UNIVERSITY OF OKLAHOMA

GRADUATE COLLEGE

DEVELOPMENT AND EVALUATION OF NOVEL AIR HANDLING UNIT CONTROL STRATEGIES FOR IMPROVED BUILDING DEMAND FLEXIBILITY AND THERMAL COMFORT

A DISSERTATION

SUBMITTED TO THE GRADUATE FACULTY

in partial fulfillment of the requirements for the

Degree of

DOCTOR OF PHILOSOPHY

By

NURAYN ADEWALE TIAMIYU

Norman, Oklahoma

2026

DEVELOPMENT AND EVALUATION OF NOVEL AIR HANDLING UNIT CONTROL STRATEGIES FOR IMPROVED BUILDING DEMAND FLEXIBILITY AND THERMAL COMFORT

A DISSERTATION APPROVED FOR THE SCHOOL OF AEROSPACE AND MECHANICAL ENGINEERING

BY THE COMMITTEE CONSISTING OF

Dr. LI SONG, CHAIR

Dr. CHOON YIK TANG

Dr. JIE CAI

Dr. HAMIDREZA SHABGARD

Dr. DONG ZHANG

Alhamdulillahi Rabbil ‘Alamin

Acknowledgement

All praise and gratitude belong to Allah, the Lord of all worlds, for His endless blessings, guidance, and mercy throughout this Ph.D. journey. Completing this dissertation would not have been possible without the unwavering support and encouragement of the many individuals who have stood by me along the way.

I would like to first express my sincere gratitude to my advisor, Dr. Li Song, for her academic mentorship, guidance, and support throughout my Ph.D. program. Her expertise, encouragement, and commitment to my development have been instrumental in my growth as an independent researcher and have motivated me to continuously strive for excellence. Thank you for your patience, understanding, and steadfast support. I am truly grateful for your kindness and encouragement.

My sincere gratitude also goes to my committee members, Dr. Choon Yik Tang, Dr. Jie Cai, Dr. Hamidreza Shabgard, and Dr. Dong Zhang, for their invaluable advice, guidance, and constructive feedback throughout the various stages of my Ph.D. program, including my advisory conference, course plan, general examination, dissertation proposal, and dissertation defense. Special thanks go to Dr. Gang Wang for his valuable feedback and technical guidance on this dissertation and the other research projects we collaborated on. His insights and expertise have been greatly appreciated.

I am also thankful to the collaborators with whom I have had the privilege of working on various research projects. My appreciation extends to my colleagues (past and present) and affiliated researchers in the Building Energy Efficiency Laboratory for their support and collaboration. I also gratefully acknowledge the financial support provided through the following scholarships and grants: the Bert Family Graduate Fellowship, the ExxonMobil Aerospace and Mechanical Engineering Scholarship, the Gallogly College of Engineering

Scholarship, the Central Oklahoma American Society of Heating, Refrigerating and Air-Conditioning Engineers (ASHRAE) Scholarship, the Graduate College Robberson Travel and Research Grant, and the School of Aerospace and Mechanical Engineering Graduate Student Travel Support.

To my parents, siblings, in-laws, and my entire family: thank you for always being there for me and for your unconditional love, encouragement, and support. I am deeply grateful for your emotional and spiritual support. Knowing that I have your love and encouragement has always given me strength, hope, and a reason to look forward with joy. My sincere appreciation also goes to my friends from all parts of the world. Your friendship, encouragement, and support have been invaluable, and I am truly grateful to each of you for being part of this journey.

Last but not least, I would like to express my deepest gratitude to my lovely wife, Dr. Toye. What do I even write about someone who means the world to me? No matter what I write, it would still be an underestimation of how grateful I am to have you in my life and for your support throughout this journey. Thank you for the sacrifices, for always being there for our family, and for being a constant pillar of support for me. Thank you for being my Nur (light) and my sakinah (tranquility). In the words of Rumi: "In your light I learn how to love. In your beauty, how to make poems. You dance inside my chest where no one sees you, but sometimes I do, and that sight becomes this art."

"*My Lord, enable me to be grateful for Your favor which You have bestowed upon me and upon my parents, and to do righteousness of which You approve. And admit me by Your mercy among Your righteous servants." (Qur'an 27:19)*

Table of Contents

List of Figures

List of Tables

Abstract

Buildings account for a significant share of electrical power demand, up to 80% in some regions in the United States. With many flexible loads, buildings have the potential to reduce power demand during peak times and provide demand flexibility. Building enables demand flexibility through measures such as shifting energy use to another time and shedding of load. Applying advanced control strategies to heating, ventilation, and air conditioning (HVAC) loads allows buildings to reduce the electricity consumed during peak hours. While various demand control (DC) strategies have been employed in commercial buildings, they often fail to accurately shift and shed loads while maintaining occupant thermal comfort. Additionally, existing DC strategies face challenges in quantifying load reduction, achieving precise DC and ensuring even distribution of the reduced cooling load across thermal zones. These limitations highlight a critical research gap in effectively integrating demand flexibility with occupant comfort in building energy management systems.

This dissertation develops and evaluates advanced control strategies for building demand control and thermal comfort using both simulation and experimental test beds. An innovative Energy Feedback (EF) control strategy and a novel Duct Static Pressure (DSP) cascade control strategy were first proposed, and their individual control performances were assessed using an experimental test bed. Subsequently, the integrated dynamic performance of the proposed EF and DSP cascade control strategies was evaluated against a baseline control strategy using a calibrated Modelica-based virtual test bed. Performance metrics such as settling time, relative error (RE), and the range of average zone temperature (RZT) are used as measures of quick response, control accuracy, and even cooling load sharing, respectively. The most effective strategy for minimizing the negative impact on occupant comfort during demand control is identified. The proposed control strategy demonstrated the fastest response and achieved precise load shedding, with a settling time of 0.03 hours, an RE of 0.01%, and an RZT of

0.00448°C. In contrast, the baseline strategy had a long settling time of 5.05 hours, an RE of 12.52%, and an RZT of 0.05°C.

An optimization-based control strategy was incorporated into the EF Controller to provide effective setpoint control for achieving load shifting through precooling and load shedding during peak demand periods while minimizing electricity cost. The optimization-based control strategy enabled the modulation of the cooling load setpoint based on weather conditions and the building's daily load profile. This involved developing a reduced-order thermal model, estimating its parameters for control purposes, and developing and implementing the Optimization-Based EF Controller on the calibrated virtual test bed. The performance of the proposed Optimization-Based EF–DSP Cascade Control strategy was evaluated and compared with the baseline demand control strategy and a non-optimized EF–DSP Control strategy that utilized constant cooling load setpoints.

The Optimization-Based EF Controller yielded a total electricity cost saving of 12.8% compared with the non-optimized controller, including an 8.7% reduction during the on-peak period and a 15.4% reduction during the off-peak period. The proposed Optimization-Based EF Control provides an effective approach for achieving demand-flexible HVAC operation by simultaneously reducing cooling energy consumption, minimizing electricity cost, maintaining occupant thermal comfort, and mitigating rebound effects. Finally, the performance of the Optimization-Based EF Controller was experimentally validated, and two practical implementation approaches for applying the optimization-derived EF setpoints on an HVAC system, namely the Schedule-Based EF Control and the Adaptive EF Control, were evaluated.

Among the key contributions of this dissertation are the following: (i) the development and experimental evaluation of novel EF and DSP cascade control strategies to achieve accurate demand control and evenly distribute the reduced cooling load among thermal zones; (ii) the development and calibration of a Modelica-based virtual test bed that comprises of an AHU system and building envelope, and its application to the integrated performance assessment of the proposed control strategies; and (iii) the development and implementation of an optimization-based control framework that generates and communicates optimized control signals to the EF controller.

1. General Introduction

1.1 Background

Globally, the main energy consuming sectors are buildings, transportation, and industrial. Buildings constitute the largest consumer of energy and a significant contributor to greenhouse gas emissions to the environment. In 2021, the total greenhouse gas (GHG) emitted in the United States amounted to 6,340 million metric tons of carbon dioxide (CO_2) equivalent emissions (US EPA, 2022). Buildings (residential and commercial) in the United States (US) account for about 75% of the electricity consumption, 40% of the total US energy consumption, and 30% of the GHG emissions (Goetsch & Deru, 2022). The total US electricity consumption reached 4.07 trillion kWh in 2022, marking the highest amount recorded by the US Energy Information Administration (EIA, 2022). For perspective, the electricity usage in 2022 is fourteen times greater than the electricity usage in 1950. The projected average annual growth rate for the total US electricity demand from 2022 through 2050 is approximately 1% (EIA, 2022). There is a need to improve the way electricity is being consumed and decrease the overall amount of electricity consumed in buildings. This would significantly reduce energy costs for consumers and aid the transition to a decarbonized economy.

Energy consumption is on the rise both in the United States and globally. While overall energy usage is increasing, there's a notable uptick in electricity consumption, which brings about specific risks. The transmission and distribution infrastructure constraints, growing peak electricity demand, and growing share of different renewable energy electricity generation are challenging the electrical grid (US DOE, 2019). Buildings account for a significant share of peak power demand. In some regions, they account for up to 80% of the peak power demand (US DOE, 2019). With many adjustable loads, buildings have the potential to maintain energy balance during peak demand times and provide demand flexibility by reducing energy wastage. Even though buildings are the primary drivers of the electricity demand in the US, they can also be part of the solution for the peak demand issues.

Applying advanced control and communication strategies to flexible loads such as lighting, heating, ventilation, and air conditioning (HVAC) loads with onsite photovoltaic systems, electric vehicle charging, and electrical storage allows a building to adjust power consumed to meet the grid. Building allows the provision of demand flexibility through measures such as reducing electricity consumption, shifting energy use to another time, and increasing the power draw from the grid for storage for later use (Schwartz et al., 2020). These demand flexibility measures are core characteristics of grid-interactive energy-efficient buildings (GEBs). GEBs are energy-efficient buildings that utilize smart end-use technologies and active on-site distributed energy resources (DER) to provide demand flexibility in a continuous and integrated way while co-optimizing energy use for grid services, energy costs reduction, occupant needs, and preferences. GEBs are critical in promoting resilience, environmental performance, affordability, and reliability across the US electric power system (Satchwell et al., 2021).

In 2019, the United States Department of Energy (U.S. DOE) initiated the GEB initiative which is aimed at optimizing DERs to enhance the benefit of building owners, occupants, and the electric grid. It was projected that the national adoption of GEBs can potentially save up to \$8 billion and \$18 billion in US power system costs annually by 2030 and save up to \$100 - \$200 billion in cumulative power system costs from 2021 to 2040 (Satchwell et al., 2021). Also, there are significant environmental benefits such as annual Co_2 emissions reduction of up to 80 million tons per year by 2030 (Li et al., 2021a).

Five demand-side management strategies were identified in the U.S. DOE technical report to manage building loads and make buildings more energy-efficient and grid-interactive (Schwartz et al., 2020). The identified strategies are efficiency, load shedding, load shifting, modulating, and generation. Figure 1.1 shows how the building load curves integrate some of the demand-side management strategies.

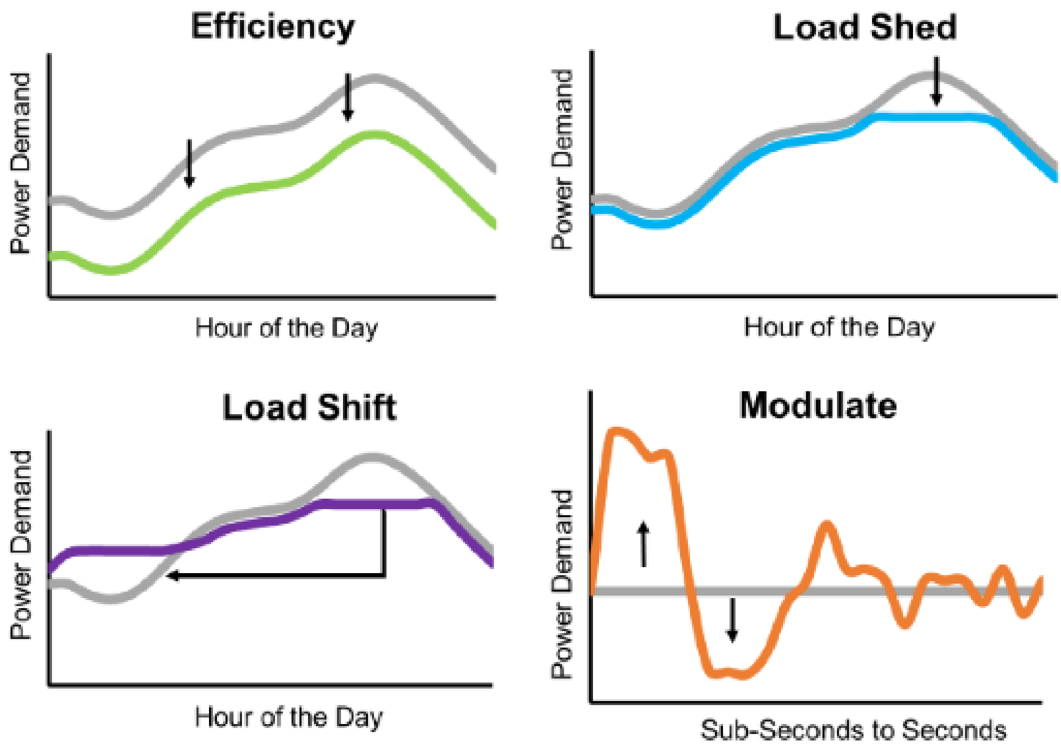

Figure 1.1: Building load curves of the demand side management strategies (Li et al., 2021)

Efficiency is the continuous reduction in energy use while maintaining or improving the functionality of the building. Load shedding refers to the ability to reduce electricity use for a short period and on short notice. Shedding is commonly deployed during peak demand periods and emergencies. Load shifting refers to the deliberate and planned shift for reasons such as minimizing demand during the peak periods and leveraging the cheapest electricity price period or mitigating the need for renewable energy curtailment. Shedding of load often leads to some level of load shifting. Modulating refers to the ability to autonomously balance power supply and demand or reactive power draw and supply within seconds to sub-seconds in response to a signal from the grid operator during the dispatch period. Lastly, generation is the ability to generate electricity for onsite use and potentially dispatch electricity to the grid in response to the signals from the grid operators.

Each demand-side management strategy offers distinct advantages and trade-offs that merit them to be explored. However, the strategies that are explored in this study would be load shedding and load shifting. This is because these strategies can be achieved by HVAC control adjustments. HVAC systems consume the most energy within the building sectors and they account for approximately 40% of the power demand in buildings (Goetzler et al., 2019). HVAC technologies are well suited to controlling peak demand because air conditioning is the biggest contributor to summer demand peaks and heating is the biggest single contributor to winter demand peaks (Goetzler et al., 2019). HVAC loads are ideally suited for demand flexibility control by utilizing the thermal mass of building structures. The building structural mass can effectively limit the variations in zone temperatures when the HVAC load changes (Xu, 2009), and HVAC systems can integrate easily with smart management systems (Chen et al., 2018).

Variable air volume (VAV) air handling units (AHU) are the most common HVAC systems in medium to large institutional and commercial buildings (Torabi et al., 2022). This is because they can meet varying heating and cooling needs of different building zones. The purpose of AHUs is to maintain indoor thermal comfort and indoor air quality (IAQ) in buildings. This is achieved by the heating, ventilation, and cooling processes. A single-duct AHU with economizer operation normally consists of a mixing/relief chamber with an interlinked outdoor damper, relief air damper, and recirculating air damper, a cooling coil (CC), a supply fan (SF), and a return fan (RF). Figure 1.2 shows the schematic of an AHU, illustrating its components and configurations.

The working principle of the AHU working principle can be summarized as follows: First, the outdoor air (Q_{oa}) is taken and mixed with the recirculating air (Q_{rec}) in the mixing chamber. Second, the mixed air is cooled and dehumidified as it passes the CC. Third, the cooled and dehumidified supply air (Q_{sa}) is delivered by the SF to conditioned spaces through terminal boxes, removing space sensible and latent cooling load. Fourth, the return air (Q_{ra}) is removed by the RF to maintain an appropriate building static pressure (P_{BLG}), which is impacted by exhaust airflow (Q_{ex}) and exfiltration airflow (Q_{exf}) in addition to the supply airflow (Q_{sa}) and return airflow (Q_{ra}). Finally, the unbalanced airflow between the return air and recirculating air, i.e., relief airflow (Q_{rel}), in the building is released to the outside through the relief chamber. To achieve indoor thermal comfort, the chilled-water flow rate through the CC is adjusted to generate cooled and dehumidified air for indoor humidity control and the SF speed is modulated through variable frequency drive (VFD) to maintain the supply air duct static pressure (P_D) at a setpoint, which ensures that all terminal boxes can receive the required supply air to maintain comfortable indoor air temperature.

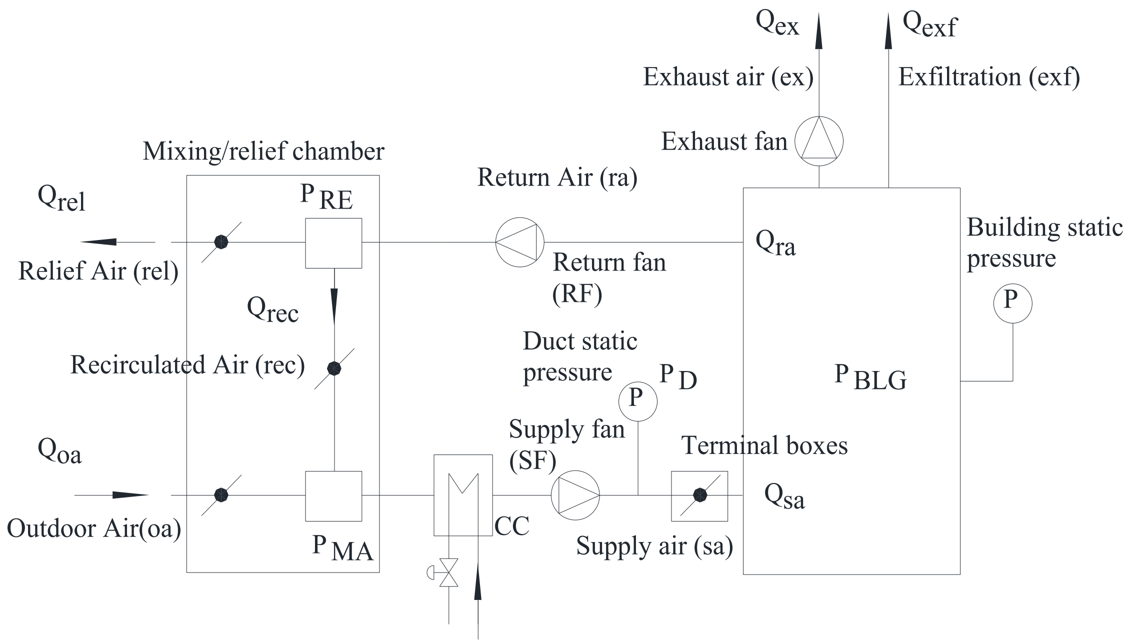

Figure 1.2: Schematic of an AHU (Tiamiyu et al., 2024)

VAV systems vary the amount of air at a variable temperature from an AHU. These systems efficiently condition building zones using flow control technologies while maintaining the required minimum flow rates for each zone. Figure 1.3 shows the VAV AHU system for two building zones.

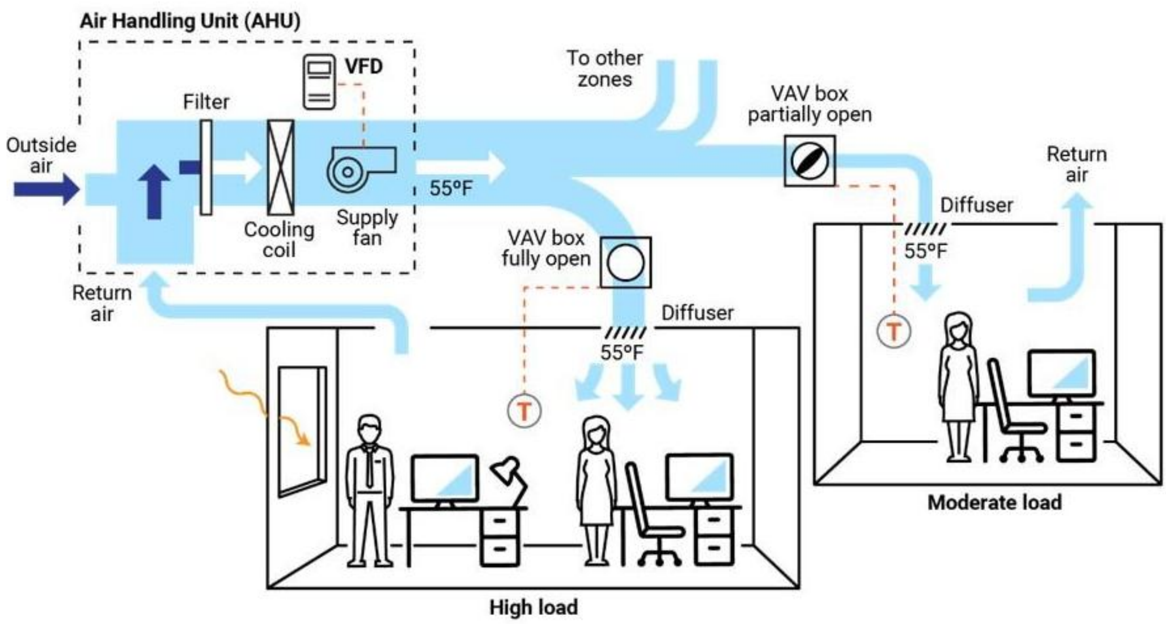

Figure 1.3: VAV AHU system for two building zones (PNNL, 2021)

The operation and control of VAV AHUs play a crucial role in enhancing the system's energy efficiency (Okochi & Yao, 2016). Dynamic variables such as ambient temperature, occupancy, and lighting loads constantly fluctuate throughout the system operation. Consequently, deviations from designated setpoints lead to significant oscillations or imbalances which cannot be ignored. Therefore, the implementation of VAV system controls becomes essential to mitigate issues such as overcooling or overheating which occur from system instability (Okochi & Yao, 2016).

The conventional AHU HVAC control has five feedback control loops to form a control flow from terminal boxes to the chiller. Figure 1.4 shows the conventional control loops for a single-duct AHU system. The different control loops are summarized as follows:

- Loop 1: The Terminal box (TB) dampers are modulated to maintain the zone temperature (ZT) at its specified ZT setpoints.

- Loop 2: The supply fan speed is modulated through the variable frequency drive (VFD) to maintain the DSP at its setpoint.

- Loop 3: The cooling coil valve is modulated to maintain the supply air temperature setpoint.

- Loop 4: The chilled water pump is modulated to maintain the water loop pressure differential (WLP).

- Loop 5: The chiller power is modulated to maintain the chilled water supply temperature (CWT) at its setpoint.

This conventional AHU system is an indoor comfort-priority control because the control actions are to align the supply side with the energy demand of the load side.

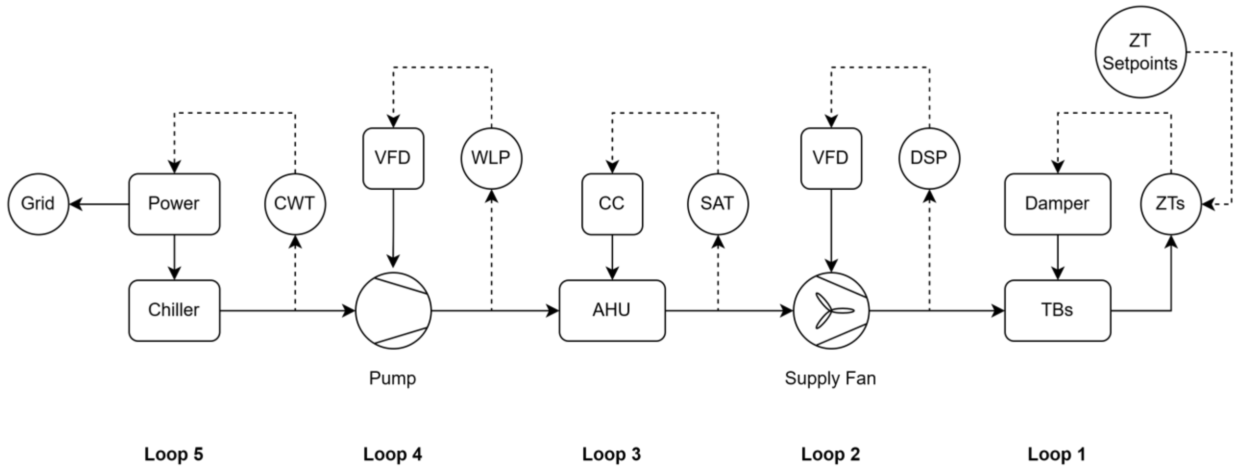

Figure 1.4: Conventional AHU feedback control loops

In an AHU, the electricity consumers are the cooling coil and supply fan. The cooling coil consumes chilled water which is generated by chillers using electricity. The cooling coil consumes electricity indirectly as it is responsible for the heat transfer from the air to the chiller water. The supply fan is the primary electricity-consuming component in the AHU, and it supplies conditioned air to the TBs for individual thermal zones in a building. The supply air is then modulated by the TB dampers for precise air temperature control. Electricity consumption in an AHU can be reduced by reducing the supply fan speed and by constraining the amount of heat removed by the cooling coil (Hurt, 2021). However, reducing the fan speed would reduce the supplied airflow rate to each thermal zone and hence, compromising the thermal comfort of building occupants. It is important to utilize HVAC load strategies that reduce the electricity consumed by the HVAC system without compromising the comfort of the building occupants. Also, the energy use of the cooling coil and supply fan is a passive response to the comfort call from the thermal zones. Thermostat settings ultimately determine the electricity usage of an HVAC system.

1.2 Research Gaps and Research Questions

1.2.1 Research Gaps

Buildings account for a significant share of electrical power demand, up to 80% in some regions (US DOE, 2019). With many flexible loads, buildings have the potential to reduce power demand during peak times and provide demand flexibility. Building allows the provision of demand flexibility through measures such as shifting energy use to another time (Schwartz et al., 2020; Tang et al., 2021; Zanetti et al., 2025; Zhou et al., 2025). The demand reduction would significantly reduce energy costs for consumers.

Heating, ventilation and air conditioning (HVAC) systems account for approximately 40% of the power demand in buildings (Goetzler et al., 2019). HVAC loads are ideally suited for demand flexibility control by utilizing the thermal mass of building structures (H. Li et al., 2021b). The building structural mass can effectively limit the variations in zone temperature (ZT) when the HVAC load changes (Xu, 2009), and HVAC systems can integrate easily with building automation systems (BAS) (Chen et al., 2018). HVAC demand response technologies have been developed to facilitate demand response operation (Kim & Braun, 2022; Wang et al., 2019; Xue et al., 2015; Young et al., 2020).

Different AHU demand control strategies have been utilized for commercial buildings to manage HVAC load (Dai et al., 2023; Ghahramani et al., 2016; Papadopoulos et al., 2019; Shan et al., 2016; Zhao et al., 2026). Global temperature adjustment (GTA) of occupied zones is the most popular approach to shift HVAC load using existing BAS (Deng et al., 2025; Yin et al., 2023). The ZT setpoints in an entire facility can be changed from one command in one location (Watson et al., 2006). GTA is typically implemented by broadcasting a signal to thermostats through the BAS. Depending on the direction of the ZT setpoint change, the broadcasted signal causes the HVAC system to increase or decrease the HVAC power demand (Keskar et al., 2022). More advanced implementations can automatically adjust ZT setpoints to follow linear or exponential curves based on the time of day, creating a customized shed profile for a building (Xu & Haves, 2006).

The adjustment of setpoints to a higher value reduces the amount of cold air needed for the thermal zones in summer (Lee & Braun, 2008). Consequently, this strategy reduces the electricity power consumed by the supply fan and the cooling load consumed by the cooling coil (Hoyt et al., 2015). The GTA method utilizes the same conventional AHU feedback control loops. There are some operational challenges associated with the GTA strategy. One of these challenges is that precise load reduction is not guaranteed, as the percentage load reduction is not explicitly correlated with the ZT rise (Hurt, 2021). This conclusion is also reported in Liu et al. (2021) study where the authors evaluated the load shedding and shifting potential for three building types which are medium office, large office, and retail store. During the demand control event day, load shifting was not achieved using the GTA. This is because there were uncertainties with the implementation of the GTA strategy. For some demand control event days, the GTA strategy performed better than the baseline, while on other days, it performed worse.

Another challenge of this GTA strategy was the slow response of the fan and the cooling coil to the space load changes introduced by the ZT setpoint reset, preventing immediate load shedding. While the GTA strategy can ensure that the reduced cooling load is evenly shared across all zones, it cannot quickly and accurately reduce HVAC power demand.

Centralized adjustment on AHUs demand control strategies makes temporary adjustments to the AHU system. Examples of these strategies include the DSP setpoint reduction, applying a supply fan speed limit, and increasing the SAT (Afroz et al., 2023; Motegi et al., 2007). The cooling and fan energy would be reduced when the DSP setpoint is reduced during demand control events. For instances where the DSP setpoint is set lower than required, the VAV TBs starve due to lack of air pressures which then causes the airflow supplied to be less than necessary to cool the space (Wang et al., 2023; Watson et al., 2006). Similarly, just as DSP setpoint reduction lowers fan speed, a fan speed limit strategy can be applied to supply fans controlled by VFDs to reduce fan power consumption. In this strategy, the supply fan speed is limited to a fixed value, which must be lower than the normal operation of the fan under closed-loop conditions (Watson et al., 2006). However, due to the open-loop nature of this fan control (fixed speed), the effect of this strategy on thermal comfort is less predictable. Finally, increasing the SAT was introduced to reduce cooling demand, and this reduction occurs at the cooling plant. However, this strategy could lead to increased fan energy use in the VAV system due to increased airflow to meet the thermal zone demand, unless the fan speed is limited to a range of use.

These centralized AHU demand control strategies respond quickly to demand and facilitate cooling load reduction comparing with the GTA control, but they possess certain inherent drawbacks. For instance, these strategies result in an uneven distribution of the demand control burden across the zones i.e. the TBs cannot evenly share the reduced AHU cooling load. Zones with low demand or TBs closer to the main supply duct operate normally while zones with high demand such as those on the sunny side of the building or TBs at the end of long duct run experience air starvation or completely go out of control (Wang et al., 2023; Watson et al., 2006). These strategies would lead to significant variation in the ZTs and airflow rates, hence, compromising the thermal comfort of building occupants. Also, increasing the SAT can potentially increase the humidity level in commercial buildings (Elehwany et al., 2024; Shehadi, 2018). These increased humidity levels associated with higher ZT would affect the indoor air quality of the occupied zones (Aghniaey & Lawrence, 2018). In addition to the thermal comfort issues associated with these AHU demand control strategies, precise demand controlcannot be achieved due to the lack of energy measurement and setpoint controls.

The shortcomings of the current demand control strategies emphasize the need to develop and evaluate the feasibility of an AHU demand control strategy that directly and precisely curtails the cooling coil load and supply fan power to provide on-demand HVAC load shifting and shedding while minimizing the negative impact on indoor thermal comfort caused by the reduced cooling load during demand control.

1.2.2 Research Hypothesis and Proposed Solution

To address the inaccurate and slow demand control, imprecise load reduction, and the inability to guarantee precise load shedding associated with GTA control and strategies such as DSP setpoint reduction, supply fan speed limiting, and SAT reset, a control strategy capable of directly regulating the cooling load is required. In addition, precise demand reduction has not been achieved by existing strategies due to the lack of direct cooling load measurement and cooling load setpoint control. This dissertation proposes an Energy Feedback (EF) control strategy to provide fast and accurate demand control, ensure precise load shedding during the on-peak period, and facilitate load shifting during the off-peak period. The EF control regulates the cooling load by modulating the supply fan speed to track prescribed cooling load setpoint, thereby enabling fast, precise, and direct demand control.

Uneven distribution of the demand control burden across the thermal zones occurs with current demand control strategies, as some zones experience air starvation and significant variations in ZTs. These conditions compromise the indoor thermal comfort of building occupants, particularly in commercial buildings with multiple thermal zones. To minimize the negative impact of reduced cooling load on indoor thermal comfort during demand control, this dissertation proposes a Duct Static Pressure (DSP) Cascade Control, which adjusts the ZT setpoints within a prescribed comfort range (minimum and maximum limits) for all terminal boxes to regulate the DSP at its setpoint. The integrated operation of the two proposed control strategies is intended to achieve precise demand control while maintaining indoor thermal comfort by distributing the reduced cooling load evenly across all thermal zones.

1.2.3 Research Questions

Based on the identified limitations of existing AHU demand control strategies, this dissertation aims to address the growing need for sustainable energy management in buildings by developing, evaluating, and validating advanced control strategies that bridge the gap between demand control and thermal comfort. The objective of this dissertation is to develop, optimize, and validate advanced HVAC demand control strategies that enable fast and precise demand control while minimizing the negative impact on occupant thermal comfort

The following research questions are formulated based on the identified research gaps:

RQ1: Can the proposed control strategies, namely Energy Feedback (EF) control and Duct Static Pressure (DSP) cascade control, provide accurate demand control and distribute the reduced cooling load evenly among all thermal zones?

RQ2: How can the integrated dynamic performance of the proposed AHU control strategies for building demand control be evaluated?

RQ3: How do the proposed control strategies perform compared to state-of-the-art demand control strategies?

RQ4: How should a simulation-based virtual test bed for an HVAC system and building envelope be designed and calibrated?

RQ5: What is the most effective EF control loop design for achieving quick control response and accurate control?

RQ6: How should an optimization strategy be integrated with the proposed novel demand control strategies in simulation and experimental test beds?

RQ7: How can an Optimization-Based EF Controller be developed and its performance evaluated?

RQ8: What is the most effective implementation approach for the Optimization-Based EF Controller on an experimental test bed?

1.3 Dissertation Overview and Unique Contributions

The outline of this dissertation is as follows:

- **Chapter 1** provides the introduction and research gap analysis of this study.
- **Chapter 2** describes state-of-the-art building demand control strategies.

- **Chapter 3** presents the development and experimental evaluation of EF and DSP Cascade Controls.
- **Chapter 4** presents the integrated performance assessment of the proposed control strategies using a developed and calibrated Modelica-based virtual test bed.
- **Chapter 5** presents the development and evaluation of an optimization-based framework coupled with the proposed control strategies.
- **Chapter 6** presents the experimental validation of the proposed Optimization-Based EF–DSP Cascade Control strategy.
- **Chapter 7** presents the general conclusions and recommendations for future work.

The unique contribution of **Chapter 3** is the development and experimental evaluation of new controls to provide accurate demand control and share the reduced cooling load evenly among all thermal zones. These controls minimize the negative impact on indoor thermal comfort caused by the reduced cooling load during demand control. This is achieved by implementing two controls: (1) modulating fan speed using cooling load for quick and precise demand management, and (2) adjusting the ZT setpoints within a comfort range (maximum and minimum limits) for all TBs to maintain duct static pressure (DSP). The proposed controls, namely Energy Feedback (EF) control and DSP cascade control, are modified to control the cooling load between the AHU and TB.

The unique contribution of **Chapter 4** includes an integrated performance assessment of the proposed EF and DSP cascade control strategies for building demand control and thermal comfort, as well as the development and calibration of a Modelica-based virtual test bed comprising an AHU system with seven individually controlled VAV boxes, their control sequences, and the building envelope. Additionally, a comparative assessment between the proposed and existing demand control strategies under identical weather conditions is conducted to verify the performance of the new controls using the calibrated virtual simulation test bed.

The unique contributions of **Chapter 5** include the development, implementation and evaluation of an optimization-based EF controller to modulate the cooling load setpoint based on outdoor air temperature and the daily load profile of the building. This also includes parameter estimation of a commercial building model and the development of an optimization control framework that communicates optimized control signals with the calibrated virtual test bed.

2. State of the Art Building Demand Control Strategies

Different building DR strategies have been utilized for commercial buildings to temporarily manage HVAC load. Currently, the most used strategy is to simply reset the ZT setpoints for some period. This adjustment of setpoints to a higher ZT reduces the amount of cold air needed for the thermal zones as the TB damper position would reduce to achieve the setpoint. Consequently, this strategy reduces the electricity consumed by the supply fan and cooling coil as there is a reduction in the supply airflow rates which results in less heat entering the chiller water. Hoyt et al. (2009) demonstrated the impact of increasing the room temperature setpoint on the energy saving for a commercial building. Increasing the cooling setpoint from 24ºC (75ºF) to 25ºC (77ºF) resulted in a cooling energy savings of 7-15% depending on the building's operational features and climate zones. When the setpoint temperature was extended from 24ºC (75ºF) to 28ºC (82ºF), the energy saving potential reported reached 35-45%, however, the impact of these energy savings on occupant thermal comfort was not reported in their study. Though ZT setpoint reset is a simple way to improve building energy flexibility, the building occupant comfort must not be sacrificed (Chen et al., 2018). Other strategies include pre-cooling and pre-heating, duct static pressure control (fresh air flow control), desiccant cooling, and chiller water temperature control (Watson et al., 2006). This section presents more details of the strategies for DR in commercial buildings.

2.1 Global temperature adjustments of zones

Global temperature adjustment (GTA) of occupied zones is the most popular approach used to shift HVAC power consumption using existing building automation systems (BAS). The space temperature setpoints of an entire facility can be changed from one command in one location (Watson et al., 2006). GTA is typically implemented by broadcasting a signal to thermostats through the BAS. Depending on the direction of the temperature setpoint change, the broadcasted signal causes the HVAC system to increase or decrease the HVAC power consumption (Keskar et al., 2022). More advanced implementations can adjust the temperature setpoints to follow linear or exponential curves (Xu et al., 2004). GTA can be implemented either absolutely or on a relative basis. Absolute implementation of GTA enables the setting of the ZT to absolute values while relative implementation of GTA allows the adjustment of ZT setpoints to new values that are the offset values of the current values (Watson et al., 2006). Table 2.1 shows examples of an absolute and relative adjustment of GTA setpoints for different DR modes.

Table 2.1: Absolute and relative implementations of GTA setpoints (Watson et al., 2006)

DR Mode	Absolute ZT Cooling setpoints (°F)	Relative ZT Cooling setpoints (°F)
Normal	74°F (globally)	Varies per zone
Moderate Shed	76°F	Normal +2°F
High Shed	78°F	Normal +4°F

The GTA method utilizes the same conventional AHU feedback control loops with no adjustments. To accurately implement the GTAs in a facility, the desired ZT setpoint is firstly determined based on thermal models of a building system considering occupants' preferences for indoor conditions under dynamic pricing. Then, the chiller power reactively adjusts to meet the desired ZT temperature setpoint. The communication from the TBs to the chillers is very slow because of the building's thermal mass and HVAC equipment. Because of this slow communication, the chiller power is not quickly and accurately controlled as predicted in different building thermal models even though ZT can be approximately controlled around its setpoint (Wang et al., 2023). HVAC load flexibility control by resetting the ZT setpoints is difficult to achieve due to the complexity of the commercial HVAC system and dynamic loads in a commercial building.

There are some operational challenges associated with the GTA strategy. One of the challenges is that precise load reduction is not guaranteed for ZT setpoint reset as it is not easy to correlate the percentage load reduction to the temperature degree rise (Hurt, 2021). This conclusion is also reported in Liu et al. (2021) study. The authors evaluated the load shedding and shifting potential for three building types which are medium office, large office, and retail store. During the DR event day in Figure 2.1, load shifting was not achieved using the GTA. This is because there are uncertainties with the implementation of the GTA strategy.

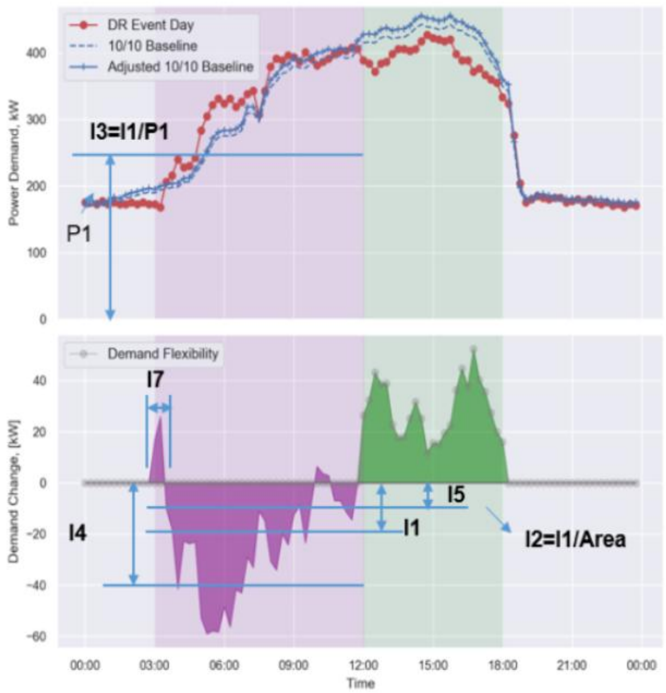

Figure 2.1: HVAC load shifting using GTA (Liu et al., 2021)

For some DR event days, the GTA DR strategy performs better than the baseline and, on some days, it performs worse than the baseline. Also, other factors affect the demand response potential of the building such as weather conditions and time of day. Yin et al. (2016) evaluated the impact of degrees of GTA on the DR performance at different ranges of outside air temperature (OAT). Large variations in the DR potential were caused by weather conditions.

When the OAT is very hot (above 35°C (95°F)), the commercial building HVAC system has less DR potential. This lower DR potential is because the HVAC system is running at its full capacity and the HVAC load exceeds the system capacity (Yin et al., 2016). Another challenge of this GTA DR strategy is the slow responses of the fan and the cooling coil to the space load changes introduced by the setpoint reset do not allow immediate response for load shedding.

2.2 Centralized adjustment on AHUs

These DR strategies make temporary adjustments to the AHU system. Examples of these strategies include the DSP setpoint reduction, applying a supply fan speed limit, and increasing the supply air temperature.

2.2.1 Reduction of DSP setpoint

The DSP in a VAV AHU system is usually measured in the supply duct and the supply fan speed is modulated by VFD to maintain the DSP at a setpoint. For most AHUs, the DSP setpoint at the supply duct is high enough to provide enough pressure to allow the proper functioning of the TBs. Also, they are set to meet the pressure requirement of the TBs with the greatest demand under design load (Watson et al., 2006).

Since the DSP is set to meet the demand of the TBs under greater demand, reducing the DSP setpoint during lesser demand conditions would reduce the energy losses associated with maintaining the DSP at a setpoint higher than the required. The cooling and fan energy would be reduced when the DSP setpoint is reduced during DR events. For instances where the DSP setpoint is set too low, the VAV TBs starve due to lack of air pressures which then cause the airflow supplied to be less than necessary to cool the space (Wang et al., 2023; Watson et al., 2006).

2.2.2 Limiting fan speed limit

This DR strategy is only applicable to supply fans controlled by VFD. The supply fan speed is limited to a fixed value which must be lower than the normal operation of the fan under closed-loop conditions (Watson et al., 2006). For example, during a high load condition, the fan speed may modulate between 90% and 100%. To apply this strategy, the supply fan speed would be limited to a speed of 90% or below to limit the fan energy during the DR event. However, due to the open-loop nature of this fan control (fixed speed), the effect of this strategy on thermal comfort is less predictable (Watson et al., 2006).

2.2.3 Increasing the supply air temperature

This DR strategy saves cooling energy, and this savings occurs at the cooling plant. During the implementation of this strategy on AHUs, it is important to avoid increasing the fan energy in the VAV system due to increased flow (Watson et al., 2006). This can be prevented only by increasing the supply air temperature (SAT) after the fan speed has been limited to a range of use.

2.2.4 Evaluation of AHU adjustment DR strategies

Although these DR strategies are effective in achieving cooling load reduction, they possess certain inherent drawbacks. For instance, these strategies result in an uneven distribution of the DR burden across the zones i.e. the TBs cannot even share the reduced AHU cooling load. Zones with low demand or TBs closer to the main supply duct operate normally while zones with high demand such as those on the sunny side of the building or TBs at the end of long duct run experience air starvation or completely go out of control (Wang et al., 2023; Watson et al., 2006). These HVAC DR strategies would lead to significant variation in the zone temperatures and airflow rates, Hence, compromising the thermal comfort of building occupants. Also, increasing the supply air temperature can potentially increase the humidity level in commercial buildings. These increased humidity levels associated with higher ZT would affect the indoor air quality of the occupied zones (Aghniaey & Lawrence, 2018).

2.3 Centralized adjustment on chillers

Most central chiller plants have the capability of reducing their power demand. This DR strategy is applied to limit the chiller power or current while other HVAC components are controlled using the AHU conventional feedback loops. Figure 2.2 shows the control loops for the centralized adjustment on chillers. This approach yields missed communication between the power control (Loop 5) and the conventional AHU feedback control loops (Loop 1 to Loop 4). Also, this strategy impacts the thermal comfort in a commercial building as there is uneven response among AHUs under the reduced chiller power (Wang et al., 2023).

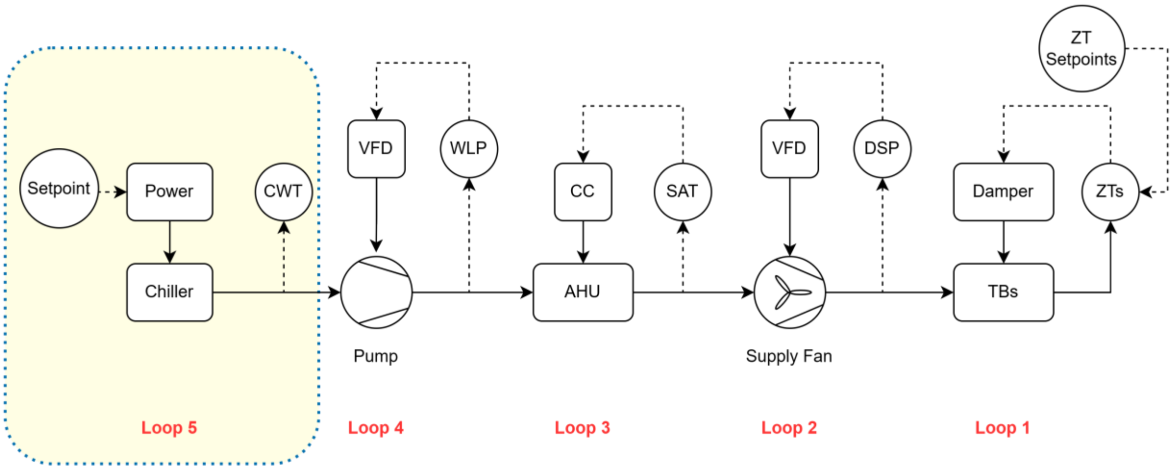

Figure 2.2: Centralized adjustment on chillers

3. Development and Experimental Evaluation of Energy Feedback and Duct Static Pressure Cascade Control

This chapter describes the development of the Energy Feedback (EF) Control and the Duct Static Pressure (DSP) Cascade Control and presents their experimental evaluation. The objective of this chapter is to experimentally evaluate the performance of each proposed controller on a fully instrumented VAV AHU experimental test bed. Two experimental tests were conducted. The first test evaluated the DSP Cascade Control, while the second test evaluated the EF Control. The aim of these tests was to assess the feasibility of implementing each controller on the experimental test bed and to evaluate its ability to accurately regulate the duct static pressure and cooling load, respectively.

3.1 Description of Energy Feedback and DSP Cascade Controls

Figure 3.1 shows the schematic of the integrated EF and DSP cascade control loops. For the EF control, the supply fan speed is modulated to maintain the cooling load at its setpoint, thereby achieving precise cooling demand control. This requires the reconfiguration of the conventional ZT feedback control loop for the supply fan. The controlled variable is the cooling load, which is not measured directly but is calculated from measured variables such as air temperature and humidity. The EF control variable can be either the sensible cooling load or the total cooling load, depending on the available instrumentation in the AHU system and the selected control implementation. The EF control is designed to provide fast and accurate regulation of the cooling load at the AHU supply side, thereby enabling precise demand control.

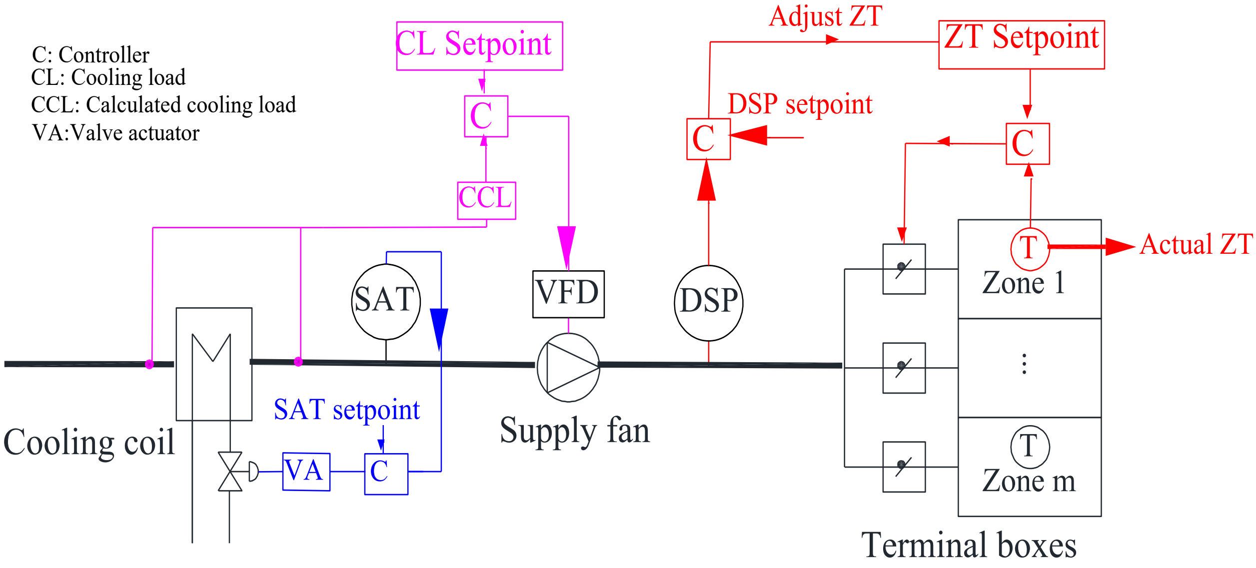

Figure 3.1: Energy feedback control loop integrated with DSP cascade control loop

The DSP Cascade Control is designed to achieve an even distribution of the demand control burden across the thermal zones. This novel DSP Cascade Control is developed to generate an adjustment factor, β through reverse control action to uniformly adjust the effective ZT setpoint $(T_{stp,i})$for all terminal boxes (TBs). This allows all the thermal zones to share the reduced cooling load evenly, thereby minimizing the negative impact on indoor thermal comfort.

$$T_{stp,i} = \beta T_{max,i} + (1 - \beta)T_{min,i} \qquad 0 \leq \beta \leq 1$$

where the maximum setpoint ($T_{max,i}$) and the minimum setpoint ($T_{min,i}$) define the allowable thermal comfort range for each thermal zone. A smaller ZT comfort range corresponds to a higher comfort priority and provides less demand flexibility, whereas a larger ZT comfort range corresponds to a lower comfort priority and provides greater demand flexibility.

Figure 3.2 shows the block diagram of the DSP Cascade Control, which consists of an outer control loop and an inner control loop. In the outer loop, the controller regulates the DSP at its setpoint and generates the adjustment factor (β) to uniformly adjust the effective ZT setpoints for all the TBs. In the inner loop, the TB controllers modulate the damper positions to maintain their respective effective ZT setpoints. Figure 3.3 shows the schematic of the DSP cascade control for seven thermal zones.

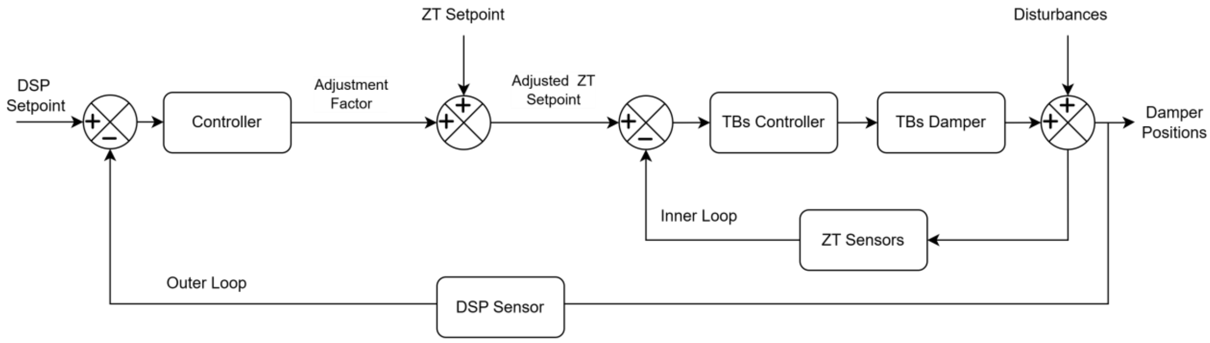

Figure 3.2: Block diagram of DSP Cascade control

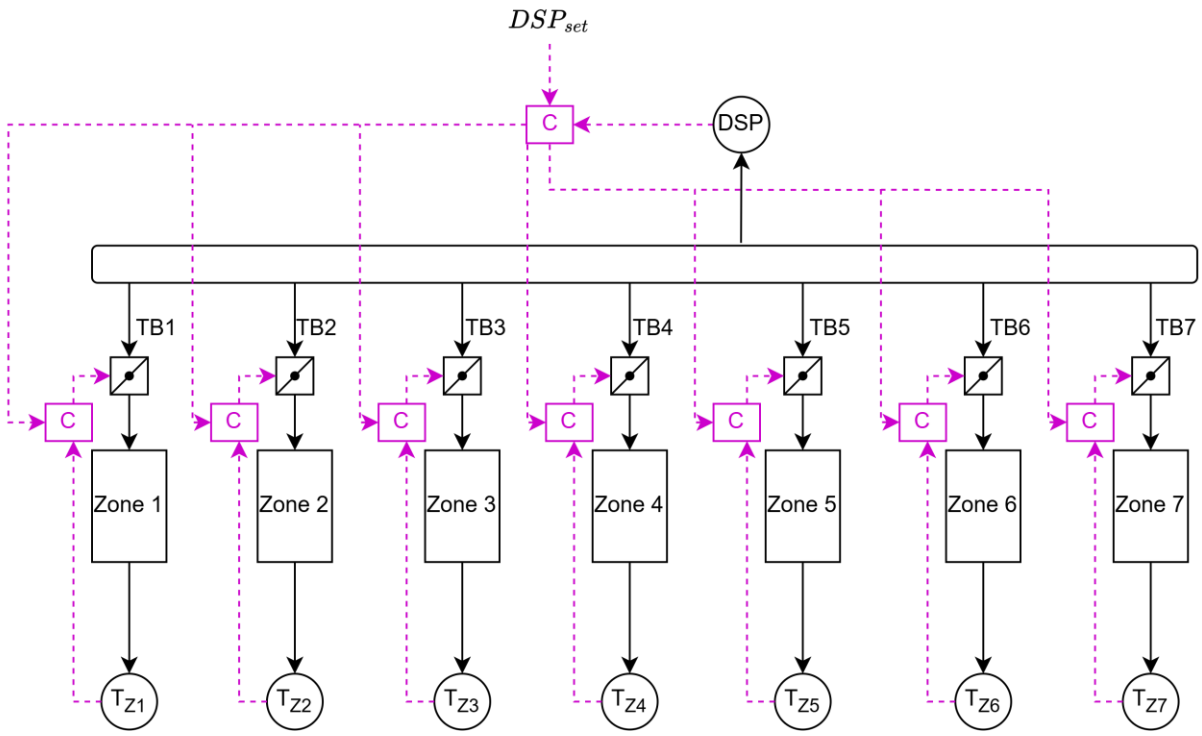

Figure 3.3: DSP Cascade Control Loop schematic for seven thermal zones

The EF and DSP Cascade Control requires the reconfiguration of the AHU control loops. Table 3.1 summarizes the differences between the conventional ZT feedback control and the proposed EF and DSP Cascade Control for the TBs and the supply fan.

Table 3.1: Differences between the ZT Feedback Control and the Proposed EF and DSP Cascade Control

System	ZT feedback control	EF and DSP cascade control	
	Primary controller	Primary controller	Secondary controller
TB	TB damper is modulated to maintain the ZT setpoint	TB damper is modulated to maintain the ZT setpoint	ZT setpoint is modulated to maintain the duct static pressure setpoint
Supply Fan	Fan speed is modulated to maintain the duct static pressure setpoint	Fan speed is modulated to maintain the cooling load setpoint	N/A
Cooling coil	Valve is modulated to maintain the SAT at its setpoint	Valve is modulated to maintain the SAT at its setpoint	N/A

Proportional–integral (PI) controllers are widely applied in HVAC control systems. Tuning the proportional (P) and integral (I) gains of a controller is essential to achieve the desired control performance. The selection of the P and I gains depends largely on the process gain of the controlled HVAC system, which is defined as the ratio of the change in the controlled variable to the change in the manipulated control input. In the proposed control loops, the controlled variables and manipulated control inputs differ from those in the conventional control loops. Consequently, the process gains of the controlled systems also differ, and the P and I gains of the controllers must be retuned to achieve the desired control performance.

3.2 Experimental Test and Results

The experimental test bed is a fully instrumented single-duct VAV AHU system that serves seven thermal zones of an office building located on a university campus. The number of occupants in the served areas varies from zero during unoccupied periods to a maximum of 16 during occupied periods. The configuration of the system is shown in Figure 3.4. The AHU includes a chilled-water cooling coil with a design cooling capacity of 28 kW, a supply fan with a design airflow rate of 1,200 L/s and a design head of 710 Pa. The VAV system is equipped with a building automation system (BAS) for data acquisition, communication, monitoring, and control. The BAS is capable of measuring:

1. the speed, pressure head, and VFD power consumption of the supply and return fans;
2. the duct static pressure (DSP);
3. the outdoor air and supply airflow rates using the duct traverse method; and
4. the outdoor, mixed, supply, and return air dry-bulb temperatures

All measurements were recorded at one-minute intervals and logged by the BAS.

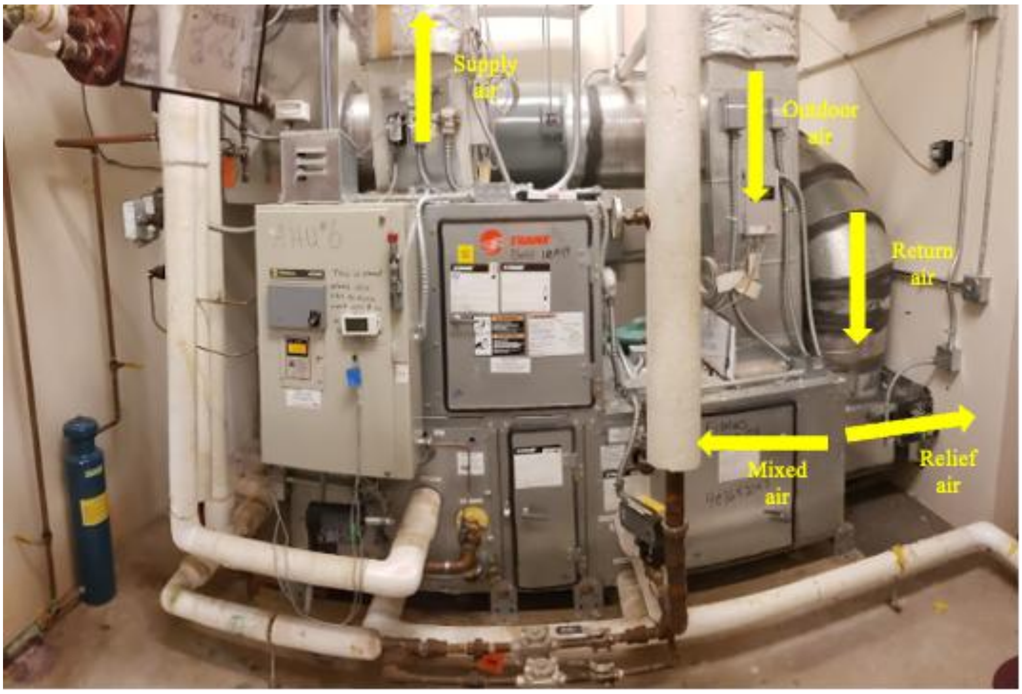

Figure 3.4: Single-duct VAV AHU system

3.2.1 DSP Cascade Control Test

For the DSP Cascade Control test, the supply fan speed was fixed at 90%. The fan speed was fixed to validate the feasibility of maintaining the DSP setpoint by adjusting the ZT setpoints, while eliminating the influence of supply fan speed control on the DSP. The TB damper response time was first systematically adjusted by reducing the driving time of the corresponding actuator, followed by tuning the proportional (P) and integral (I) gains of the corresponding ZT controller. This process ensured that the dampers responded quickly to changes in the ZT while avoiding excessive overshoot of the DSP and maintaining overall control stability. Afterwards, open-loop tests were conducted by applying step changes to the ZT setpoints to determine the process gain, defined as the ratio of the change in DSP to the change in ZT. Based on the identified process gain, the DSP controller was designed and tuned. After controller tuning, the DSP was maintained at its setpoint by modulating the ZT setpoint adjustment factor.

Figure 3.5(a) shows the controlled SAT, while Figure 3.5 (b) shows the measured DSP (blue curve) together with the adjusted ZT (orange curve). Both the SAT and DSP were well maintained at their setpoints of 13°C and 250 Pa, respectively. More importantly, Figure 3.5 (b) demonstrates that the DSP Cascade Control successfully maintained the DSP at its setpoint by adjusting the ZT setpoints within the prescribed comfort range. During the precooling period, the ZT was reduced by a maximum of 0.3°C , while during the cooling release period, it was increased by a maximum of 0.5°C.

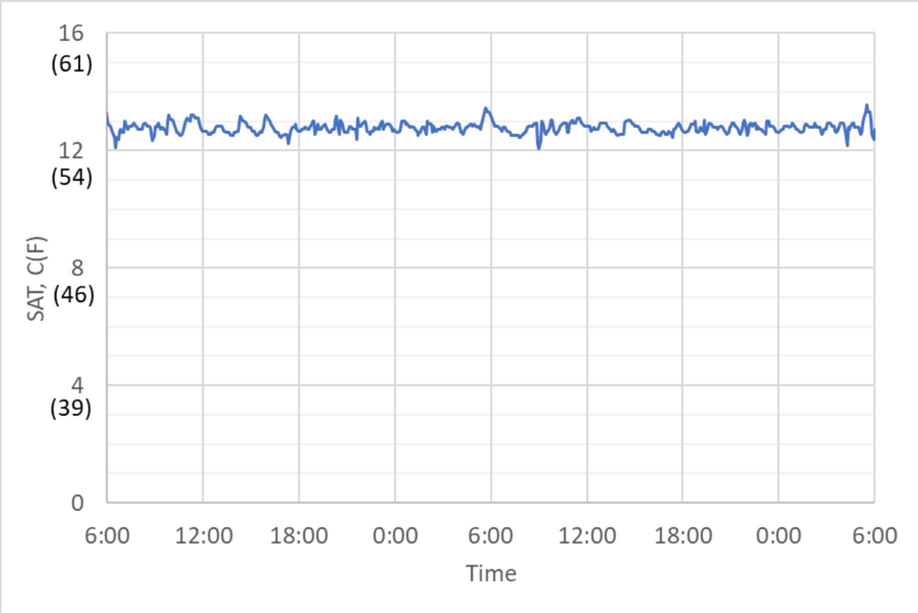

(a) SAT

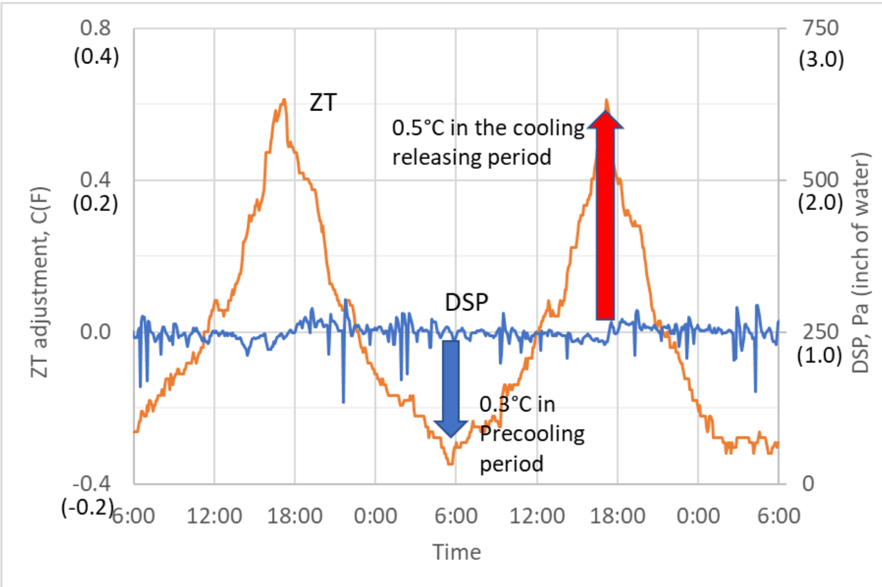

(a) DSP and ZT adjustment

Figure 3.5: DSP Cascade Control Test with fixed fan speed

3.2.2 EF Control Test

In this EF Control test, the supply fan speed was modulated to maintain the adjusted sensible cooling load (ACL) at a constant setpoint of 7.3 kW, while the DSP and SAT controls remained the same as those in the DSP Cascade Control test. This test was conducted to validate the performance of the proposed HVAC load management strategy in the considering the interactions among the supply fan, cooling coil, and TB dampers. Figure 3.6 shows the controlled ACL (blue curve) together with the supply fan speed (orange curve). The ACL was well maintained at its setpoint by increasing the supply fan speed to 100% during the morning precooling period and decreasing it to approximately 70% during the afternoon cooling release period.

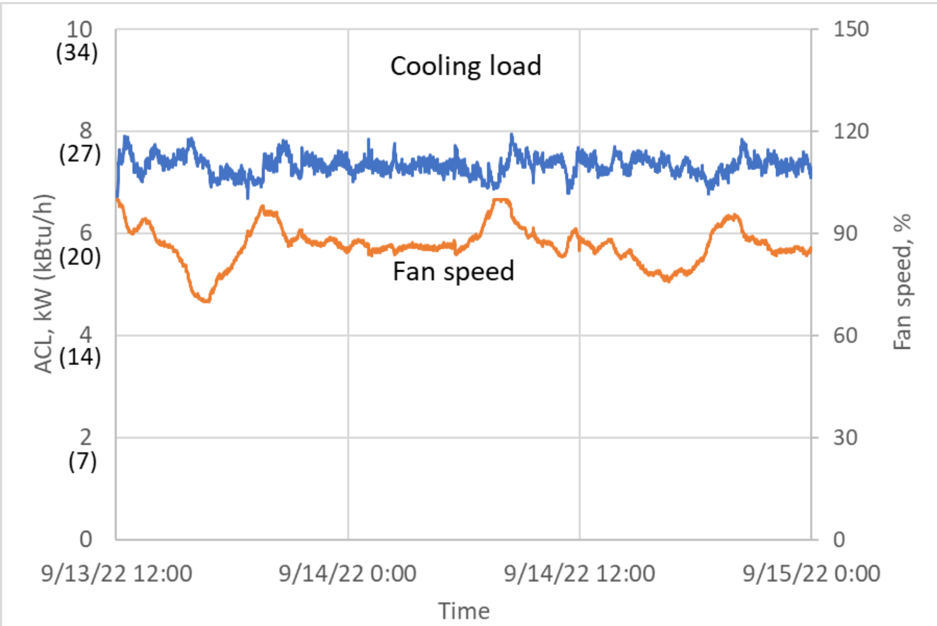

Figure 3.6: Supply fan speed and controlled cooling load for EF control test

3.3 Summary

This chapter presented the development and experimental evaluation of the proposed EF Control and DSP Cascade Control. The experimental results demonstrated the feasibility of implementing each control strategy on a fully instrumented VAV AHU experimental test bed. The EF Control accurately regulated the cooling load by modulating the supply fan speed, demonstrating its capability to provide precise cooling demand control. The DSP Cascade

Control successfully maintained the DSP at its setpoint by uniformly adjusting the ZT setpoints within the prescribed comfort range. These results confirm that both proposed control strategies achieved their intended control objectives under experimental operating conditions. The successful implementation of the individual controllers establishes the foundation for the comprehensive evaluation of their integrated performance presented in the following chapter, which also examines different EF–DSP control strategies to identify the configuration that provides the best overall performance. In addition, the proposed control strategies are compared with existing demand control strategies under identical weather conditions to further verify their effectiveness.

4. Integrated Performance Assessment of Proposed Air Handling Unit Control Strategies and Performance Comparison Using a Modelica-Based Virtual Test Bed

This chapter investigates the integrated dynamic performance assessment of these proposed control strategies. This study evaluates and compares performance of four air handling unit (AHU) control strategies using a Modelica-based virtual test bed. Control strategies were first developed and described. These strategies include Sensible EF without DSP, Sensible EF with DSP, Total EF with DSP, with state-of-the-art zone temperature (ZT) control serving as the baseline. Then, a virtual test bed representing an existing AHU system was developed and calibrated. Four control strategies were implemented. Finally, the performance of EF strategies was evaluated against baseline strategy using settling time, relative error (RE), and the range of average ZT (RZT) as measures of quick response, control accuracy, and even cooling load sharing, respectively.

4.1 Description of state-of-the-art demand control and strategies using the EF and DSP cascade control technologies

The state-of-the-art demand control is the ZT feedback control using GTA. This baseline control strategy ensures that reduced cooling load burden is evenly shared across thermal zones. However, it does not achieve fast and accurate demand control due to the slow response of the supply fan and cooling coil. This state-of-the-art control is utilized as a baseline for the other strategies using EF and DSP cascade control technologies. Figure 4.1a shows the schematic of the feedback control loops of the state-of-the-art control. These loops are described in the introduction.

Different control strategies based on the EF and DSP cascade control technologies are evaluated in this study. The first EF control strategy, Sensible EF without DSP, employs EF control without the DSP cascade control to ensure fast demand control during on-peak hours. The utilized EF control variable is the sensible cooling load, which allows the reduced cooling load to be quantifiable. Figure 4.1b shows the EF control (marked in Pink) without the DSP cascade control to be evaluated in this study. The EF control involves the reconfiguration of the AHU control loops that allows fan speed to be controlled in response to cooling load set point for precise cooling demand response operation. The supply fan speed is controlled to maintain the cooling load at a set point since it is no longer needed for duct static pressure control. The sensible cooling load is the calculated and controlled variable for the EF controller.

The second EF control strategy, Sensible EF with DSP, integrates both EF control and DSP cascade control to achieve quick demand control while ensuring even sharing of reduced cooling load among the thermal zones. The EF control variable utilized for this control strategy is the sensible cooling load. A novel DSP cascade controller is utilized to achieve even modulation on the demand side while the EF control is utilized to achieve quick and accurate power at the supply side. A novel DSP cascade controller is designed to create an adjustment factor (β) with a reverse action to evenly adjust the effective ZT setpoint ($T_{stp,i}$) for all the TBs, which allows all the zones to share the adjusted cooling load evenly and consequently minimize the negative impact on indoor comfort.

$$T_{stp,i} = \beta T_{max,i} + (1-\beta) T_{min,i} \qquad 0 \leq \beta \leq 1$$

where a maximum setpoint ($T_{max,i}$) and a minimum setpoint ($T_{min,i}$) define a comfort range for the thermal zones. A smaller ZT range means a higher comfort priority and provides less demand flexibility while a larger ZT range means a lower comfort priority and provides more demand flexibility.

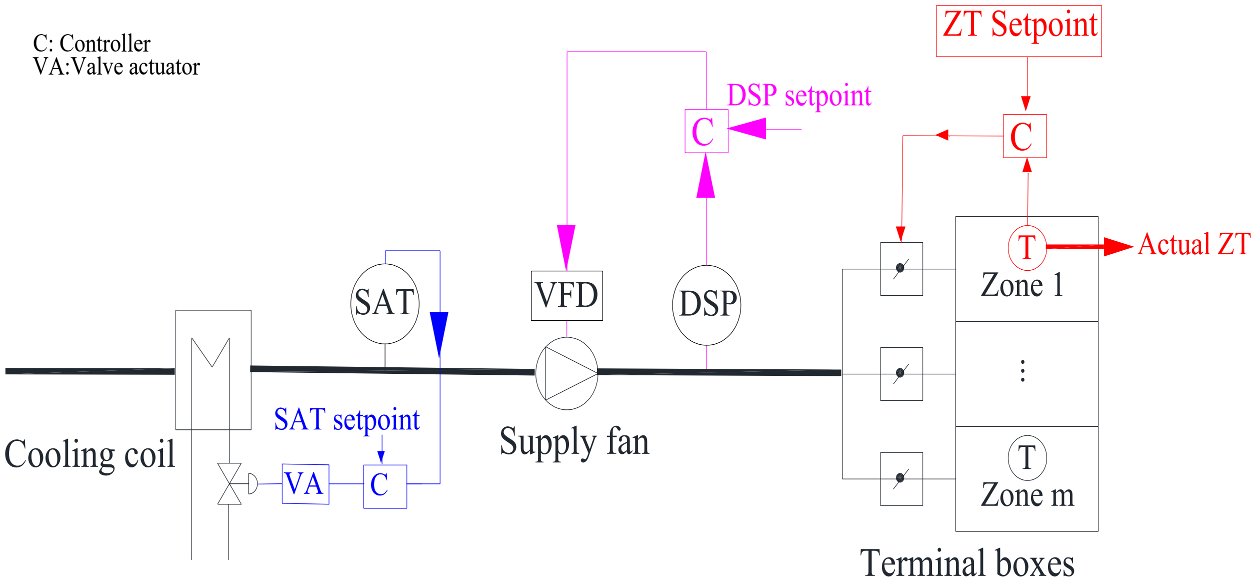

(a) ZT feedback control using GTA

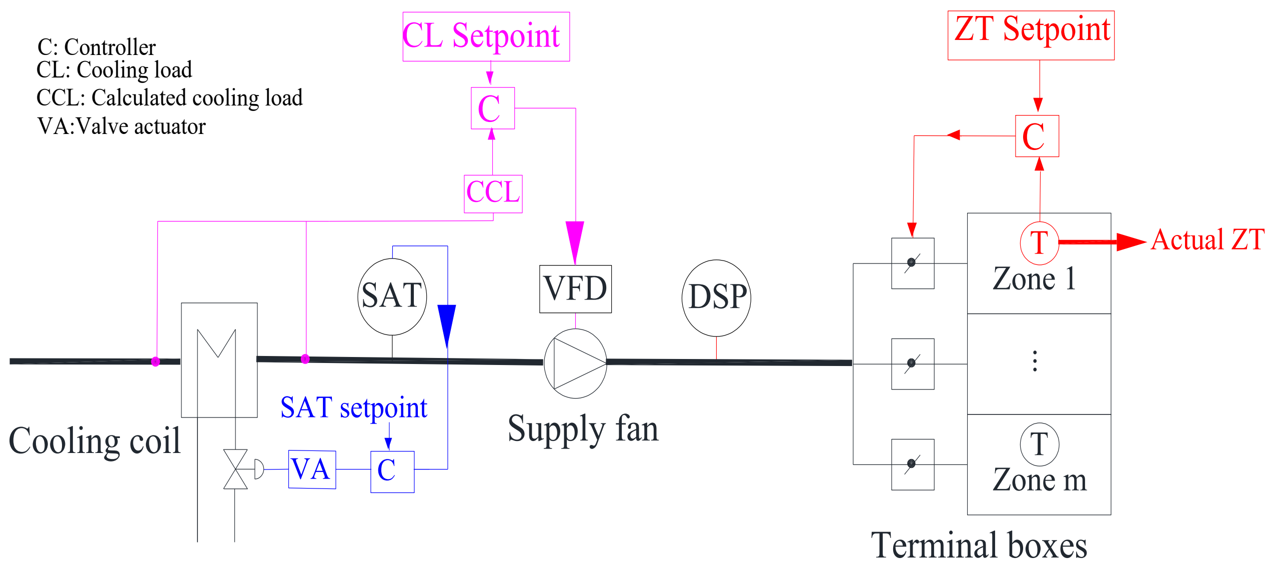

(b) EF control without DSP cascade control

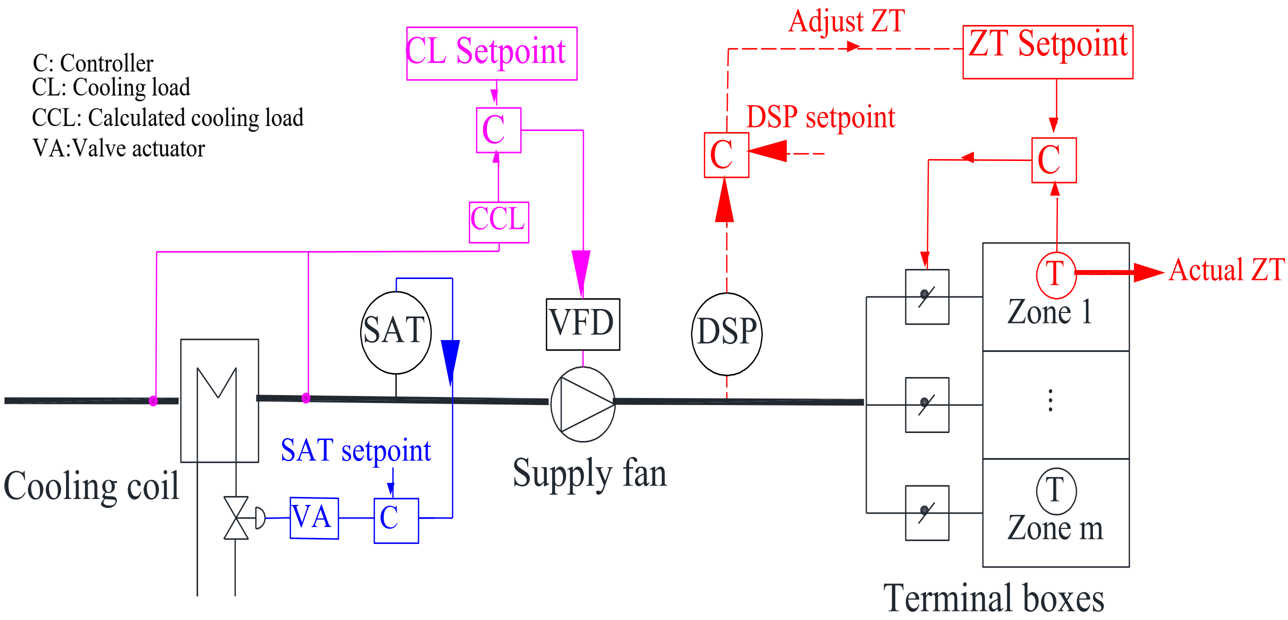

(c) EF control integrated with DSP cascade control

Figure 4.1: Demand control strategies

Figure 4.1c shows the EF control loop integrated with the DSP cascade control loop (marked in Red). The TB loop adopts the DSP cascade control to regulate the ZT. This DSP cascade control has two loops which are the outer and inner control loop. In the outer loop (dashed red line), a controller is utilized to maintain the DSP at a setpoint and create an adjustment factor to adjust the effective ZT setpoint for all the TBs evenly. In the inner loop (solid red line), the TB controllers then modulate the TB dampers position to maintain the adjusted ZT setpoint. This cascade controls allows all the zones to share the adjusted cooling load (CL) and minimize the thermal comfort problems of other demand control strategies. The DSP control shifts the responsibility of maintaining duct static pressure from the supply air fan, as is common in traditional AHU operation, to the TB temperature set points, which now are reset to regulate the duct static pressure instead.

The third control strategy, Total EF with DSP, also employs EF control but uses the total cooling load (TCL) as the control variable, combined with DSP cascade control. The purpose of this strategy is to achieve both fast and accurate demand control while evenly sharing the reduced cooling load across thermal zones. The cooling control in all the demand control strategies are the same as the cooling coil valve is modulated to maintain the SAT at its setpoint. Table 4.1 presents a summary of the state-of-the-art demand control and strategies utilizing EF and DSP cascade control technologies.

Table 4.1: State-of-the-art and proposed demand control strategies

Nomenclature		Baseline	Sensible EF without DSP	Sensible EF with DSP	Total EF with DSP
On- Peak hours	Control strategy	ZT feedback control using GTA	EF control without DSP cascade control	EF control and DSP cascade control	EF control and DSP cascade control
	EF control variable	N/A	Sensible cooling load	Sensible cooling load	Total cooling load
Off- Peak hours	Control strategy	ZT feedback control			
Purpose of control strategies		Slow demand control with sharing reduced load	Quick demand control without sharing load	Quick demand control Even sharing reduced cooling load	Quick and accurate demand control Even sharing reduced cooling load

4.2 Methodology

To evaluate the performance of the AHU demand control strategies, key variables such as cooling load and zone temperature (ZT), along with operating parameters including SAT, mixed air temperature, airflow rates, and enthalpy, are required to assess building demand control and thermal comfort. These variables are obtained using a calibrated virtual simulation test bed.

This section outlines the methodology employed to compare the demand control strategies using the EF and DSP cascade technologies with the state-of-the-art demand control. It describes the experimental test bed and the virtual simulation test bed used in this study. The virtual simulation test bed is calibrated using experimental tests conducted on the AHU system, and the calibration procedure is also presented. Additionally, the performance metrics used to evaluate the control strategies performance are presented.

4.3 Experimental and virtual simulation test beds

The experimental test bed utilized in this study is a fully instrumented single-duct VAV AHU system that serves seven thermal zones of an office building located on a university campus. The configuration of the system and its thermal zones are shown in Figure *3.4* and Figure 4.2. The AHU includes a chilled water-cooling coil with a design cooling capacity of 28 kW, a supply fan with a design flow rate of 1,200 L/s and a design head of 710 Pa. The supply fan, driven by a 2.2 kW motor, equipped with VFD. The supply fan speed was modulated to maintain the duct static pressure at its setpoint of 250 Pa.

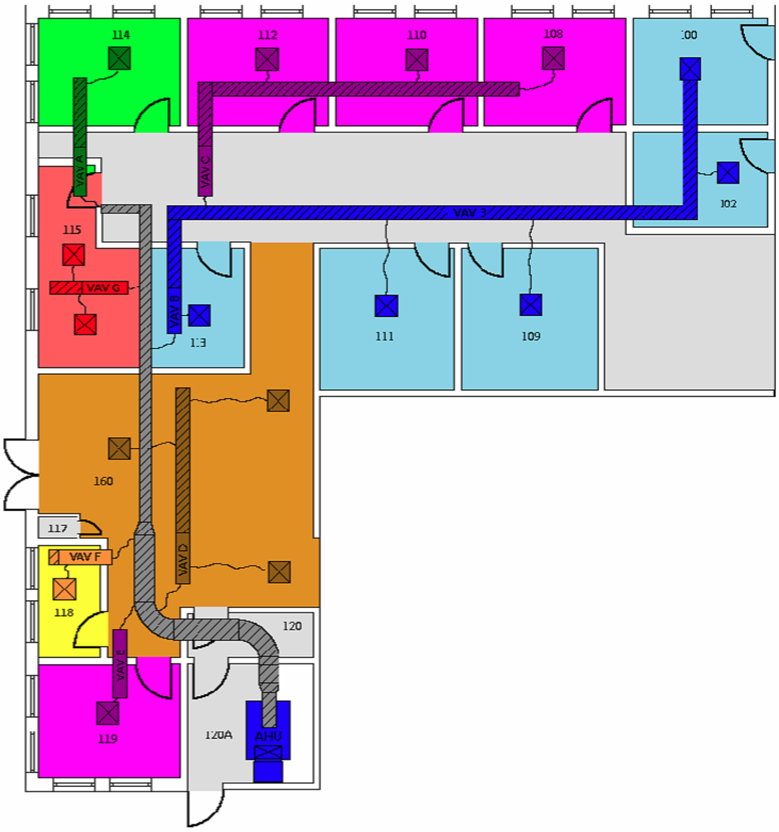

Figure 4.2: Seven thermal zones served by the VAV AHU

The virtual simulation test bed comprises of an HVAC system and building model that contains seven thermal zones. The HVAC system in this test bed is a VAV AHU system with heating and cooling coils. The test bed also includes VAV TBs with components such as reheat coils and air dampers in each of the seven-zone inlet branches. The AHU system's control sequence follows the traditional operational sequences (ASHRAE, 2006). The conventional AHU control has three feedback control loops related to space thermal comfort in addition to the return fan control for building pressurization and outdoor air control for the indoor air quality. These three controls form a control flow from terminal boxes to the cooling coil and are summarized as follows (Figure 4.3): (i) The terminal box (TB) dampers are modulated to maintain the ZT at its setpoints (ii) The supply fan speed is modulated through the variable frequency drive (VFD) to maintain the duct static pressure (DSP) at its setpoint (iii) The cooling coil valve is modulated to maintain the supply air temperature (SAT) at its setpoint. This conventional AHU system prioritizes indoor comfort by aligning its control actions with meeting the load, rather than meeting power demand.

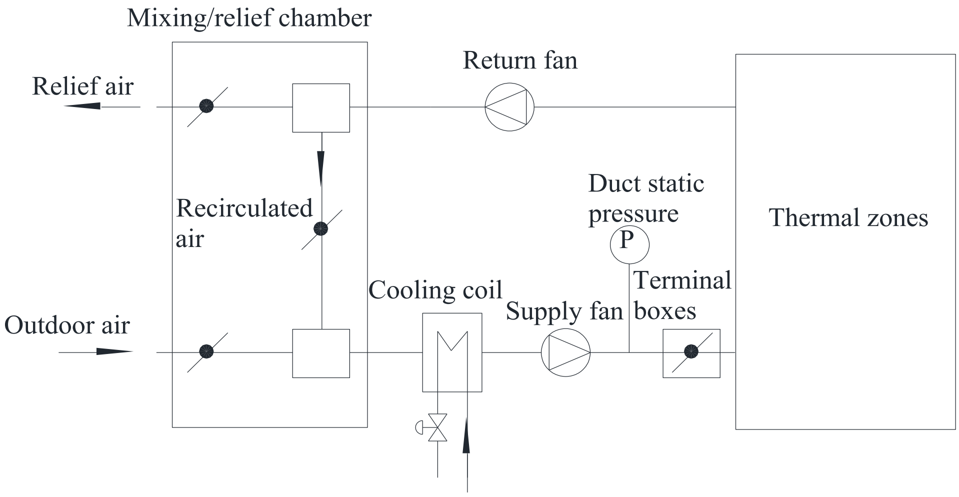

Figure 4.3: Schematic of an AHU

Spawn facilitates co-simulation between the HVAC system in Modelica and building energy simulation in EnergyPlus (Wetter et al., 2024). Spawn is DOE's next-generation simulation engine that leverages open standards for equation-based modeling (Modelica) and co-simulation (functional mock-up interface). Spawn is DOE's next-generation simulation engine that leverages open standards for equation-based modeling (Modelica) and co-simulation (functional mock-up interface). It combines software such as OpenStudio, Modelica Buildings Library, Optimica, QSS solvers, and PyFMI. EnergyPlus and Modelica are partitioned, with Figure 4.4 showing the variables interacting between them. Modelica simulates everything related to air and controls, while EnergyPlus simulates heat conduction in the building envelope model.

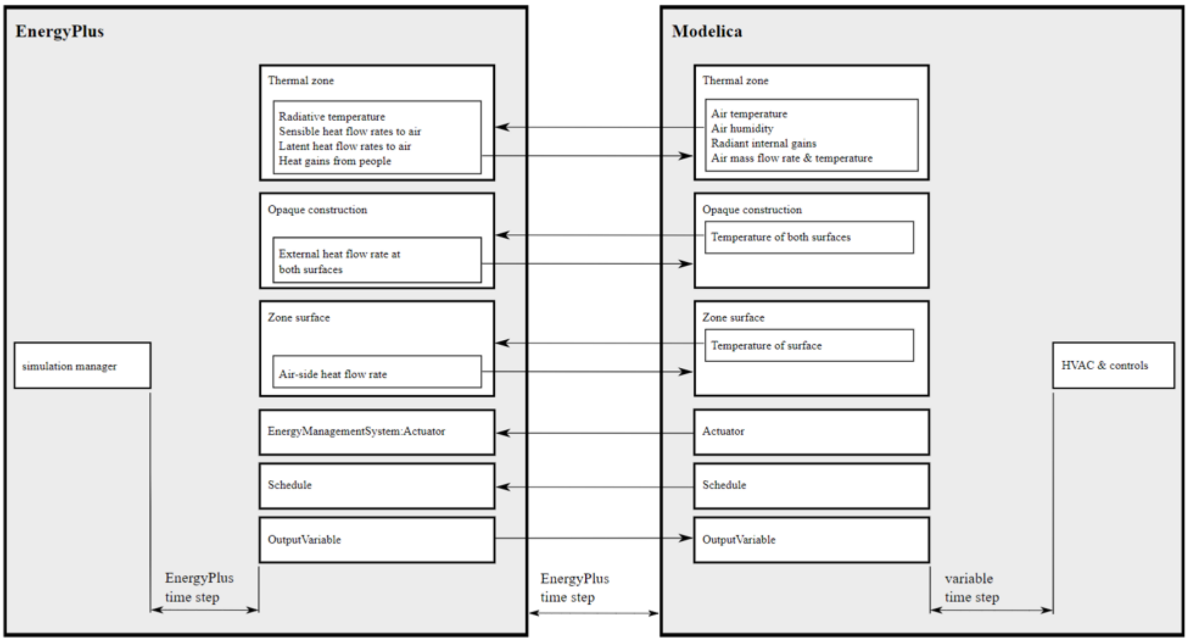

Figure 4.4: Partitioning of the EnergyPlus and Modelica domain

Two different software, namely OpenStudio (version 3.6.1) and EnergyPlus (9.6.0) were used in the development and simulation of the building envelope model for the virtual test bed. The building's floor plan was created in OpenStudio using FloorSpaceJS, an open-source software module used for building geometry creation. The building model was properly scaled and the fenestration areas and all the associated loads for each space types were included. The model utilizes four main types of boundaries: outdoor, adiabatic, ground, and surface. An outdoor boundary describes the surface exposed to the environment, while the ground boundary condition is applied to the floor. Also, the building materials and construction type of the walls and ceiling were then specified for each surface. The 3D model of this office building with seven conditioned zones (Zone A to Zone G) is served by a single-duct AHU is shown in Figure 4.5.

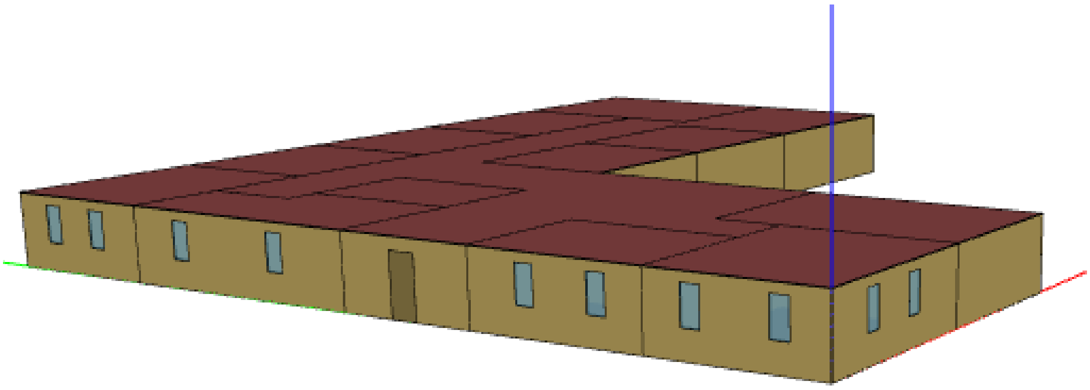

Figure 4.5: 3D model of the building envelope

Figure 4.6 shows the reference simulation test bed and Figure 4.7 with the top-level view of the AHU system and its control.

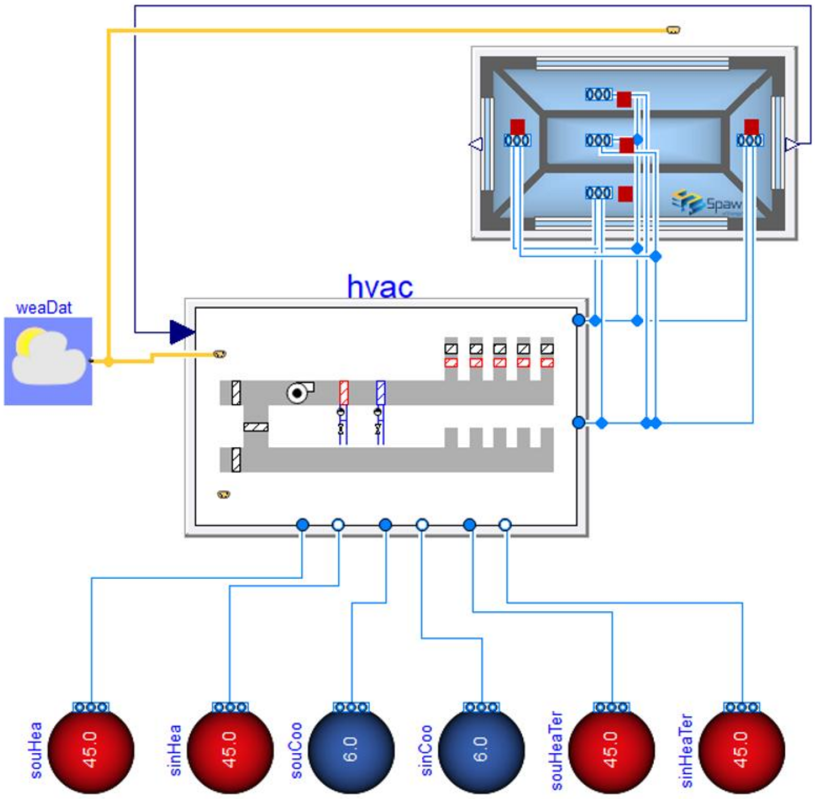

Figure 4.6: Reference simulation test bed

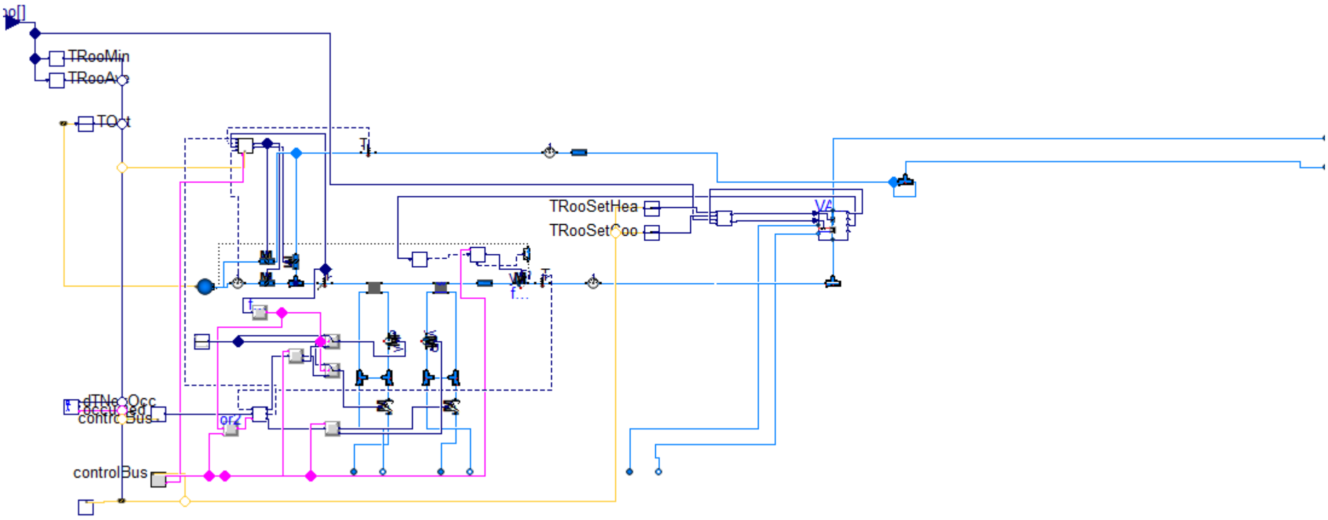

Figure 4.7: Top-level view the reference AHU system and its control

Several modifications were made to the reference virtual simulation test bed in Modelica Buildings Library (Wetter et al., 2018) to ensure that the virtual test bed is adequate for this study. In the reference virtual test bed, VAV boxes and their controllers were modelled using an index-based array structure, enabling uniform updates across all thermal zones while inherently prohibiting the simulation of pressure losses between upstream and downstream VAV boxes. Pressure losses between the VAV boxes are critical to studying various comfort losses among different VAV boxes when AHU is in demand response operation. Therefore, the present study decomposed the VAV boxes and their controllers into individual components, allowing for independent modification and tuning of specific boxes and enabling more precise zonal control and incorporating the corresponding pressure loss fittings between the decomposed VAV boxes. Figure 4.8 shows the top-level of the developed virtual test bed.

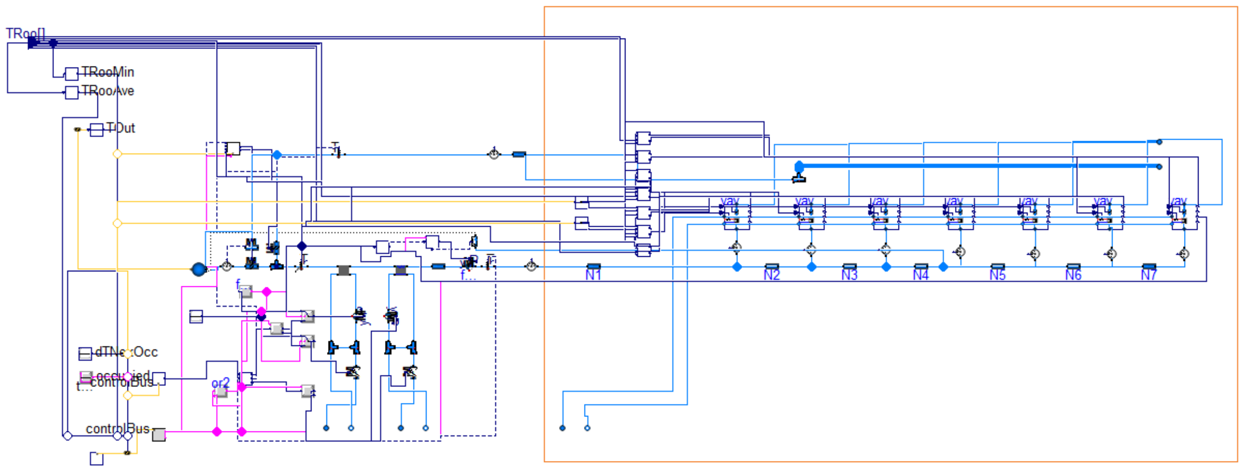

Figure 4.8: AHU system serving seven zone with decomposed VAV boxes And pressure loss fittings

Additionally, the reference test bed consists of a building layout with five thermal zones, which has been utilized in multiple studies without modification to the VAV box arrangement or the thermal zones (Lu et al., 2021, 2023). In this study, the floor layout was extended to seven thermal zones, each served by its own VAV box. These modifications ensure the virtual test bed meet the need for the study and its layout and system architecture form a robust design equivalent to the experimental setup, thereby creating a high-fidelity platform for subsequent simulation and control analysis.

4.4 Calibration of the virtual simulation test bed

The virtual simulation test bed was calibrated to represent the experimental test bed. This was achieved by comparing the operational performance of the AHU system and the dynamics of the building envelope. Experimental tests were carried out to compare the simulated parameters from the virtual test bed with the measured parameters from the experimental test bed.

The virtual test bed, which consists of the building energy model and the AHU system, was calibrated at the zone level based on three key metrics: the flow rate supplied to the seven thermal zones, the total supply flow rate from the AHU, and the cooling load. An overview of the calibration process of the virtual test bed used in this study is provided in Figure 4.9. The building's physical information, weather data, and the Energy Plus input files were incorporated into the simulation test bed for co-simulation with the HVAC system in Modelica. The next step involved specifying the operational parameters of the AHU system in the model, followed by defining the design parameters for the VAV terminal boxes (TBs) in all zones. The occupancy schedules and internal heat gains for the seven thermal zones were modeled as heterogeneous, i.e., each thermal zone had different daily schedule. These individual zone schedules and internal heat gains were then adjusted during calibration to ensure the simulated cooling load, required VAV flow rate and zone temperatures accurately matched the experimental data for each thermal zone.

The step-by-step calibration process, as illustrated in Figure 4.9, begins with specifying the operational parameters of the AHU components. An experimental test is then conducted to compare the simulated operation data from the virtual test bed with the measured data from the experimental test bed. A decision point follows, where the virtual test bed dynamics are evaluated against the experimental test bed. If there is a significant difference in performance data, calibration parameters are updated, and the process is repeated until the virtual test bed accurately represents the experimental test bed. The comparison indices for the calibration between the simulated and measured parameters were the supply flow rate, which represents the HVAC air-side system and controls; the sensible cooling load, which represents the building physics and internal loads; and the average zone temperature, which represents the thermostat settings and thermal comfort within the zones. Calibrating these parameters was essential to provide a holistic and accurate indication of the virtual test bed's overall performance.

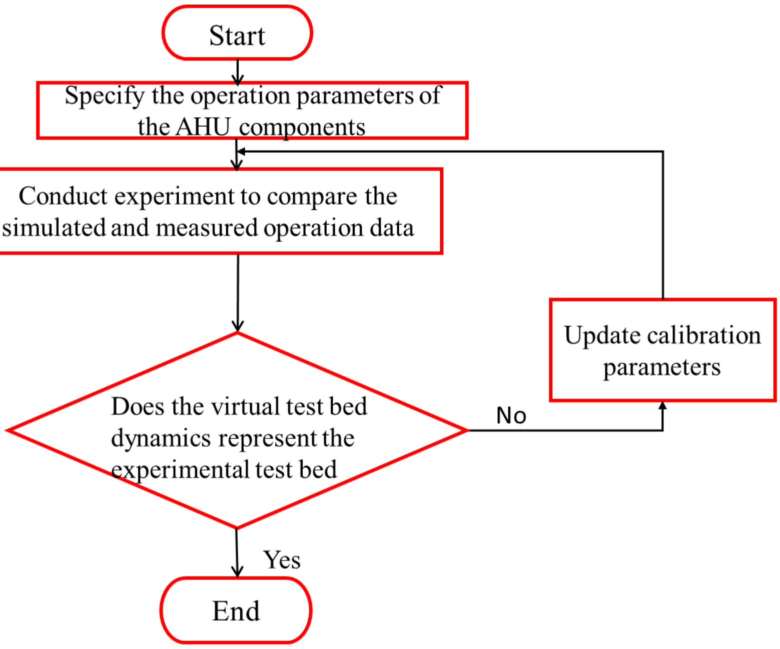

Figure 4.9: Calibration workflow of the virtual test bed

The calibration experimental test was conducted on the 1st of July, 2025. On this Summer Day, the settings of the virtual test bed were adjusted to match those of the experimental setup. These settings include;

- ZT setpoint for all the thermal zones was set to 22°C.
- The weather information of this day was utilized for the virtual test bed.
- The SAT setpoint was 12.8°C.

Figure 4.10a shows the comparison of the simulated and measured supply fan flow rate, on the test date. The simulated and measured sensible cooling loads for this test day were compared. The sensible cooling load was determined using a heat-balanced equation, which is a function of the difference between the average ZT and the SAT. Figure 4.10b and c shows the average ZT and the cooling load respectively. The simulated average ZT of the thermal zones matches well with the measured average ZT as the difference in temperature is small. Additionally, the simulated cooling load dynamics correspond well with the measured cooling load dynamics.

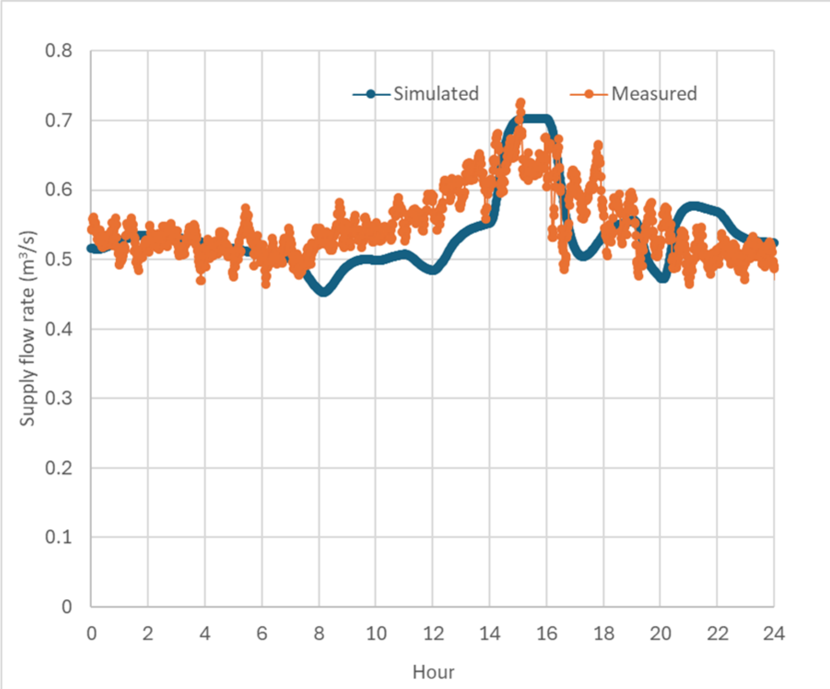

(a) Supply flow rate

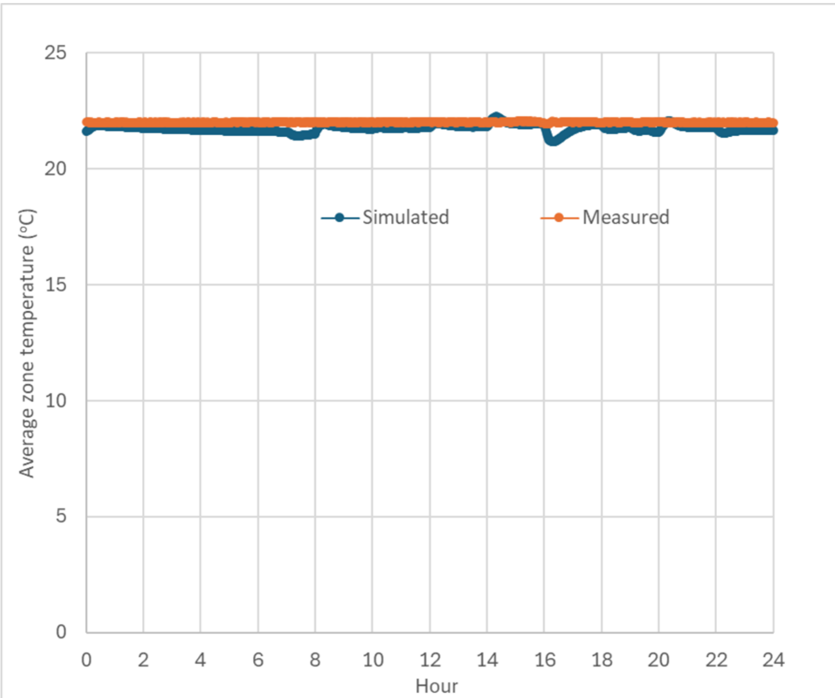

(b) Average ZT

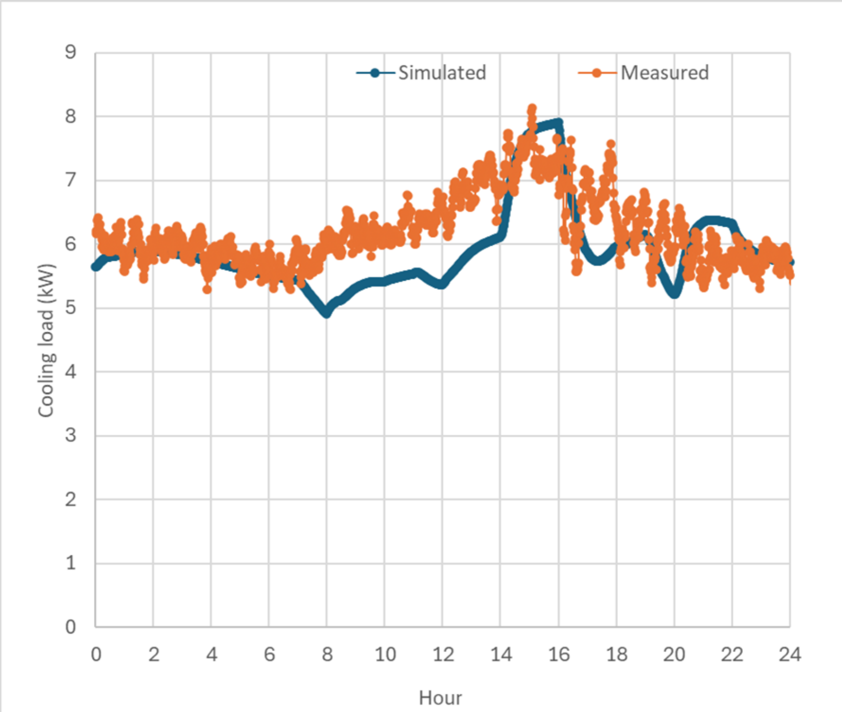

(c) Cooling load

Figure 4.10: Comparison of simulated and measured supply fan flow rate, average ZT, and cooling load for a summer day

The calibration quality of the virtual test bed was evaluated using the statistical indices recommended by ASHRAE Guideline 14 (ASHRAE, 2014), which are the Normalized Mean Bias Error (NMBE) and Coefficient of Variation of the Root-Mean-Square Error (CV(RMSE)). The NMBE measures the overall bias between the simulated and measured parameter values and is mathematically expressed as:

$$\text{NMBE (\%)} = \frac{\sum_{i=1}^{n}\left(y_{measured,i} - \hat{y}_{simulated,i}\right)}{n \times \bar{y}_{measured,i}} \times 100$$

Where $y_{measured,i}$ is the measured value, $\hat{y}_{simulated,i}$ is the simulated value, $\bar{y}_i$ is the mean of measured values, and n is the total number of data points.

The CV(RMSE) measures the magnitude of randomness and variability between the simulated and measured values and is mathematically expressed as:

$$\text{CV(RMSE)}\ (\%) = \frac{\sqrt{\frac{\sum_{i=1}^{n}(y_{measured,i}-\hat{y}_{simulated,i})^2}{n}}}{\bar{y}_{measured,i}} \times 100$$

Table 4.2 shows a summary of the calibration metrics for the difference between the simulated and measured parameters. The NMBE values for the cooling load and supply flow rate are 5.1% and 6.1% respectively. These results are well within the 10% limit considered acceptable in ASHRAE Guideline 14 for hourly values. However, the simulated and measured data were collected at a one-minute interval over a period of one day. The hourly benchmark was utilized for comparison since the ASHRAE Guideline 14 does not specify limits for one-minute intervals. The CV(RMSE) values for the cooling load and supply flow rate are 10.4% and 10.7%, respectively, which are comfortably below the 30% limit for hourly values. The NMBE and CV(RMSE) for the average zone temperature are 1.2 % and 1.4%, respectively.

Table 4.2: Summary of Calibration Metrics

	NMBE (%)	CV(RMSE) (%)
Cooling load (kW)	5.1	10.4
Supply flow rate (m^3/s)	6.1	10.7
Average zone temperature (ºC)	1.2	1.4

The simulated parameters match well with the measured parameters across all the indices. The virtual test bed satisfies the NMBE and CV(RMSE) thresholds specified by ASHRAE Guideline 14 for hourly data, even when validated against the higher-resolution, one-minute interval dataset. This outcome confirms the accurate calibration of the virtual test bed for subsequent control studies. It also demonstrates that the operational performance of the AHU system and the building envelope dynamics agree well with the experimental test bed.

4.5 Performance metrics for evaluating control performance

Different performance metrics are utilized to evaluate the demand control strategies, using key variables such as cooling load and ZT. These metrics assess both demand control performance (e.g., control response and accuracy) and thermal comfort performance (e.g., temperature stability and occupant comfort). More details on how the indices are applied to these variables are presented below:

4.5.1 Settling time for evaluating the response time of the EF control

The EF control is to modulate the supply air fan speed in response to the cooling load setpoint. Settling time in this study is the time required in dynamic response analysis (O'Neill et al., 2017) for the cooling load to stabilize and remain within a defined tolerance band. The tolerance band used is 2% of the stable cooling load value for the demand control strategies. This metric is used to evaluate the control response time of the HVAC system during a demand control event. A short settling time indicates a fast control response time, while a long settling time signifies a slow response time.

4.5.2 Mean absolute and relative errors for evaluating the accuracy of the EF control

The Mean Absolute Error (MAE) represents the average absolute deviation of the TCL from the setpoint. It is mathematically expressed as:

$$MAE = \frac{\sum_{i=1}^{n}\left|TCL_i - TCL_{sp}\right|}{n}$$

where TCL_i is the TCL at time i, and TCL_{stp} is the TCL setpoint. This metric evaluates the accuracy of demand control strategies in maintaining the TCL setpoint. A low MAE indicates better performance, while a higher MAE signifies greater deviations from the setpoint.

Relative error (RE) is a measure of accuracy for the demand control strategies. It indicates the magnitude of error relative to the cooling load setpoint. The percentage RE is mathematically expressed as:

$$RE\ (\%) = \frac{MAE}{TCL_{stp}} \times 100$$

4.5.3 Range of Mean ZT for evaluating evenly cooling load sharing

The range of mean ZTs (RZT) is used to evaluate the thermal comfort performance of the control strategies and to assess whether the thermal zones evenly share the reduced cooling load during the demand control. The RZT for each control strategy is mathematically expressed as:

$$RZT = \overline{ZT}_{farthest} - \overline{ZT}_{closest}$$

where $\overline{ZT}$ is the average ZT over the evaluation period, and the subscripts farthest and closest refer to the thermal zones farthest from and closest to the main supply duct, respectively.

4.6 Simulation of demand control strategies with the virtual test bed

The four demand control strategies and the conventional AHU control strategy were simulated using the calibrated virtual test bed. This section presents the simulation results of these strategies and their implementation on the test bed. The demand control event (peak period) considered in this study spans from 2 PM to 9 PM. A summer day was selected for the simulations due to the typically high electricity demand during this period. This allows for a robust assessment of the demand control performance using the virtual test bed. The simulation time step is 1 min, and the convergence tolerance is 1×10^{-7} to ensure simulation accuracy.

The conventional strategy utilizes ZT feedback control without any modifications to the conventional control loops. This control loop serves as the reference for demand control strategies because it prioritizes indoor thermal comfort. Throughout the simulation period, the ZT cooling setpoint (TZoneSet) is fixed at 21.5ºC. In this study, this conventional strategy forms the foundation for evaluating the performance of the demand control strategies. Figure 7 shows the ZTs, supply fan flow rate and speed, TB damper positions, and DSP over a one-day simulation period for the conventional strategy. As shown in Figure 4.11a, the zone temperatures (ZTs) for Zones A through G are maintained at the setpoint of 21.5ºC, with minor transient deviations (a maximum rise of 0.30ºC and a maximum dip of 0.36ºC). In Figure 4.11b, the supply fan speed and airflow rate remain low during the early unoccupied hours but subsequently increase during non-peak and peak occupied periods to meet the increased thermal demand. Figure 4.11c illustrates that the terminal box dampers for all thermal zones are partially open (with positions ranging from approximately 0.36 to 0.65), enabling modulated airflow in response to instantaneous zone loads. In Figure 4.11d, the DSP is maintained precisely at its setpoint of 250 Pa throughout the day.

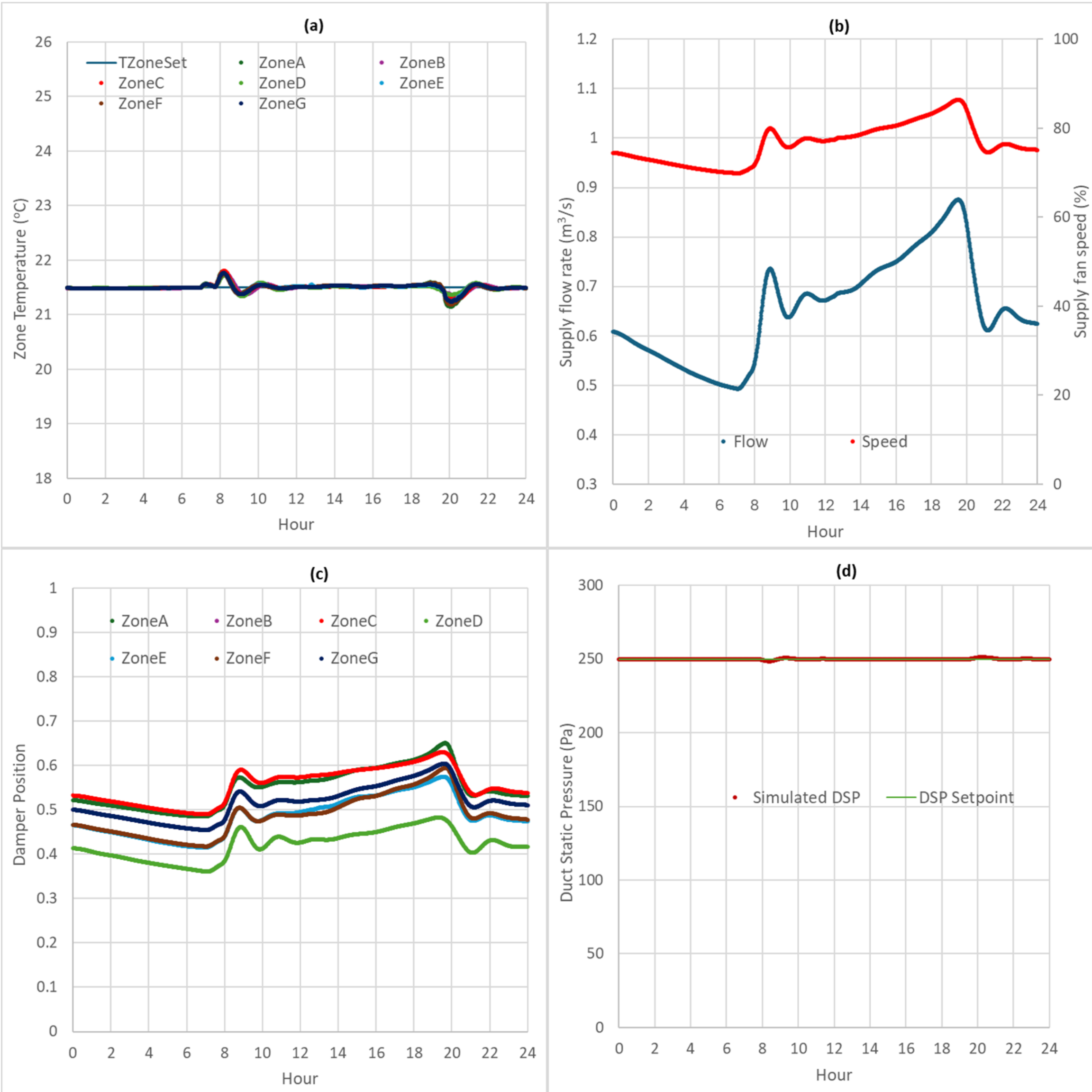

Figure 4.11: ZTs, supply fan airflow rate, and speed, damper position and duct static pressure for the conventional strategy

4.6.1 Baseline

This strategy involves GTA control during peak hours. TZoneSet remains fixed at 21.5°C during unoccupied and occupied non-peak hours, but during peak hours, it is automatically adjusted to 22.8°C using a pulse signal. No changes were made to the AHU's conventional control loop. Figure 4.12 shows the ZTs, supply fan flow rate and speed, terminal box damper positions and DSP for the baseline scenario.

At 2 pm (14 hours), TZoneSet increases from 21.5°C to 22.8°C (Figure 4.12a). This change reduces the required cooling load, resulting in a corresponding decrease in the supply fan speed and airflow rate (Figure 4.12b). The TB dampers also reduce their positions during setpoint adjustment to match the lower instantaneous zone loads (Figure 4.12c). For this scenario, the DSPis maintained at its setpoint of 250 Pa throughout the day. Only minor transient deviations are observed, coinciding with the TZoneSet transitions at t = 14 hours and t = 21 hours.

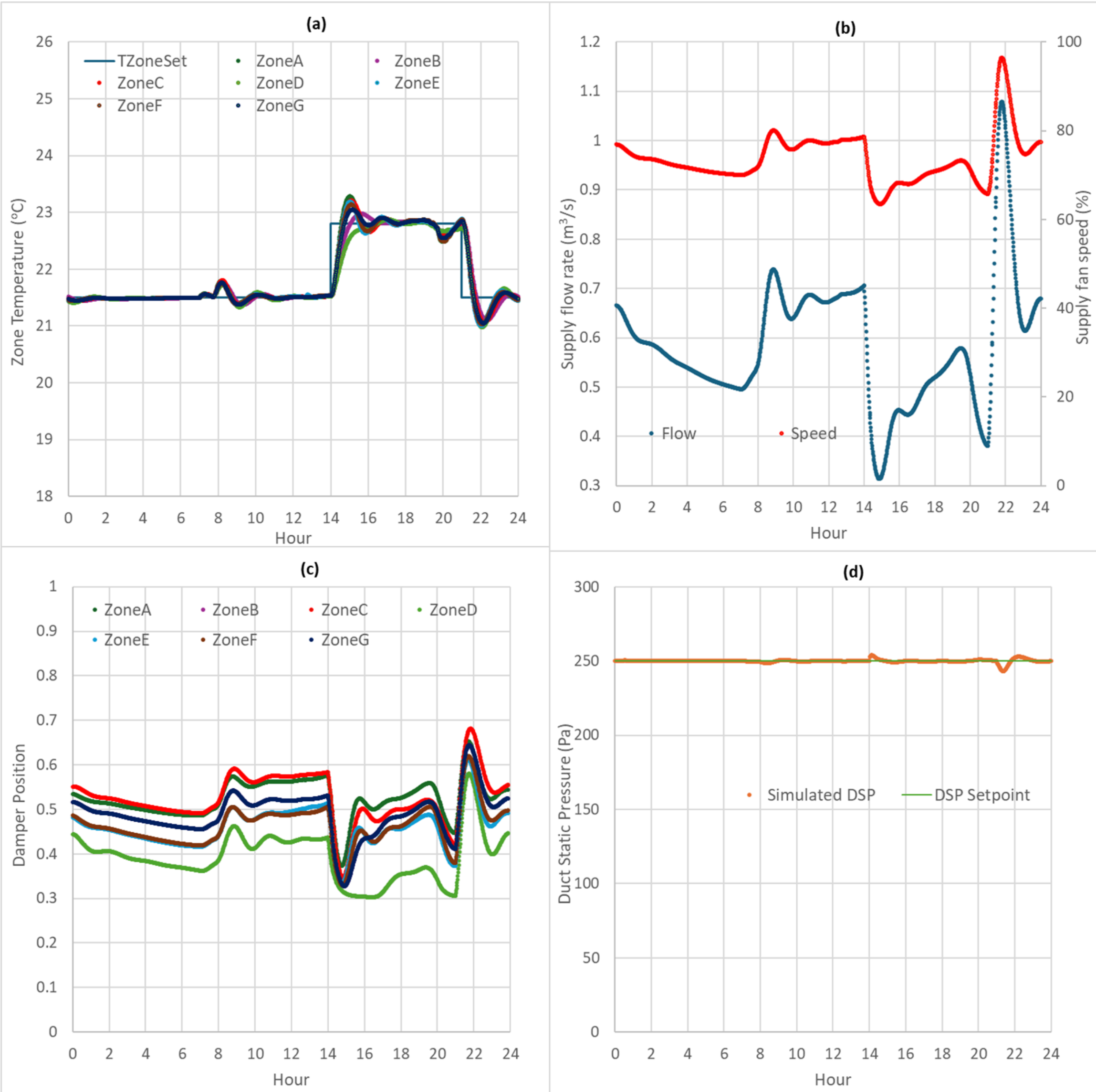

Figure 4.12: ZTs, supply fan airflow rate, and speed, damper position and duct static pressure for the baseline strategy

4.6.2 Sensible EF without DSP

This strategy involves two reconfigurations of the conventional control loops. Firstly, the supply fan speed is modulated to maintain the sensible cooling load (SCL) at a setpoint during peak hours. Secondly, the DSP cascade controller is not utilized. The SCL is mathematically expressed as;

$$Q_{SCL} = \dot{m}_{ma} Cp_{air}(T_{ma} - T_{sa})$$

Where Q_{SCL} is the cooling coil sensible load, $\dot{m}_{ma}$ is the mass flow rate of the mixed moist air, Cp_{air} is the specific heat capacity of moist air, T_{ma} is the mixed air temperature, and T_{sa} is the supply air temperature. The SCL setpoint during the peak period is 8.96 kW and this value is set based on the shed load intended for the simulation day. During the non-peak hours, the ZT feedback control loop is utilized during non-peak hours. Figure 4.13 shows the EF controller operation for this scenario. During peak hours, the supply fan speed is modulated to maintain the SCL at the setpoint of 8.96 kW.

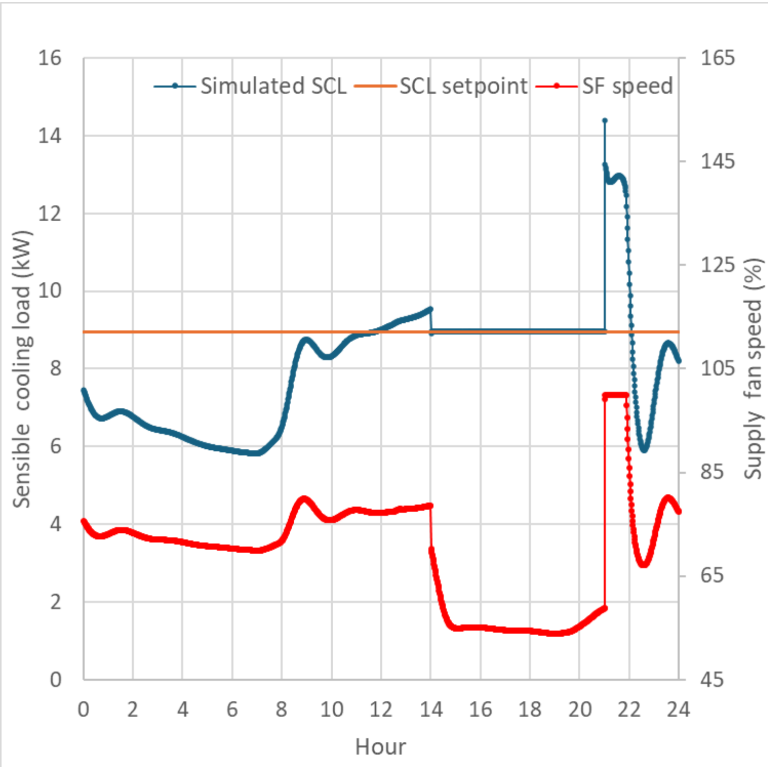

Figure 4.13: EF controller operation for Sensible EF without DSP

Figure 4.14 shows the ZTs, supply fan airflow rate and speed, TB damper positions, and DSP for Sensible EF without DSP. TZoneSet remained fixed at 21.5°C, as no setpoint adjustment was applied during the peak period. During the non-peak hours, the DSP was effectively maintained at its setpoint. In contrast, during the peak hours, the DSP was not maintained because the DSP cascade controller was not utilized. This resulted in an abrupt decrease in DSP, reaching a minimum of 30 Pa (Figure 4.14d).

The TB dampers for all zones are fully open during peak hours (Figure 4.14c), as the TB controllers attempt to compensate for the lack of duct pressure. As shown in Figure 10a, the ZTs are not maintained at the TZoneSet. Zone D, which has the TB closest to the main supply duct, has the lowest ZT while Zones A and C, which have TBs farthest from the supply duct, experience the highest ZTs among the thermal zones. These ZT profiles indicate a clear imbalance in the distribution of the reduced cooling load among the thermal zones.

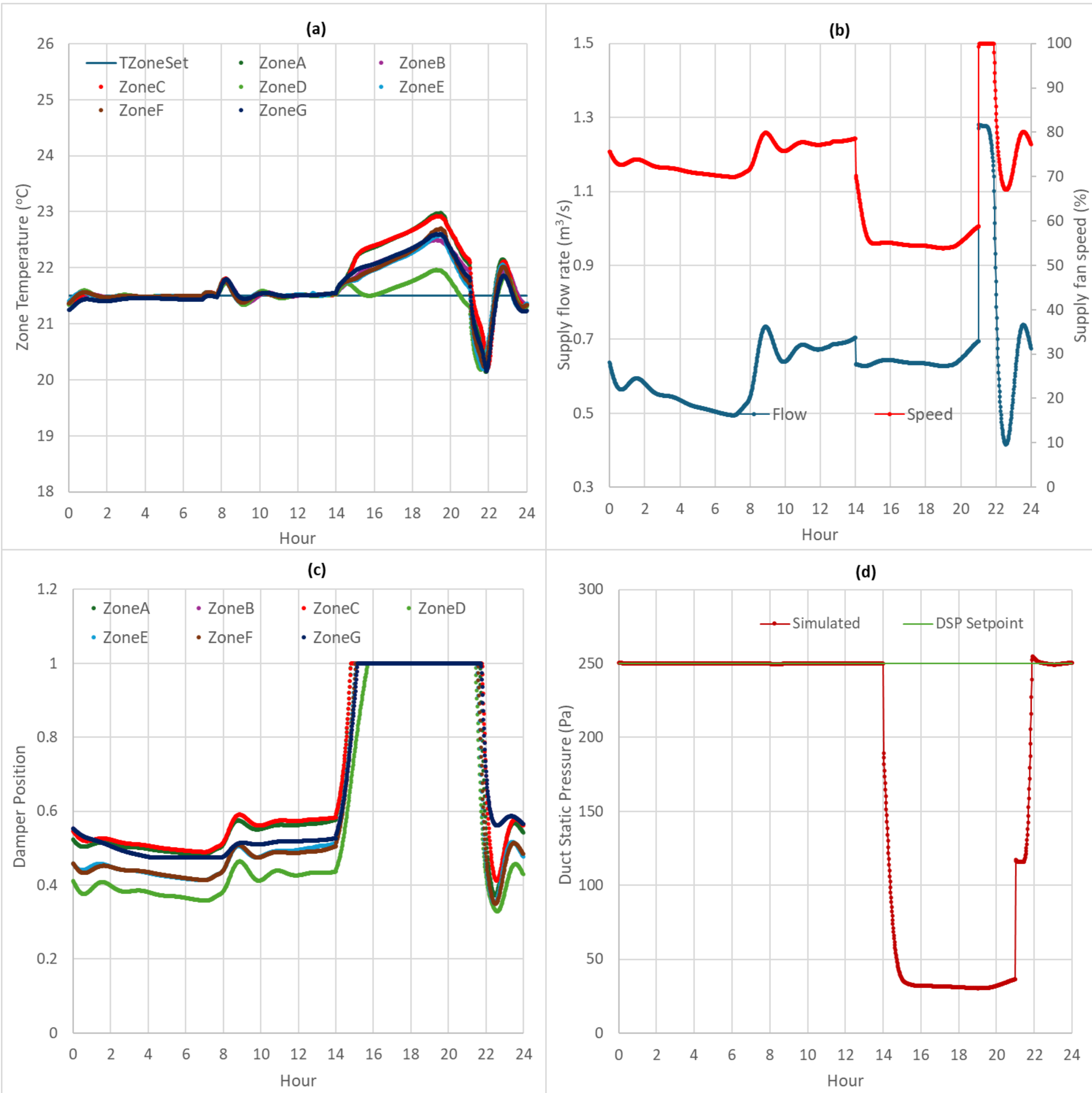

Figure 4.14: ZTs, supply fan airflow rate, and speed, TB damper positions and duct static pressure for Sensible EF without DSP

4.6.3 Sensible EF with DSP

This strategy utilizes a combination of energy feedback control, DSP cascade control, and ZT feedback control loops. The ZT feedback control loop is active during non-peak hours. During this period, the supply fan speed is modulated to maintain the DSP at its setpoint (250 Pa), while TZoneSet is fixed at 21.5°C. During peak hours, the supply fan speed is modulated to maintain the SCL at a setpoint of 8.96 kW, and a DSP cascade controller is utilized to maintain the DSP setpoint and readjust TZoneSet. Figure 4.15 illustrates the EF controller operation, showing the modulation of the supply fan speed to maintain the SCL at its setpoint during the peak hour.

Figure 4.16 shows the ZTs, supply fan airflow rate and speed, TB damper positions, and DSP for Sensible EF with DSP. A reduction in the supply fan speed and airflow rate occurs during the peak hours (Figure 4.16b), followed by a corresponding reduction in TB damper positions (Figure 4.16c). The ZTs are maintained at the adjusted TZoneSet (Figure 4.16a), and the DSP is maintained at the setpoint of 250 Pa during peak hours, demonstrating the effectiveness of the DSP cascade controller. A noticeable overshoot of DSP and TZoneSet occurs at the transition time (t = 14 hours). This initial transient instability resulted from switching from the non-peak control strategy to the peak-hour control strategy. Following this transient response, the combined control strategy successfully maintains the ZTs at the adjusted TZoneSet, maintains DSP at its setpoint, and simultaneously adheres to the system SCL limit.

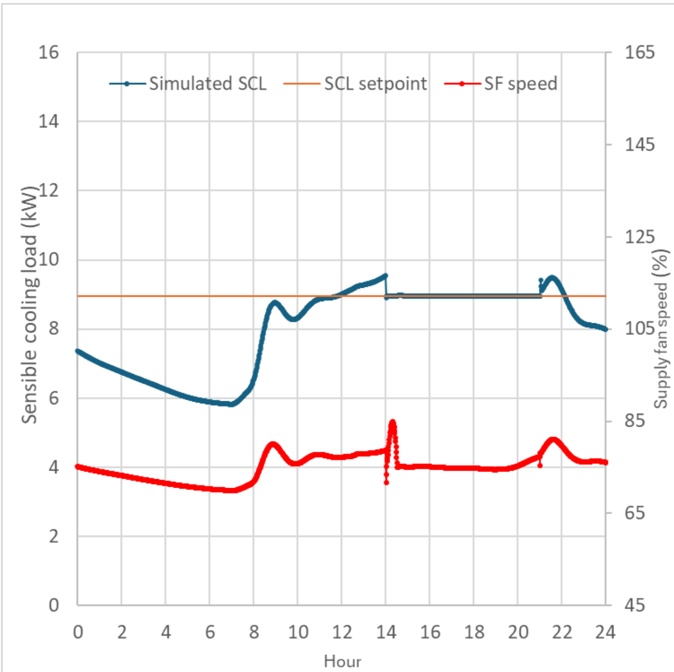

Figure 4.15: EF controller operation for Sensible EF with DSP

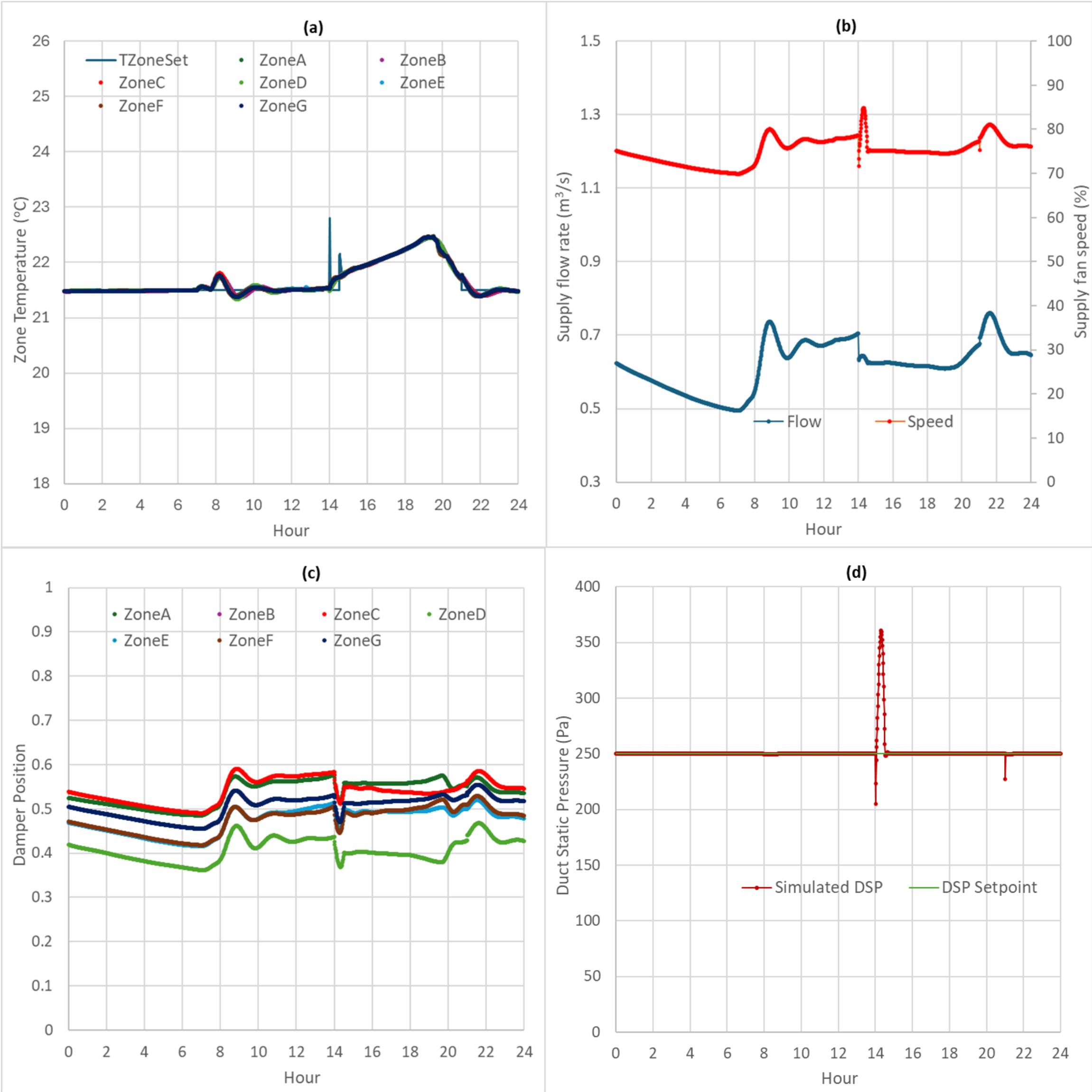

Figure 4.16: ZTs, supply fan airflow rate, and speed, TB damper positions and duct static pressure for Sensible EF with DSP

4.6.4 Total EF with DSP

This strategy utilizes the same hybrid combination of energy feedback controllers and ZT feedback controllers. However, the difference is that the supply fan speed is modulated using TCL. TCL is mathematically expressed as

$$Q_{TCL} = \dot{m}_{ma}(H_{ma} - H_{sa})$$

Where Q_{TCL} is the cooling coil total load, $\dot{m}_{ma}$ is the mass flow rate of the mixed moist air, H_{ma} is the specific enthalpy of mixed air, and H_{sa} is the specific enthalpy of supplied air. The TCL setpoint utilized to reset the supply fan speed is 11.9 kW. Figure 4.17 shows the EF controller operation, with the supply fan speed being modulated to maintain the TCL at its setpoint during the peak hour.

Figure 4.18 shows the ZTs, supply fan flow rate and speed, TB damper positions, and DSP for Total EF with DSP. During the peak hours, the DSP is maintained at its setpoint (Figure 4.18d), the supply fan speed and flow rate (Figure 4.18b) reduce to maintain the TCL setpoint, the ZTs are maintained at the adjusted TZoneSet (Figure 4.18a), and the TB damper position of all thermal zones (Figure 4.18c) reduces accordingly.

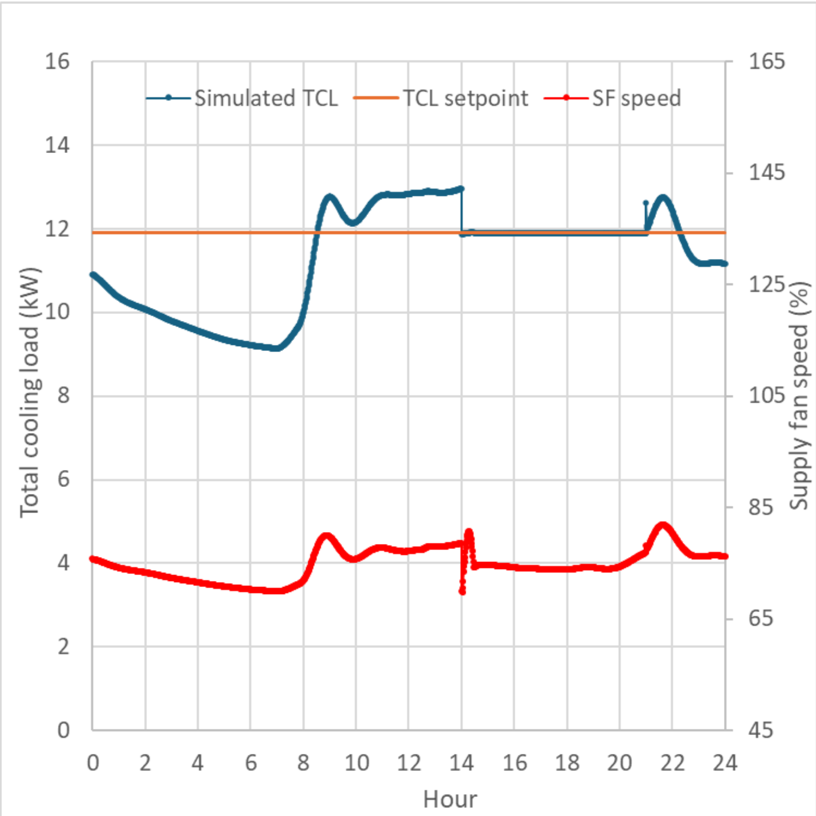

Figure 4.17: EF controller operation for Total EF with DSP

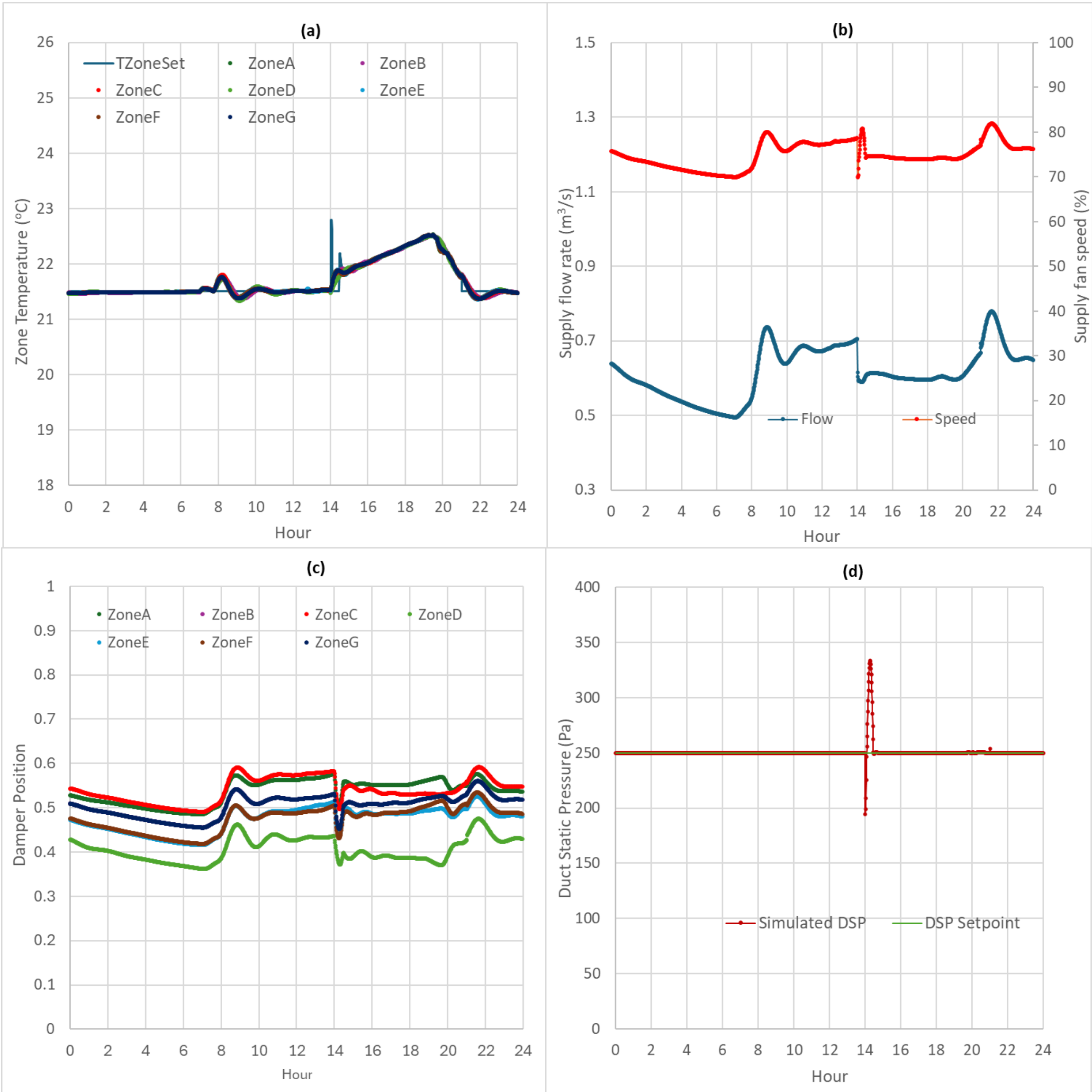

Figure 4.18: ZTs, supply fan airflow rate, and speed, TB damper positions and duct static pressure for Total EF with DSP

4.7 Comparative Analysis and Discussion

In this section, the strategies are evaluated based on the building demand control and thermal comfort.

4.7.1 Building demand control

For these strategies, the TCL is utilized as the primary comparison index for the building demand control, as it allows for the determination of the energy use for each strategy.

Figure 4.19 shows the TCL profile for the different demand control strategies evaluated in this study. The figure indicates that normal operation was maintained during the non-peak hours, as the TCL remained consistent before the peak hours (demand control event). However, due to the dynamic nature of the HVAC system and building envelope, the TCL profile for the strategies wasn't perfectly maintained after the demand control event. Specifically, a spike was observed for the baseline strategy and Sensible EF without DSP. This spike in cooling load, known as a demand rebound, occurs when the HVAC system returns to normal operation after the end of the demand control event (Sehar et al., 2016).

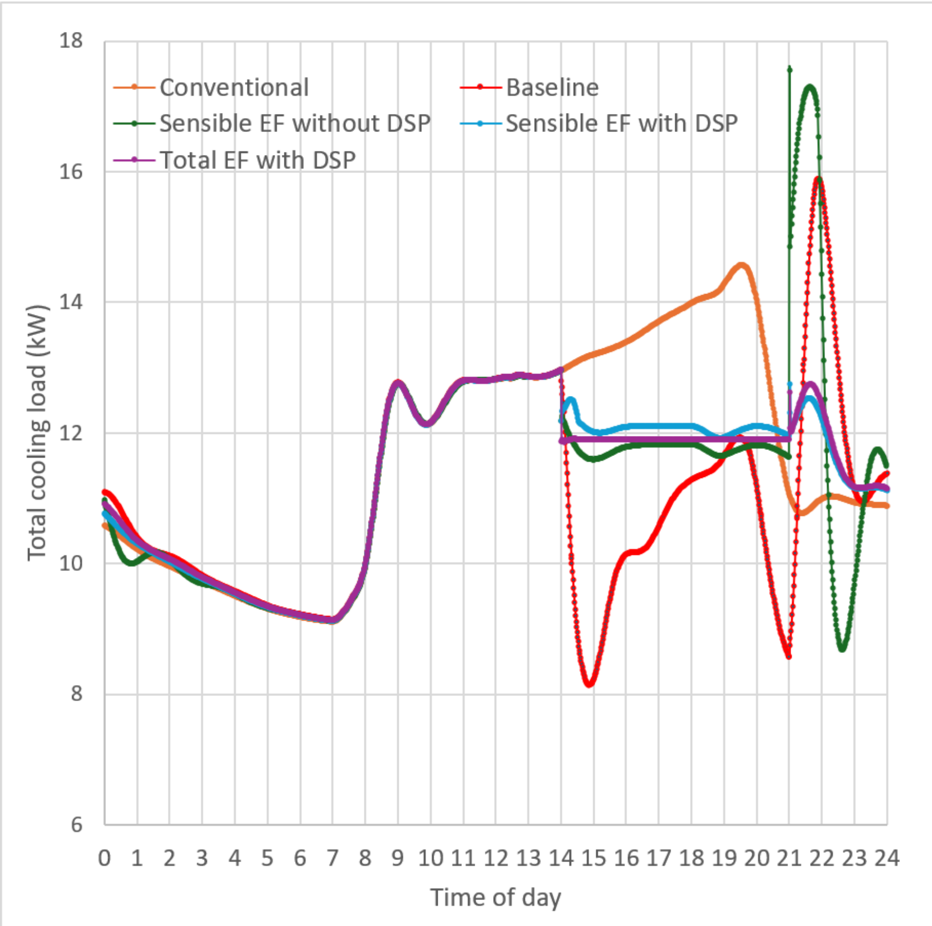

Figure 4.19: Total cooling load profile of the evaluated strategies

Generally, the evaluated demand control strategies resulted in varying magnitudes of cooling load shed when compared to the baseline. For the baseline strategy, which utilizes the GTA of the ZT setpoint during the peak period, there was not accurate cooling load shedding.

In contrast, strategies that utilize the EF controller during the demand control event achieved precise load shedding based on the setpoint utilized for the specific strategy. The TCL setpoint in Total EF with DSP was precisely maintained throughout the demand control event. The implementation of the Total EF with DSP strategy demonstrates that accurate energy use control can be achieved by utilizing the EF controller with the TCL as the control variable.

The settling time for each strategy was determined to evaluate how quickly the cooling load stabilizes and remains within a defined tolerance band during the peak period. Table *4.3* presents the cooling load settling times and stable cooling load values for each strategy. The tolerance band used for this analysis is 2% of the stable cooling load value of the evaluated strategies during the peak hour. The total EF with DSP has the shortest settling time, taking only 0.03 hours to reach a stable value of 11.9 kW, which matches the TCL setpoint. All the strategies utilizing the EF controller have a shorter settling time compared to the baseline.

Sensible EF without DSP has a settling time of 0.18 hours and a stable cooling load value of 11.82 kW, while Sensible EF with DSP has a settling time of 0.03 hours and a stable load value of 12.16 kW. Although these strategies share the same SCL setpoint, they reached different stable cooling load values and profiles. This is because Sensible EF without DSP, which did not incorporate the DSP cascade control, resulted in higher airflow than Sensible EF with DSP, thereby leading to a difference in the sensible heat ratio and TCL. The baseline has a settling time of 5.05 hours, which is the longest among the evaluated strategies. This long settling time indicates a slow response of the HVAC system to the ZT reset. These results demonstrate that the EF controller strategies provide comparatively faster and more accurate HVAC demand control, with Total EF with DSP and Sensible EF with DSP achieving the fastest response.

The mean absolute error (MAE) and relative error (RE) of the strategies were evaluated to assess how effectively they met the reference TCL setpoint. Table 4.3 shows the error metrics for the demand control strategies. The baseline strategy resulted in an RE of 12.52% and an MAE of 1.49 kW, while Sensible EF without DSP had an RE of 1.26% and an MAE of 0.15 kW. Sensible EF with DSP yielded an RE of 1.60% and an MAE of 0.19 kW. The significant RE and MAE in the baseline strategy indicate inaccurate load control, as the precise load setpoint was not achieved. In contrast, the EF control strategies exhibited smaller REs than baseline, highlighting improved demand control performance. Total EF with DSP, which has the shortest settling time, also achieved the lowest RE of 0.01% and an MAE of 0.001 kW. Among all strategies, Total EF with DSP exhibits the best demand control performance, achieving the lowest RE, lowest MAE, and fastest stabilization.

Table 4.3: Performance metrics of the evaluated demand control strategies

Strategy	Stable cooling load value (kW)	Mean cooling load (kW)	Settling time (hrs)	Mean absolute error (kW)	Relative error (%)	RZT (°C)
Baseline	11.92	10.43	5.05	1.49	12.52	0.05
Sensible EF without DSP	11.82	11.77	0.18	0.15	1.26	0.78
Sensible EF with DSP	12.16	12.09	0.03	0.19	1.60	0.00027
Total EF with DSP	11.90	11.90	0.03	0.001	0.01	0.00448

4.7.2 Thermal comfort

The range of ZTs (RZT) was evaluated to assess the thermal comfort performance of the demand control strategies during the peak period and to quantify how evenly the cooling load was shared among the thermal zones. A minimal or negligible RZT across the seven thermal zones indicates an even distribution of the reduced cooling load. Conversely, a high

RZT denotes uneven load sharing and significant temperature variability across the thermal zones.

Figure 4.20 and Table 4.3 show the RZT values for the demand control strategies. The baseline strategy has a minimal RZT of 0.05°C, while Sensible EF without DSP has the highest RZT of 0.78°C. Sensible EF with DSP and Total EF with DSP have negligible RZT values of 0.00027°C and 0.00448°C, respectively, indicating that the reduced cooling load burden is shared evenly across all the thermal zones. In contrast, Sensible EF without DSP results in a significantly higher RZT value than the baseline and the other EF control strategies, reflecting an uneven sharing of the reduced cooling load among the thermal zones. These results validate the importance of incorporating DSP cascade control alongside EF control to achieve equitable load sharing during demand control events.

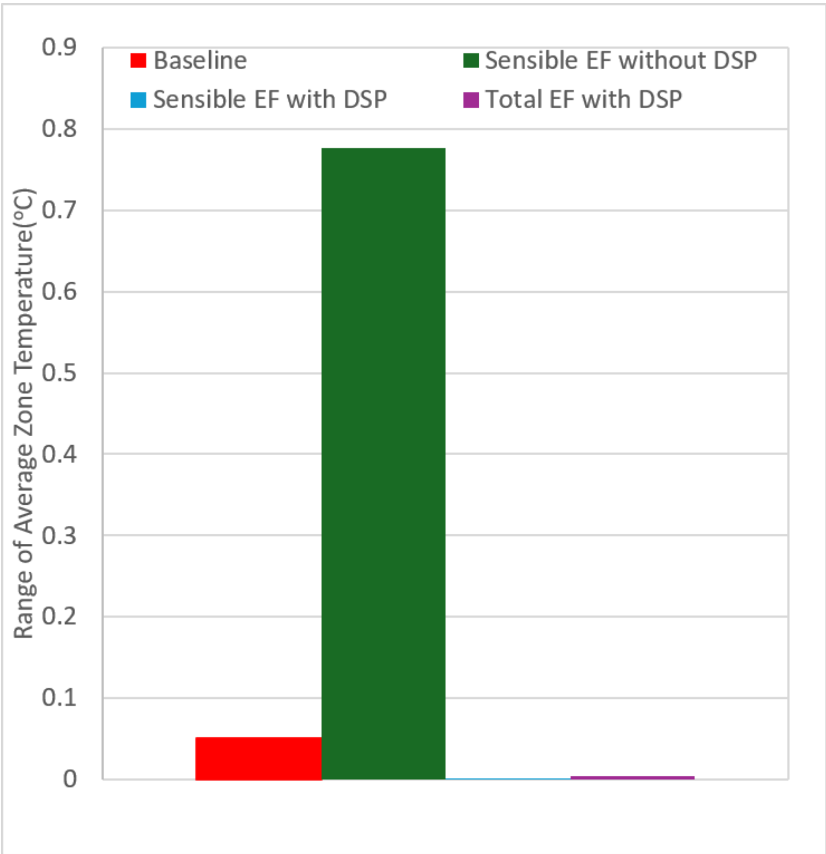

Figure 4.20: Range of average ZT (RZT) for the evaluated strategies

4.8 Summary

This study evaluated and compared the performance of four AHU control strategies using a Modelica-based virtual test bed to assess building demand control and thermal comfort. Baseline strategy resulted in the longest settling time of 5.05 hours, an RE of 12.52%, and an RZT of 0.05°C. This long settling time and high RE indicate inaccurate demand control during the peak period. The Total EF with DSP achieved precise load shedding, with a settling time of 0.03 hours, an RE of 0.01%, and an RZT of 0.00448°C. Total EF with DSP improves energy control accuracy by 1.59% relative to Sensible EF with DSP, while Sensible EF with DSP achieves more even cooling load sharing than Sensible EF without DSP, as indicated by RZT values of 0.00027°C and 0.78°C, respectively. These results indicate uneven sharing of the reduced cooling load in Sensible EF without DSP, whereas the baseline, Sensible EF with DSP, and Total EF with DSP exhibit even distribution of the reduced cooling load.

Overall, the strategies that utilized the EF controller performed better than baseline, as they resulted in comparatively faster and accurate HVAC demand control. Sensible EF without DSP performed the worst among the EF control strategies while the Total EF with DSP performed the best in demand control. This study demonstrates that integrating the DSP cascade controller and EF controller minimizes the negative impact on occupant comfort during demand control. For AHU systems equipped with enthalpy or humidity sensors, the Total EF with DSP strategy is recommended for building demand control and thermal comfort. However, implementing the Total EF with DSP control loop can be challenging in AHU systems that are not fully instrumented, as it requires accurate enthalpy measurement derived from both relative humidity and dry-bulb temperature sensors. For such systems, Sensible EF with DSP is recommended.

5. Development and Evaluation of an Optimization-Based Energy Feedback and Duct Static Pressure Cascade Control

This chapter incorporates an optimization-based control into the EF controller. This enables the modulation of the cooling load setpoint based on weather conditions and the building's daily load profile. The objective of this chapter is to develop and evaluate the performance of an optimization-based EF–DSP cascade control strategy that employs setpoint adjustment signals to achieve load shifting through precooling and load shedding during peak demand periods while maintaining minimum energy cost.

This chapter involves: (i) a reduced-order thermal modeling of an educational building and parameter estimation for control purpose; (ii) the development of an optimization-based EF controller and its implementation on the calibrated virtual test bed; and (iii) the evaluation of the optimal EF–DSP control strategy and its comparison with the EF-DSP control with constant setpoints and baseline demand control strategy.

5.1 Development of Optimization-Based EF Controller

Figure 5.1 illustrates the optimization-based EF control integrated with the DSP cascade control. To determine the optimal total cooling load setpoints for the EF controller, several steps are undertaken. First, a reduced-order thermal model of the building is developed, and its parameters are estimated. Next, an optimization-based control formulation is developed and integrated into the EF controller within the calibrated virtual test bed. Finally, the optimization framework is coupled with the virtual test bed through the BuildingsPy interface, enabling communication between the optimization algorithm and the Modelica-based HVAC model.

.

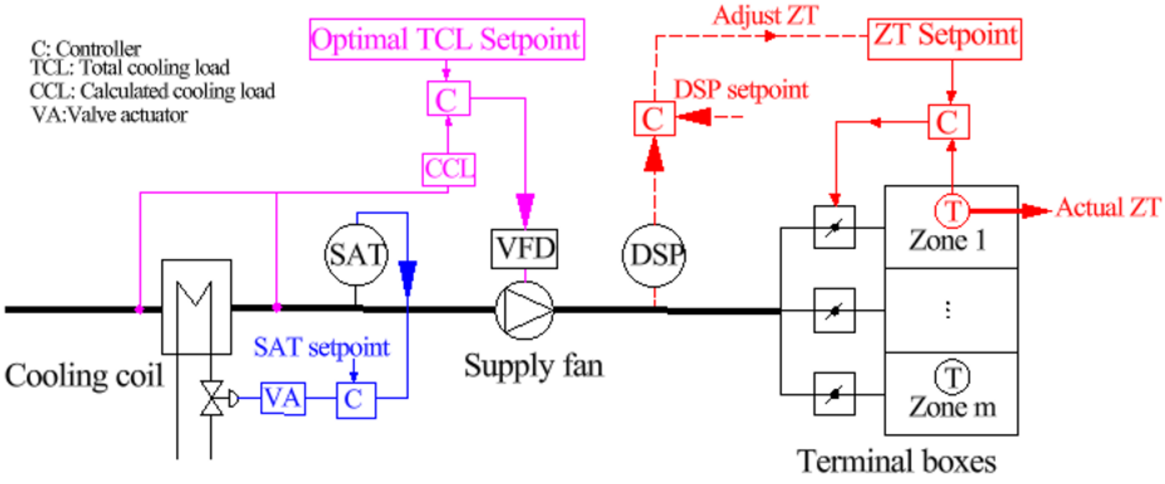

Figure 5.1: Optimization-based EF Control Integrated with the DSP cascade control

5.1.1 Reduced-order RC-based gray-box model of Building thermal dynamics

Building thermal dynamics involve heat and mass transfer processes, solar radiation through windows, air infiltration through cracks in windows and doors, and internal heat gains (Jiang, 2023). Grey-box modeling, also referred to as reduced-order modeling, is simpler and computationally more efficient than white-box modeling, which is fundamentally based on the conservation of mass, energy, and momentum. Resistance-capacitance (RC) modeling is the most widely used grey-box modeling approach and has been extensively employed in the literature for building energy modeling and control applications (Li et al., 2021).

The modeled building represents a portion of an engineering laboratory building at the University of Oklahoma and consists of seven thermal zones (Zones A–G). Figure *5.2* shows the architectural layout of the building. This section of the engineering building is served by a single air handling unit (AHU) and seven variable air volume terminal boxes (VAV TBs).

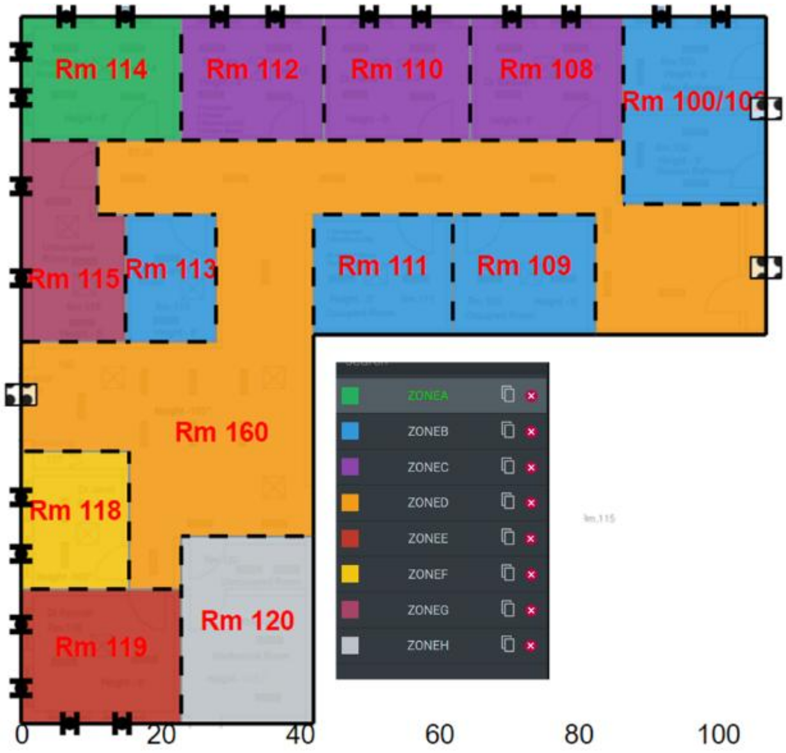

Figure 5.2: Thermal zones of the building

Five of the thermal zones are exterior zones (Zones A, C, E, F, and G), as they are exposed to the outdoor environment and are represented using second-order resistance-capacitance (2R2C) networks. Zones B and D are fully interior zones with no direct solar exposure and are represented using first-order resistance-capacitance (1R1C) networks. Table 5.1 summarizes the thermal zone classifications and their interactions with adjacent zones.

Table 5.1: Grouping and Interactions of Thermal Zones

Thermal Zones	Rooms	Adjacent Zones (interactions)
Zone A	114	C and D
Zone B	100, 102, 109, 111, 113	C, D, and G
Zone C	108, 110, 112	A, B, and D
Zone D	Corridor	A, B, C, E, F, G
Zone E	119	D and F
Zone F	118	D and E
Zone G	115	B and D

Figure 5.3 presents the 2R2C network used to model the thermal dynamics of the exterior zones of the building.

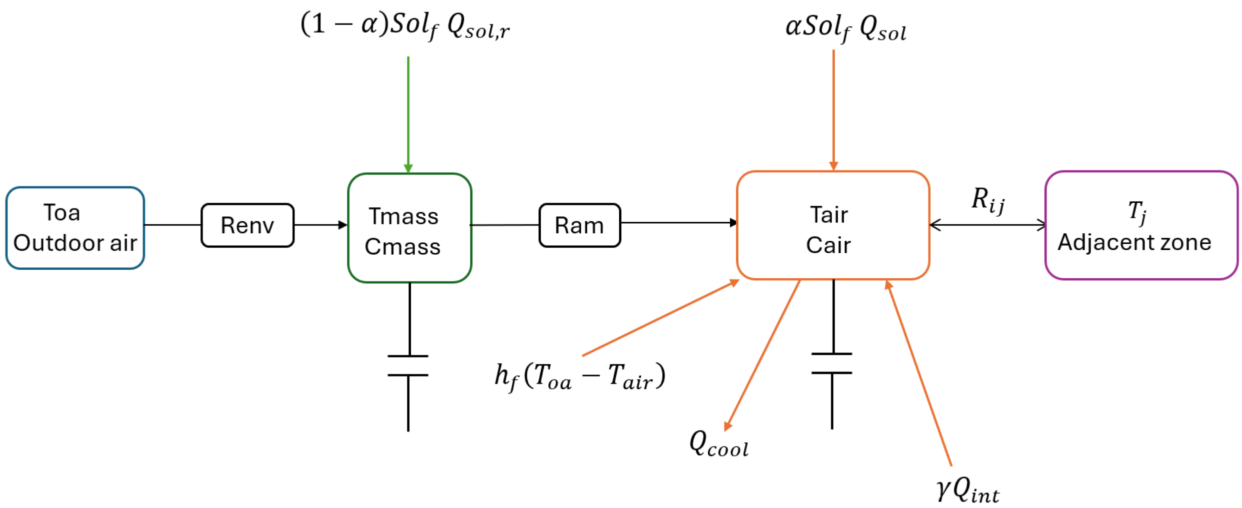

Figure 5.3: Schematic of the RC network of the exterior zones

Each exterior zone is modelled as two coupled thermal capacitances: an air node at temperature T_{air} representing the zone air and lightweight contents, and a mass node at temperature T_{mass} representing the thermally heavy envelope and structure. The two nodes are linked by an internal air–mass resistance R_{am}, while the mass node is connected to the outdoor air temperature T_{oa} through the envelope resistance R_{env}

The general 2R2C model equation for an exterior zone i ∈ { Zones A, C, E, F, G} is given by:

Mass node:

$$C_{mass,i}\frac{dT_{mass,i}}{dt} = \frac{T_{oa}-T_{mass,i}}{R_{env,i}} + \frac{T_{air,i}-T_{mass,i}}{R_{am,i}} + (1-\alpha_i)Sol_{f,i}\, Q_{sol,r}$$

Air node:

$$C_{air,i}\frac{dT_{air,i}}{dt} = \frac{T_{mass,i}-T_{air,i}}{R_{am},i} + \alpha_i Sol_{f,i}\, Q_{sol,r} + \gamma_i Q_{int,i} - Q_{cool,i} + h_{f,i}\left(T_{oa}-T_{air,i}\right) + \sum_{j\in\mathcal{N}_i}\frac{T_j - T_{air,i}}{R_{ij}}$$

Where C_{air} is the thermal capacitance of the zone air volume [J K⁻¹], C_{mass} is the thermal capacitance of the building mass [J K⁻¹]. The mass capacitance represents the building envelope and is characterized by the mass temperature (T_{mass}). The air capacitance represents the zone air and is characterized by the air temperature, T_{air}. Both capacitances are connected through the air-to-mass thermal resistance, R_{am} while the mass node exchanges heat with the outdoor environment through the envelope thermal resistance, R_{env}. h_f [W K⁻¹] is the lumped ventilation and infiltration conductance to air exchange with outdoors. $Q_{sol,r}$ is the solar radiation [W m⁻²], Sol_f [m²] is the effective solar aperture, and α is the fraction of the solar radiation hitting the air node directly. Q_{int} represents internal heat gains and γ is a multiplier used to account for uncertainties in the occupancy and equipment loads. Q_{cool} represents the cooling load in each thermal zone.

The interior zones are represented using first-order resistance-capacitance (1R1C) models with thermal coupling to adjacent zones. The general 1R1C model for an interior zone, i ∈ $\{B, D\}$, is given by:

$$C_{air,i}\frac{dT_{air,i}}{dt} = \gamma_i Q_{int,i} - Q_{cool,i} + h_{f,i}\left(T_{oa} - T_{air,i}\right) + \sum_{j\in\mathcal{N}_i}\frac{T_j - T_{air,i}}{R_{ij}}$$

5.1.2 Parameter Identification

The continuous-time state-space representation of the thermal model for each zone is given by:

$$\dot{\mathbf{x}}_i = \mathbf{A}_i(\theta_i)\,\mathbf{x}_i + \mathbf{B}_i(\theta_i)\,\mathbf{u}_i$$

Where $\mathbf{x}_i = [T_{air}, T_{mass}]^\top$ represents the states for the exterior zone and $\mathbf{u}_i = [T_{oa}, Q_{sol,r}, Q_{int,i}, Q_{cool,i}, \{T_{air,j}\}_{j\in\mathcal{N}_i}]^\top$, represents the input vector for exterior zones. For interior zones, $\mathbf{x}_i = [T_{air}]^\top$ and $\mathbf{u}_i = [T_{oa},\ Q_{int,i},\ Q_{cool,i},\ \{T_{air,j}\}_{j\in\mathcal{N}_i}]^\top$. θ_i represents the thermal parameters to be identified for each zone.

Each exterior zone has 8 parameters to be identified in addition to its inter-zone thermal resistances ($\theta_i = \{R_{env,i},\ R_{am,i},\ C_{air,i},\ C_{mass,i},\ \gamma_i,\ Sol_{f,i}\ ,\ h_{f,i},\ \alpha_i\} \cup \{R_{ij}\}_{j\in\mathcal{N}_i}$), while each interior zone has a set of 3 parameters, in addition to its inter-zone thermal resistances ($\theta_i = \{\ C_{air,i},\ \gamma_i,\ h_{f,i}\} \cup \{R_{ij}\}_{j\in\mathcal{N}_i}$).

The continuous-time model is converted into a discrete-time model using the Forward Euler method, which is a first-order explicit single-step numerical integration scheme.

The general discrete-time state equation is expressed as

$$x_{k+1} = x_k + \Delta t\, f(x_k, \mathrm{u}_k, \theta)$$

The discretized 2R2C model of the exterior zones is given by:

$$T_{mass,i,k+1} = T_{mass,i,k}$$
$$+ \frac{\Delta t}{C_{mass,i}}\left[\frac{T_{oa,k} - T_{mass,i,k}}{R_{env,i}} + \frac{T_{air,i,k} - T_{mass,i,k}}{R_{am,i}} + Sol_{f,i}\,(1-\alpha_i)\,Q_{sol,r,k}\right]$$

$$T_{air,i,k} + \frac{\Delta t}{C_{air,i}}\left[\frac{T_{mass,i,k} - T_{air,i,k}}{R_{am,i}} + \gamma_i Q_{int,i} + Sol_{f,i}\,\alpha_i Q_{sol,r,k} - Q_{cool,i,k}\right.$$
$$\left. + h_{f,i}\big(T_{oa,k} - T_{air,i,k}\big) + \sum_{j\in\mathcal{N}_i} \frac{T_{air,j,k} - T_{air,i,k}}{R_{ij}}\right]$$

The discretized equation for the 1R1C model of the interior zones is given by:

$$T_{air,i,k+1} = T_{air,i,k} + \frac{\Delta t}{C_{air,i}}\left[\gamma_i Q_{int,i} - Q_{cool,i,k} + h_{f,i}\left(T_{oa,k} - T_{air,i,k}\right) + \sum_{j\in\mathcal{N}_i} \frac{T_{air,j,k} - T_{air,i,k}}{R_{ij}}\right].$$

The discretized model is subsequently employed in the parameter identification scheme to estimate the unknown thermal parameters by minimizing the prediction error between the measured and simulated zone temperatures.

5.1.2.1 Objective Formulation

The objective of the parameter estimation process is to determine the set of thermal parameters that minimizes the discrepancy between the measured zone temperatures in the training dataset and those predicted by the grey-box thermal models. The identified parameters are obtained by minimizing a weighted error function that considers both temperature prediction accuracy and the ability of the model to replicate the dynamic thermal response of the building.

The optimization problem is posed as the minimization of the loss between the measured and simulated temperatures. The objective function is expressed:

$$\mathcal{L}\left(T^{meas}, T^{sim}\right) = \mathcal{L}_T + \lambda\,\mathcal{L}_D$$

$$\mathcal{L}\left(T^{meas}, T^{sim}\right) = \frac{1}{N}\sum_{k=1}^{N} w_k\ (T_k^{meas} - T_k^{sim})^2 + \frac{1}{N-1}\sum_{k=1}^{N-1}(\Delta T_k^{meas} - \Delta T_k^{sim})^2,$$

where N is the number of data points, w_k is the weighting factor, and λ is the derivative error weighting coefficient.

The first term, $\mathcal{L}_T$, minimizes the prediction error between the measured and simulated temperatures. In this study, the measured temperatures are obtained from the training dataset, while the simulated temperatures are generated using the identified thermal parameters. A weighting factor, w_k, is employed to assign greater importance to periods characterized by large temperature deviations. This increases the influence of peak operating conditions during the optimization process and improves model accuracy during periods that are most relevant to demand response applications.

The weighing factor is defined as

$$w_k = 1 + 4\,\frac{|T_k^{meas} - \text{median}(T^{meas})|}{\max(T^{meas}) - \min(T^{meas})}$$

The second term, $\mathcal{L}_D$, constrains the rate of temperature change and enables the identified model to reproduce the dynamic thermal response characteristics of the building. By minimizing both $\mathcal{L}_T$ and $\mathcal{L}_D$, the parameter estimation framework captures both the steady-state temperature behavior and the transient thermal dynamics of the building.

For the exterior zones, the thermal parameters are estimated by minimizing a weighted objective function that simultaneously considers both the air-node and mass-node temperatures:

$$J_i(\theta_i) = 0.6\,\mathcal{L}\left(T_{air,i}^{meas}, T_{air,i}^{sim}\right) + 0.4\,\mathcal{L}\left(T_{mass,i}^{meas}, T_{mass,i}^{sim}\right)$$

The joint fitting of the air-node and mass-node temperatures is necessary for exterior zones because the envelope parameters, $R_{env,i}$ and $C_{mass,i}$ are weakly identifiable when only the air temperature is used for calibration. Incorporating the mass-temperature measurements improves the identifiability of these parameters and enables a more accurate representation of the building thermal inertia. For the interior zones, the objective function is formulated using only the air-temperature measurements because the 1R1C model does not include a separate mass node.

5.1.2.2 Parameter Estimation Method

Due to the non-convex nature of the objective function, this study employs a multi-stage hybrid optimization framework to estimate the thermal parameters of the 2R2C and 1R1C models. The optimization combines a population-based global search with successive gradient-based local refinement across three stages. The first stage employs Differential Evolution (DE) to perform a global search of the parameter space. The second stage applies the Limited-memory Broyden–Fletcher–Goldfarb–Shanno algorithm with bound constraints (L-BFGS-B) to refine the solution obtained from the global search. The third stage performs a second L-BFGS-B optimization with tighter convergence tolerances to further improve the numerical accuracy of the identified parameters. The hybrid framework combines the global exploration capability of with the fast local convergence of L-BFGS-B, thereby improving the robustness, accuracy, and computational efficiency of the parameter estimation process.

The DE algorithm is a simple and efficient global optimization technique first proposed by Storn & Price (1997). It has been widely applied to building thermal parameter identification problems because of its ability to solve nonlinear, complex, and multidimensional optimization problems. Furthermore, DE is recognized for its ability to maintain population diversity and reduce the likelihood of premature convergence to local minima, making it well suited for the calibration of complex building energy models (Shen, 2026; Storn & Price, 1997)**.** The effectiveness of DE for building thermal parameter estimation has been demonstrated by Shen (2026) who employed a hybrid modelling approach to identify the thermal parameters of four RC model configurations (4R1C, 6R1C, 7R1C, and 7R2C) for an educational building. DE is characterized by its simple algorithmic structure, ease of implementation, computational efficiency, and robust convergence performance (Yang et al., 2016)**.**

The DE algorithm begins by randomly generating an initial population of candidate solutions (parameter vectors) within the prescribed parameter bounds. The population then evolves over successive generations through the operations of mutation, crossover, and selection until a stopping criterion is satisfied.

L-BFGS-B is a limited-memory quasi-Newton algorithm designed to solve large-scale nonlinear optimization problems subject to bound constraints on the optimization variables (Byrdt et al., 1995; Zhu et al., 1997). In the optimization framework, L-BFGS-B is employed in Stage 2 to refine the solution obtained from Differential Evolution (DE). The optimization is performed with a maximum of 8,000 iterations, a function tolerance of 10^{-15}, and a gradient tolerance of 10^{-12}. Starting from the near-optimal solution identified by DE, L-BFGS-B exploits the locally smooth structure of the objective function to rapidly converge to a more accurate local optimum while ensuring that all parameters remain within their prescribed physical bounds.

In Stage 3, the L-BFGS-B refinement is repeated using tighter convergence criteria, consisting of a maximum of 16,000 iterations, a function tolerance of 10^{-16}, and a gradient tolerance of 10^{-13}. This fine refinement stage further improves the numerical accuracy of the identified parameters by reducing the residual optimization error remaining after the Stage 2 optimization. The additional refinement increases confidence that the final parameter estimates have converged to a stable local optimum.

5.1.2.3 Dataset description and Error Metrics

The dataset used for parameter estimation consists of one week of data collected at one-minute intervals for each thermal zone. The dataset was generated using the calibrated virtual test bed, which had previously been validated against the experimental test bed. The data represents a typical summer week.

For each day, the zone temperature setpoint is maintained at 21.5°C during the off-peak period and increased to 22.8°C during the on-peak period. The setpoint change introduces thermal excitation into the building and creates variations in the zone thermal response, which improves the identifiability of the thermal parameters and supports more reliable estimation of the building's dynamic thermal behavior.

The Root Mean Squared Error (RMSE), Mean Absolute Error (MAE), and Maximum Absolute Error (MaxErr) are the error metrics used to evaluate the accuracy of the of the temperature predictions generated using the identified parameters, by comparing the measured and simulated temperatures for each thermal zone.

RMSE is used to valuate the overall accuracy of the temperature predictions and is mathematically expressed as:

$$\mathrm{RMSE} = \sqrt{\frac{1}{N}\sum_{k=1}^{N}(T_k^{meas} - T_k^{sim})^2}$$

MAE is used to quantify the average absolute difference between the measured and simulated air temperatures, and mass temperatures for the exterior zones, and is mathematically expressed as:

$$\mathrm{MAE} = \frac{1}{N}\sum_{k=1}^{N}|T_k^{meas} - T_k^{sim}|$$

MaxErr is used to represent the largest discrepancy between the measured and simulated air and mass temperatures and is mathematically expressed as:

$$\text{MaxErr} = \max_k |T_k^{meas} - T_k^{sim}|$$

5.1.2.4 Parameter Estimation Result

Table 5.2: Identified Parameters for exterior and interior zones

Parameter	Zone A	Zone B	Zone C	Zone D	Zone E	Zone F	Zone G
R_{env} (K/W)	2.5×10^{-2}	—	1.05×10^{-2}	—	1.52×10^{-2}	2.14×10^{-2}	1.88×10^{-2}
R_{am} (K/W)	1.02×10^{-2}	—	2.31×10^{-3}	—	5.14×10^{-3}	7.04×10^{-3}	5.46×10^{-3}
C_{air} (J/K)	1.75×10^{6}	3.16×10^{6}	3.16×10^{6}	3.16×10^{6}	1.74×10^{6}	1.61×10^{6}	1.33×10^{6}
C_{mass} (J/K)	7.32×10^{6}	—	1.25×10^{7}	—	1.17×10^{7}	7.74×10^{6}	1.19×10^{7}
γ (–)	5.51×10^{-1}	5.30×10^{-1}	5.18×10^{-1}	4.64×10^{-1}	3.78×10^{-1}	4.26×10^{-1}	4.23×10^{-1}
Sol_f	4.77×10^{-1}	—	7.11×10^{-1}	—	6.80×10^{-1}	4.95×10^{-1}	7.70×10^{-1}
h_{inf} (W/K)	4.61×10^{1}	4.42×10^{1}	2.74×10^{1}	8.73×10^{0}	3.75×10^{1}	2.17×10^{1}	2.71×10^{1}
α (–)	1×10^{-2}	—	5.06×10^{-1}	—	1×10^{-2}	1×10^{-2}	1×10^{-2}
Inter-zone R	R_{AC}= 1.04×10^{-3} R_{AD}= 1.42×10^{-2}	R_{BC}= 3.49×10^{-3} R_{BD}= 3.79×10^{-4} R_{BG}= 2.05×10^{-2}	R_{CD}= 2.56×10^{-2}	R_{DE}= 3.56×10^{-3} R_{DF}= 9.92×10^{-2} R_{DG}= 2.35×10^{-2}	R_{EF}= 8.30×10^{-4}		

Table 5.2 shows the identified parameters for the exterior and interior thermal zones of the building. A total of 54 parameters were identified for all thermal zones. Table 5.3 presents the RMSE, MAE, and MaxErr for T_{air} and T_{mass} of the thermal zones. Figure 5.4 shows the corresponding measured and simulated T_{air} profiles using the identified parameters, while Figure *5.5* shows the measured and simulated T_{mass} profiles for the exterior zones.

The RMSE of T_{air} for all thermal zones ranges from 0.111 to 0.246°C, while the MAE ranges from 0.082 to 0.194°C. These error indices remain within a comparatively narrow range for most thermal zones, indicating good prediction accuracy. As shown in Figure 3, the simulated T_{air} closely tracks the measured T_{air} and accurately captures the dynamic thermal response of the building. Among all the thermal zones, Zone D produced the largest prediction error, with an RMSE of 0.246°C, an MAE of 0.194°C, and a maximum absolute error of 0.918°C. As an interior zone with six adjacent thermal couplings, Zone D's T_{air} prediction is influenced by the simulated temperatures of more neighboring zones than any other zone in the building. Error in any one neighbour's fit therefore propagates into Zone D's own prediction and this contributes to the comparatively elevated error relative to zones with fewer inter-zone coupling

The RMSE of T_{mass} for the exterior thermal zones ranges from 0.252 to 0.338°C. As shown in Figure 4, the simulated T_{mass} closely tracks the measured T_{mass} for all exterior zones, demonstrating that the identified parameters of the model reasonably capture the thermal mass dynamics of the building. Among the exterior zones, Zone A yielded the largest prediction error, with an RMSE of 0.338°C, an MAE of 0.285°C, and a maximum absolute error of 0.804°C.

Table 5.3: Summary of Error Metrics

Zone	Model	RMSE T_{air} (°C)	MAE T_{air} (°C)	Max. error T_{air} (°C)	RMSE T_{mass} (°C)	MAE T_{mass} (°C)	Max. error T_{mass} (°C)
Zone A	2R2C	0.156	0.114	0.592	0.338	0.285	0.804
Zone B	1R1C	0.111	0.082	0.447	n/a	n/a	n/a
Zone C	2R2C	0.145	0.110	0.572	0.252	0.206	0.631
Zone D	1R1C	0.246	0.194	0.918			
Zone E	2R2C	0.139	0.098	0.618	0.292	0.238	0.717
Zone F	2R2C	0.122	0.087	0.559	0.281	0.223	0.733
Zone G	2R2C	0.142	0.108	0.540	0.258	0.203	0.709

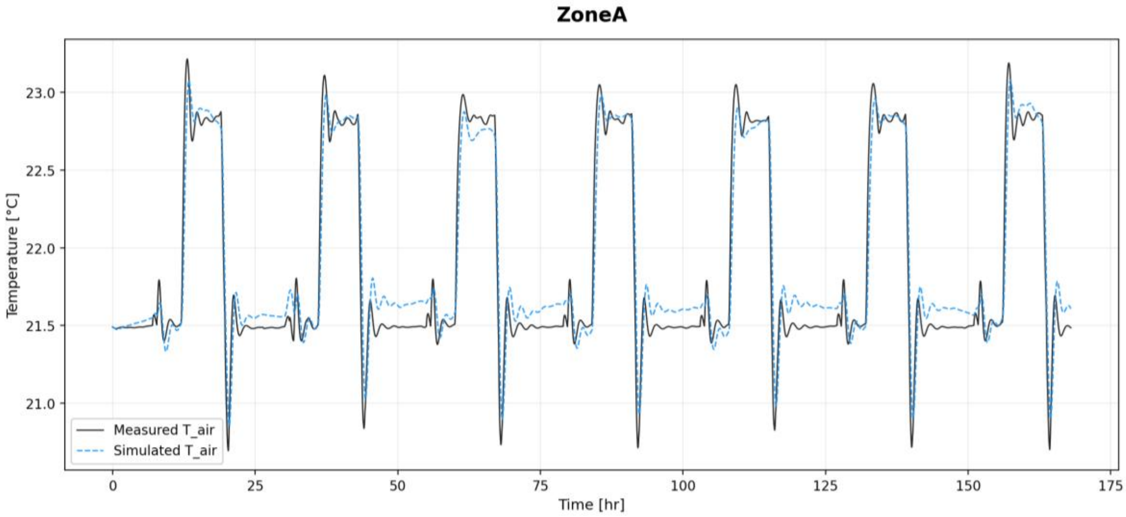

(a) Zone A

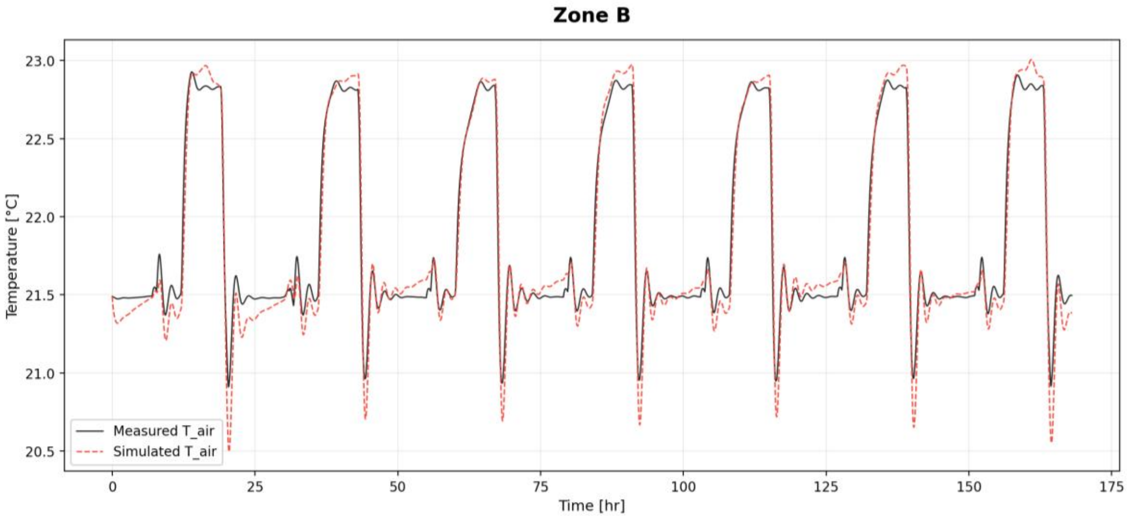

(b) Zone B

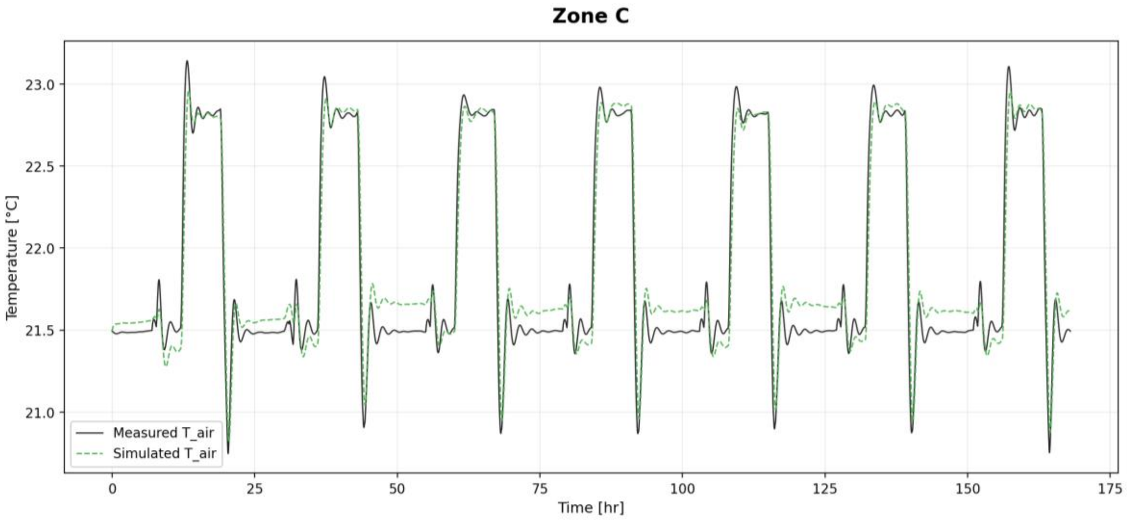

(c) Zone C

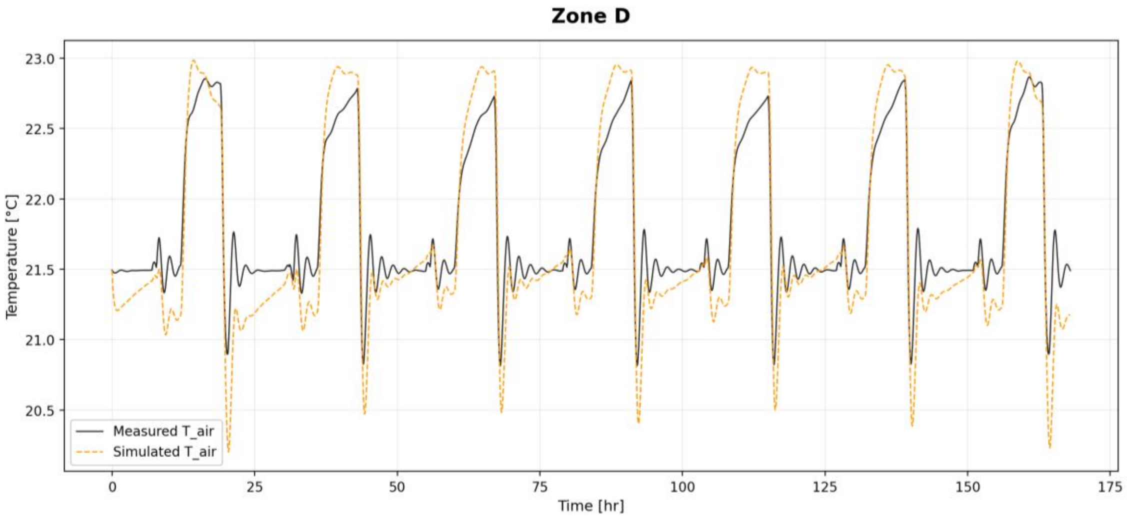

(d) Zone D

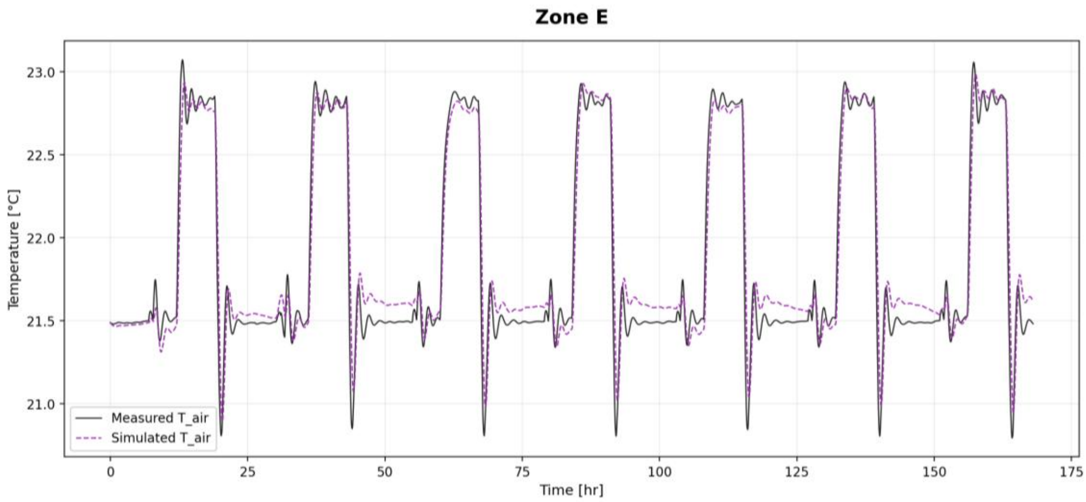

(e) Zone E

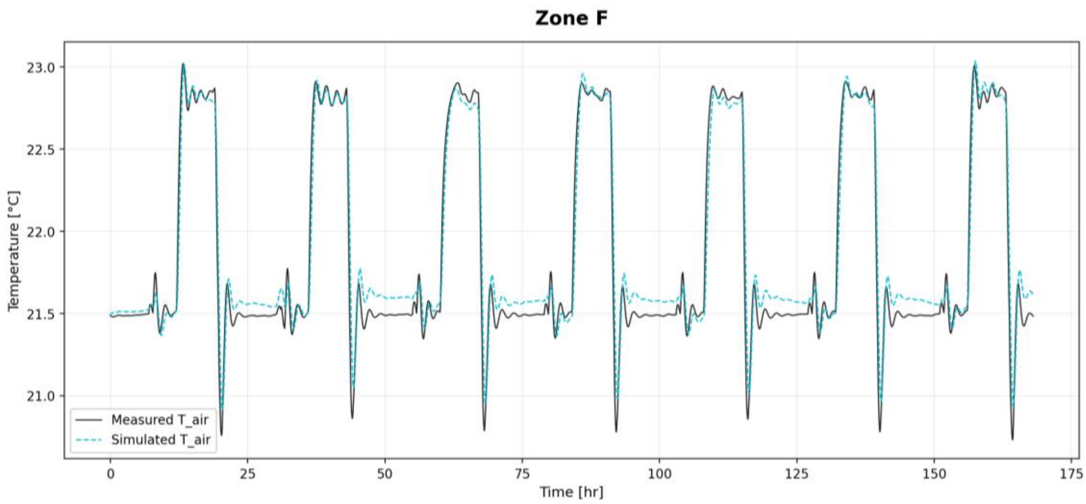

(f) Zone F

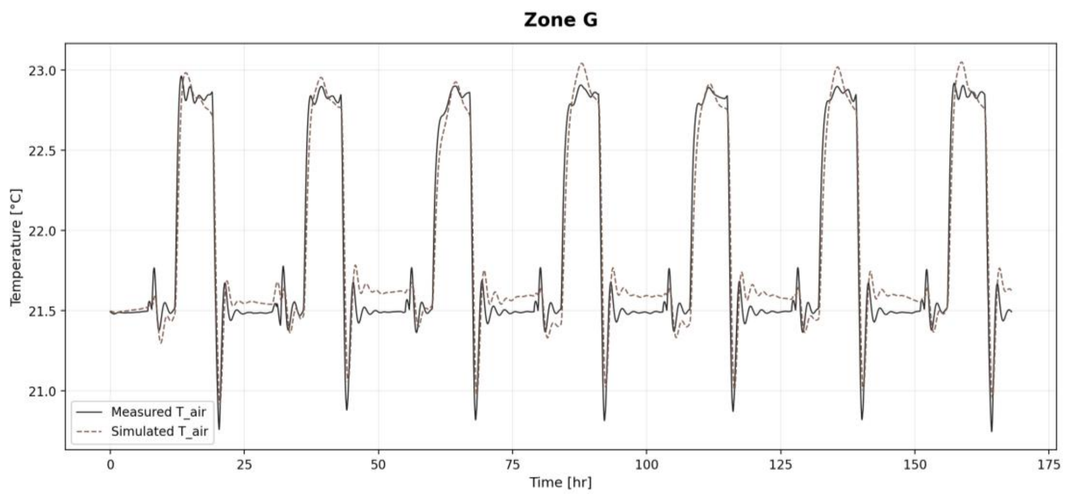

(g) Zone G

Figure 5.4: Simulated and measured zone air temperatures

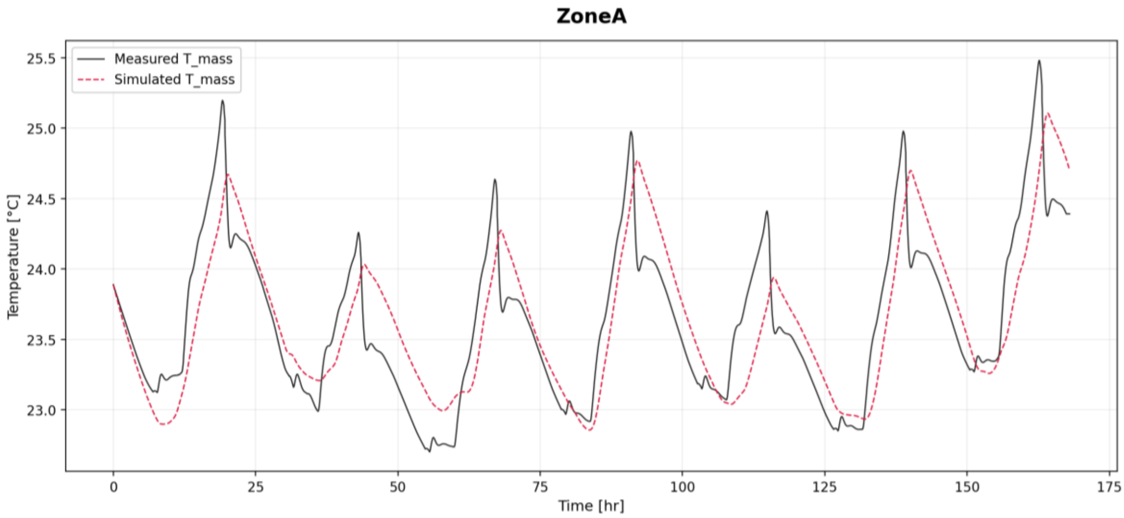

(a) Zone A

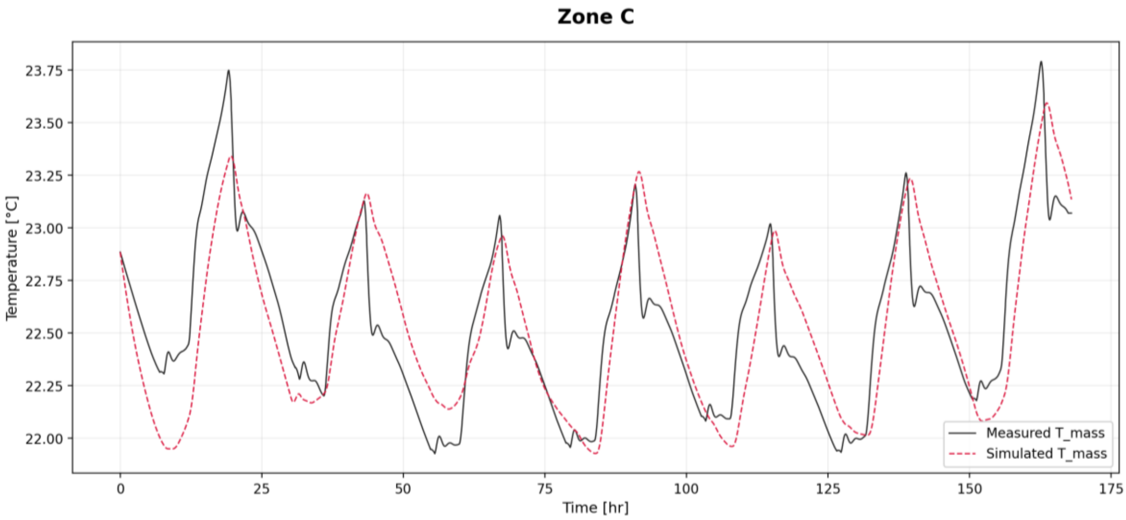

(b) Zone C

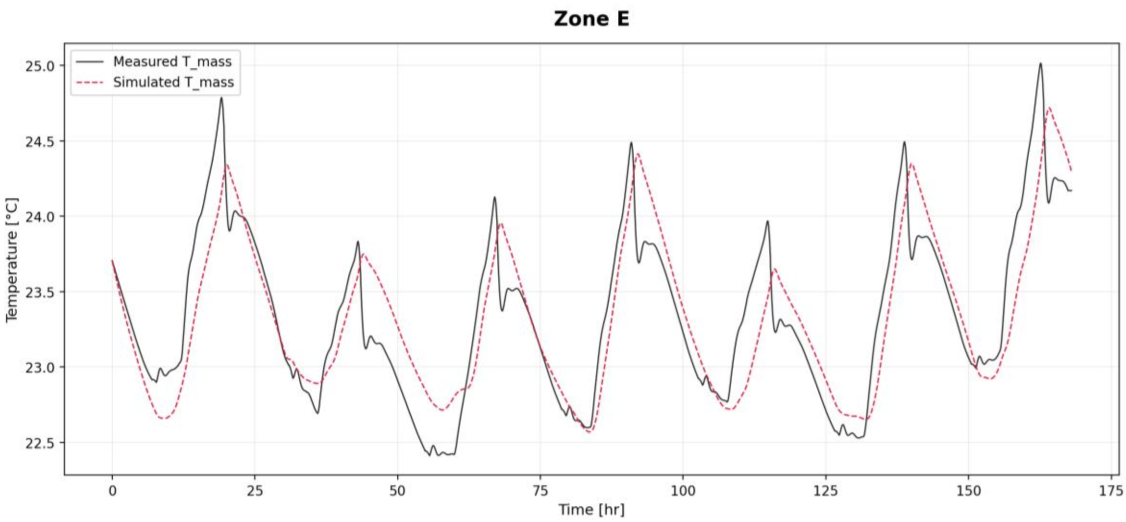

(c) Zone E

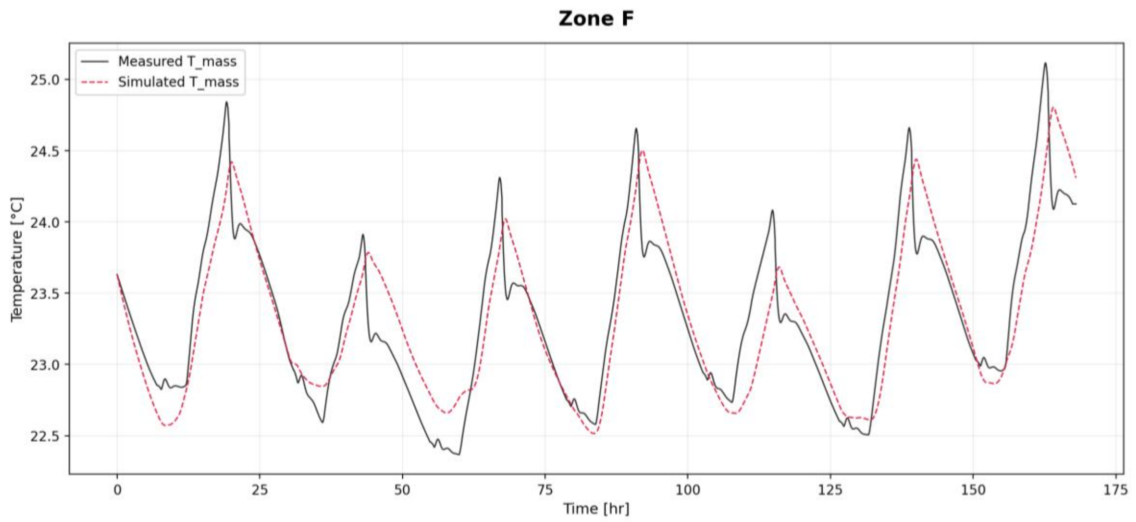

(d) Zone F

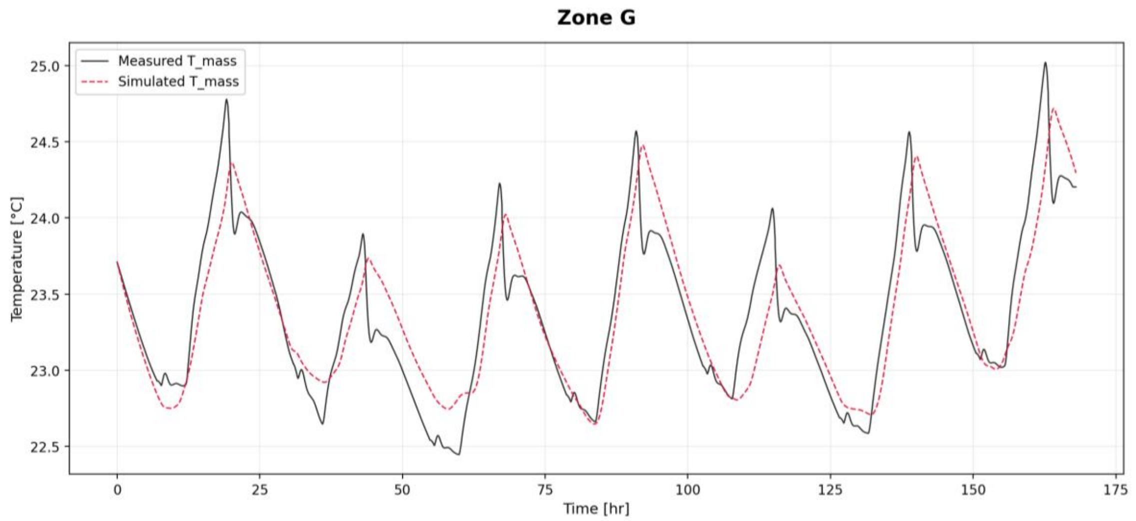

(e) Zone G

Figure 5.5: Simulated and measured zone mass temperatures

5.1.3 Optimization Control Formulation

Having described the reduced-order grey-box thermal model and its parameter identification process, the optimization control formulation used to determine the optimal cooling load setpoint is presented. The optimization problem is formulated as a linear programming problem, and the objective function is given by:

$$min \sum_{i=1}^{N} E_i \, C_{i,e} + \rho\epsilon$$

$$E_i = P_{cc,i}\Delta t$$

The first term represents the cost of electricity, while the second term represents the comfort penalty. E_i is the electrical energy consumed, $C_{i,e}$ is the dynamic electricity price, which varies between the peak and off-peak periods, ρ is a comfort penalty weighting factor that makes violating the comfort bound expensive and $\boldsymbol{\epsilon}$ is the total comfort slack variable summed over all seven thermal zones and time steps.

The total comfort slack variable is defined as:

$$\epsilon = \sum_{zones} \sum_{i=1}^{N} (\epsilon_i^+ + \epsilon_i^-)$$

where ϵ_i^+ and ϵ_i^- represent the upper and lower comfort-bound slack variables, respectively. These slack variables quantify the magnitude of the thermal comfort constraint violation at each time step.

The upper and lower slack variables are

$$\epsilon_i^+ = max(0, T_{zone,air} - T_{ub})$$

$$\epsilon_i^- = max(0, T_{lb} - T_{zone,air})$$

$$min \sum_{i=1}^{N} E_i \, C_{i,e} + \rho \sum_{zones} \sum_{i=1}^{N} (\epsilon_i^+ + \epsilon_i^-)$$

The objective of the optimization is to minimize the energy cost during both the off-peak and peak periods while maintaining the thermal comfort within an acceptable range. This enables energy cost minimization, load shedding during the peak period, and load shifting through precooling. The decision variable of the optimization problem is the cooling load setpoint (q_{cc}) at each time step. The electrical power consumption (P_{cc}) is determined from the cooling load setpoint as

$$P_{cc,i} = \frac{q_{cc,i}}{COP(T_{oa})}$$

The optimization is subject to thermal comfort constraints and cooling load constraints. The thermal comfort constraints are implemented as soft constraints and are expressed as

$$T_{lb} \leq T_{air,i} \leq T_{ub}$$

$$T_{air,i} \leq T_{ub} + \epsilon_i^+$$

$$T_{air,i} \geq T_{ub} - \epsilon_i^-$$

Where T_{lb} and T_{ub} are the lower and upper temperature comfort bounds, respectively, that are maintained for all thermal zones.

On-Peak period: $T_{ub} = 24^oC$, $T_{lb} = 22^oC$

Off-peak period: $T_{ub} = 22^oC$ $T_{lb} = 20^oC$

The cooling load capacity bound is expressed mathematically below with the minimum capacity set to zero.

$$0 \leq q_{cc} \leq q_{cc,max}$$

In summary, the optimizer inputs are the time-of-use electricity price, thermal comfort bounds, and weather data, including the outdoor air temperature (T_{oa}) and solar irradiance ($Q_{sol,r}$).

5.1.4 Implementation of optimized control with the virtual test bed

This optimization framework is coupled with and implemented on the virtual test bed using the BuildingsPy package. Figure 5.6 illustrates the communication between BuildingsPy and the EF controller in the virtual test bed. BuildingsPy is a Python-based interface that enables the loading and simulation of Modelica models, extraction of simulation results, and automation of simulation tasks, including parameter sweeps and model calibration (Fuchs et al., 2016).

In this study, BuildingsPy was adopted because it provides a robust interface for coupling the optimization framework with the Modelica virtual test bed. It is used to communicate the optimized cooling load setpoints generated by the optimization algorithm to the EF controller, execute the simulations, and extract the simulation results for subsequent analysis.

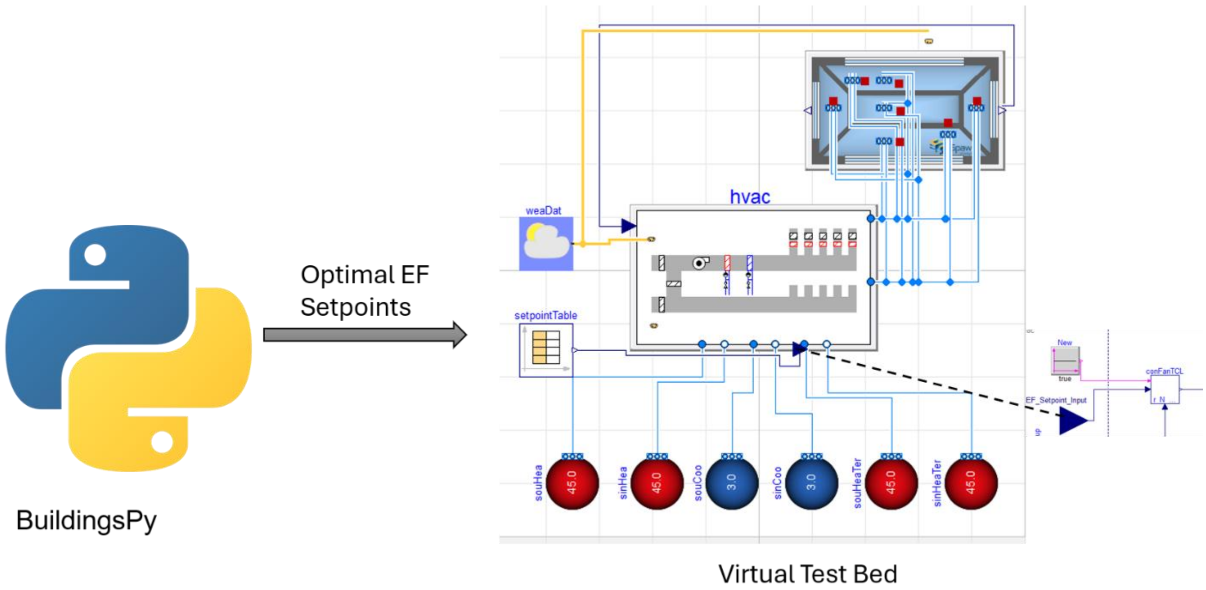

Figure 5.6: Communication between the BuildingsPy and EF controller in the virtual test bed

The following steps were followed to integrate the optimization framework with the virtual test bed. First, the optimizer output is offset by the outdoor air-cooling load to obtain the total cooling load setpoint. The optimal EF cooling load setpoint is then converted into a time-value schedule array. This optimization schedule is communicated to the setpointTable object at the Dymola top level, which subsequently passes the schedule to the EF controller through its input signal. Next, the BuildingsPy simulator object is configured, and the simulation settings, including the start time, stop time, and output intervals, are specified to match the optimization horizon. Finally, upon completion of the simulation, the simulation results are retrieved in the native binary (.mat) file format for subsequent analysis.

5.2 Scenario Design and Simulation

This section presents the control strategies evaluated in this study, their implementation on the calibrated virtual test bed, and the corresponding simulation results. The control strategies are summarized in Table 5.4. The control strategies are summarized in Table 5.4.

The baseline demand control strategy utilizes zone temperature (ZT) feedback control during the off-peak period and implements a change in the zone temperature setpoint during the on-peak period. Two demand control strategies based on the proposed EF–DSP cascade control are also evaluated. Both strategies utilize the total cooling load as the EF control variable, as identified in Chapter 4. The first strategy, EF with Constant Setpoints, employs the EF controller with the DSP cascade controller to achieve rapid demand control during the peak period and precooling during the off-peak period. The second strategy, Optimization-Based EF Control, utilizes the optimized EF cooling load setpoints.

Table 5.4: Summary of the baseline demand control strategy, EF control with Constant setpoint, and Optimization-Based EF Control

Nomenclature		Baseline	EF control with Constant Setpoints	Optimization-Based EF Control
On- Peak hours (2:00 PM – 9:00 PM)	Control strategy	ZT feedback control using GTA	EF control and DSP cascade control	EF control and DSP cascade control
	EF control Setpoints	N/A	Constant	Optimal
Off- Peak hours (10:00 AM – 2:00 PM)	Control strategy	ZT feedback control	EF control and DSP cascade control	EF control and DSP cascade control
Off- Peak hours (9:00 AM – 10:00 AM)	Control strategy	ZT feedback control	ZT feedback control	EF control and DSP cascade control

The demand control event (peak period) considered in this study spans from 2:00 PM to 9:00 PM. Simulations are conducted over a four-day period, with the first day used as a warm-up period to minimize the influence of the initial conditions. The remaining three days are used to evaluate the performance of the control strategies under varying weather conditions.

5.2.1 Baseline

This strategy utilizes GTA control during the peak period. The zone temperature setpoint ($T_{ZoneSet}$) is maintained at 20°C during the off-peak period. This setpoint corresponds to the lower thermal comfort bound used in the optimization. During the peak period, $T_{ZoneSet}$ is increased to 24°C, which corresponds to the upper thermal comfort bound for this period.

Figure 5.7 shows the zone temperatures (ZTs), supply fan airflow rate and speed, and duct static pressure (DSP) for the baseline strategy. After the demand control period, a noticeable trend is observed. The supply fan operates at its maximum speed (100%, 1), while the duct static pressure is not maintained at its setpoint of 250 Pa. This period is referred to as the demand rebound, which occurs when the HVAC system returns to normal operation at the end of a demand control event (Sehar et al., 2016).

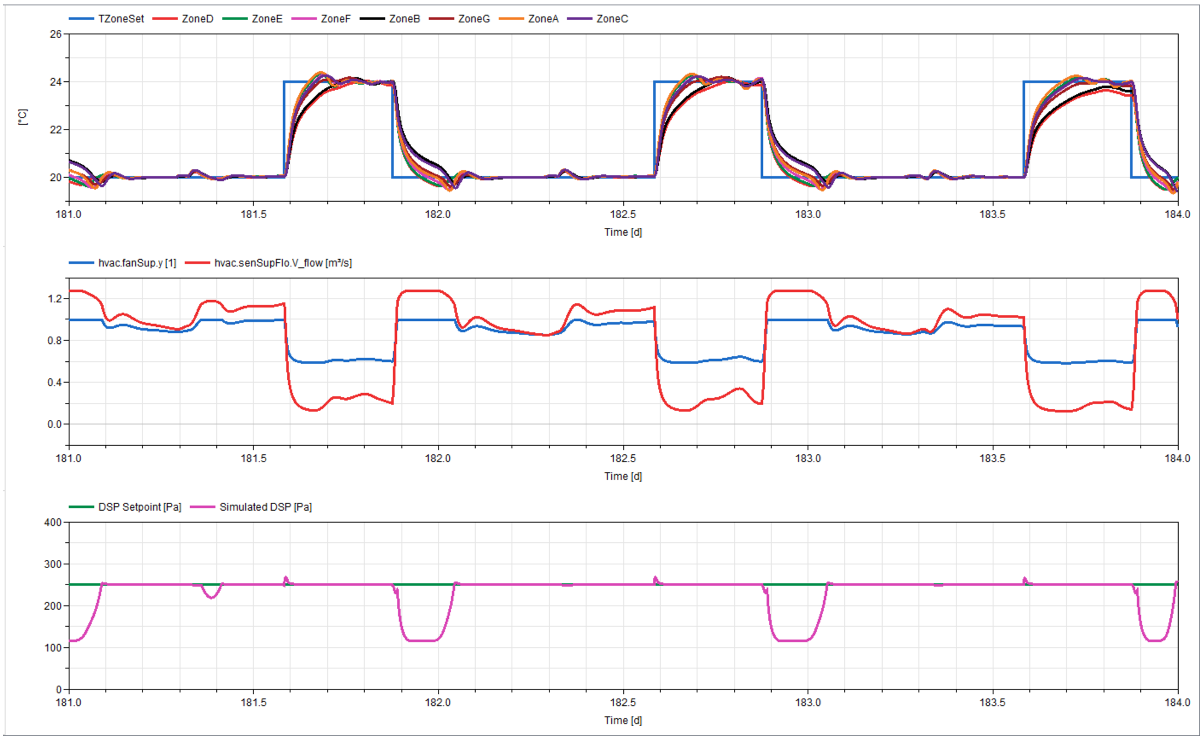

Figure 5.7: Zone temperatures, supply fan airflow rate, fan speed, and duct static pressure for the baseline

5.2.2 EF Control with Constant Setpoints

This strategy utilizes a combination of EF control, DSP cascade control, and ZT feedback control for all the days in the simulation period. The EF–DSP cascade control is active during the on-peak period and a portion of the occupied off-peak period (4 hours before the peak period), while the ZT feedback control is active during the remaining off-peak period.

For the EF controller, two constant cooling load setpoints identified from the baseline strategy are utilized. During the peak period, the supply fan is modulated to maintain a total cooling load (TCL) setpoint of 9.07 kW. During the off-peak precooling period, the supply fan is modulated to maintain a TCL setpoint of 16 kW. The DSP cascade controller is used to maintain the DSP setpoint while readjusting the $T_{ZoneSet}$ within the lower and upper thermal comfort bounds during both the off-peak and on-peak periods. Figure 5.8 shows the EF controller operation for the EF control with Constant Setpoints.

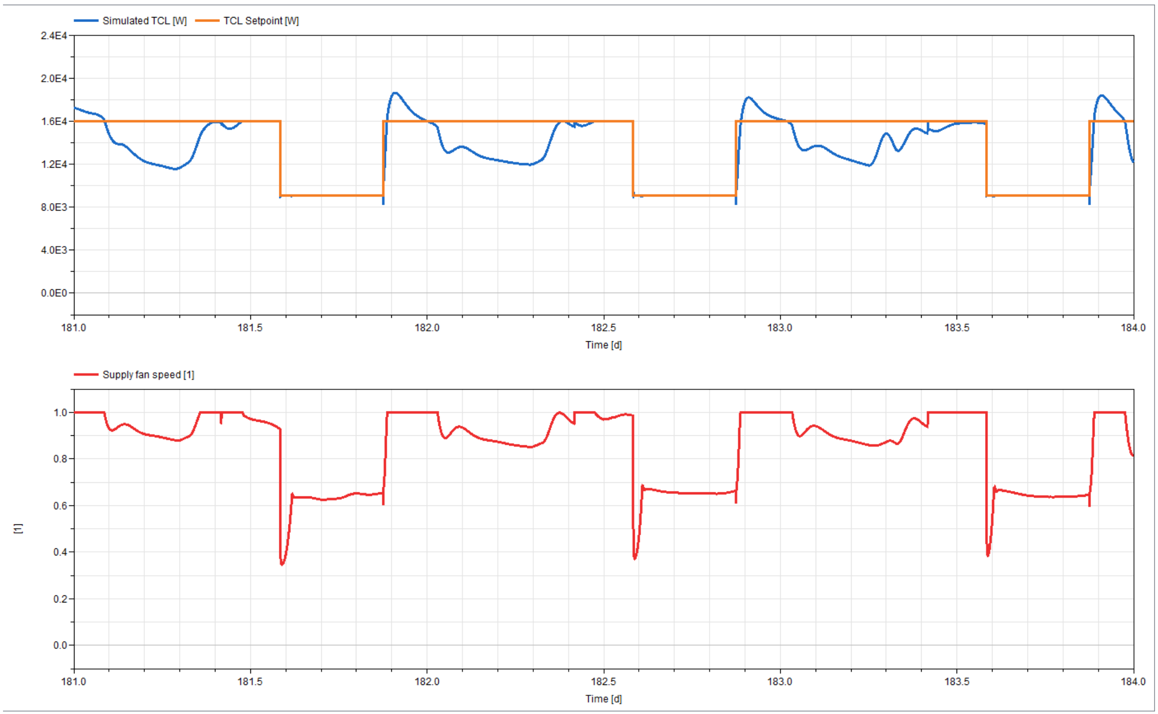

Figure 5.8: EF controller operation for EF Control with Constant Setpoints

Figure 5.9 shows the zone temperatures (ZTs), supply fan airflow rate and fan speed, and duct static pressure (DSP) for the EF control strategy with constant setpoints. An initial transient response is observed during the transition from the conventional ZT feedback control to the EF–DSP cascade control. Another transient response occurs during the change in the cooling load setpoint from 16 kW to 9.07 kW. During these transition periods, the DSP is not maintained at its setpoint. After the demand control period, a demand rebound is observed for approximately 3 hours, during which the supply fan operates at full speed and the DSP is not maintained at its setpoint.

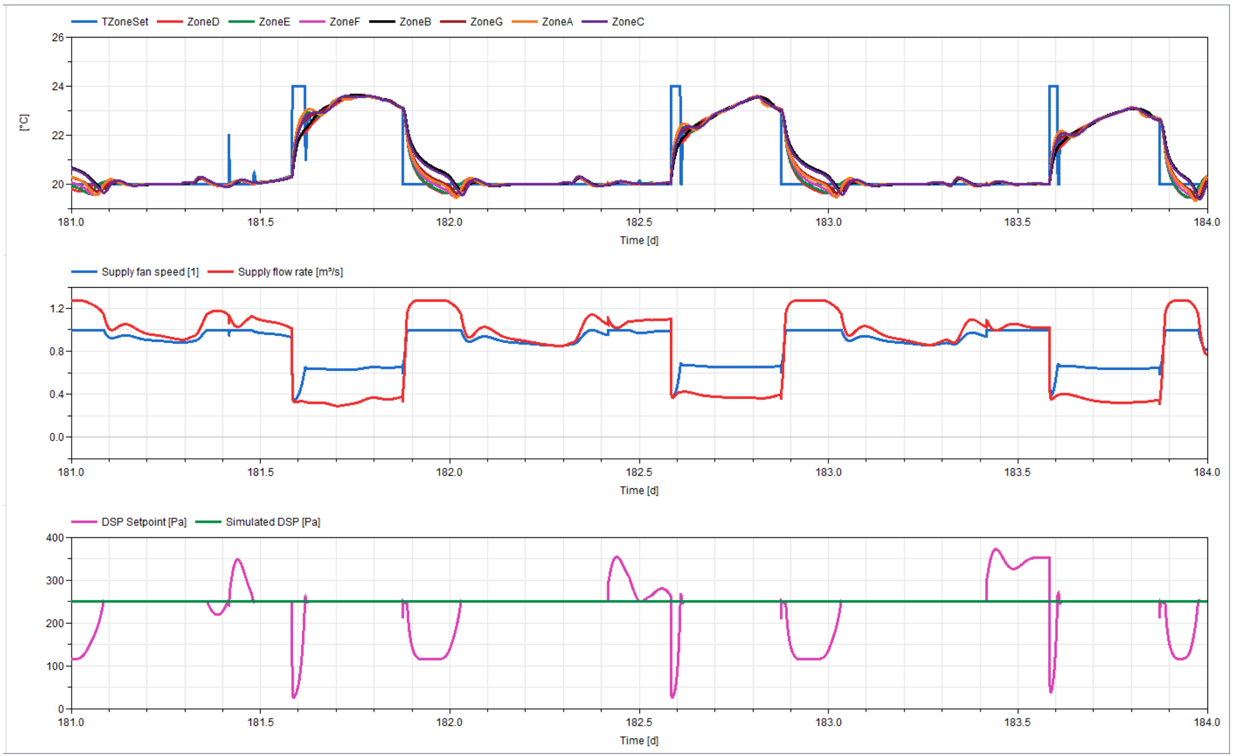

Figure 5.9: Zone temperatures, supply fan airflow rate, fan speed, and duct static pressure for EF control with Constant Setpoints

5.2.3 Optimization-Based EF Control

The Optimization-Based EF Control strategy utilizes the EF–DSP cascade control throughout the simulation period, as described in Table 5.4. Figure 5.10 shows the operation of the Optimization-Based EF Controller and the corresponding supply fan speed response. For the majority of the simulation period, the measured total cooling load (TCL) closely tracks the optimal TCL setpoint.

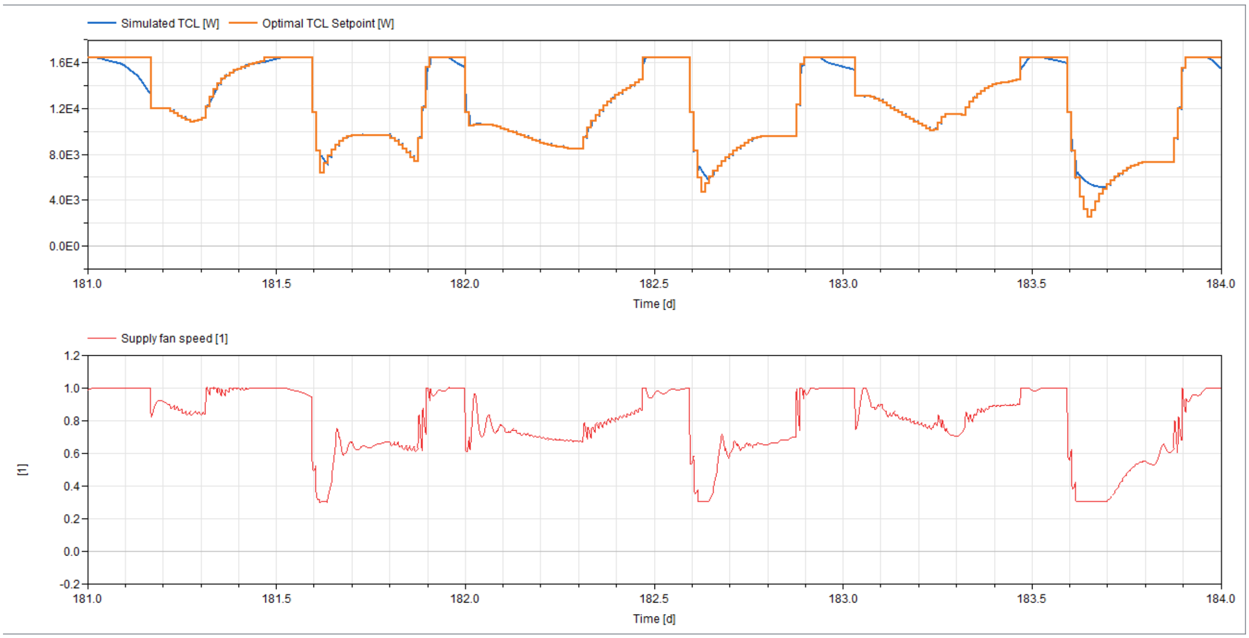

Figure 5.10: EF Controller Operation for Optimization-Based EF Control

Figure 5.11 shows the zone temperatures (ZTs), supply fan airflow rate, fan speed, and duct static pressure (DSP) for the Optimization-Based EF Control strategy. The Optimization-Based EF controller successfully maintains all zone temperatures within the prescribed thermal comfort bounds throughout the simulation period while achieving both precooling and peak load reduction. During the off-peak period, the controller increases the cooling load to precool the building (Figure 5.11), thereby reducing the thermal load entering the peak period. During the peak period, the optimized reduction in the total cooling load (TCL) results in a corresponding reduction in the supply fan airflow rate and fan speed, demonstrating effective load shedding. Transient deviations in the duct static pressure (DSP) are observed during changes in the optimized cooling load setpoint. During these periods, the DSP temporarily deviates from its setpoint before rapidly returning to the desired value, indicating that the DSP cascade controller effectively recovers from transient disturbances.

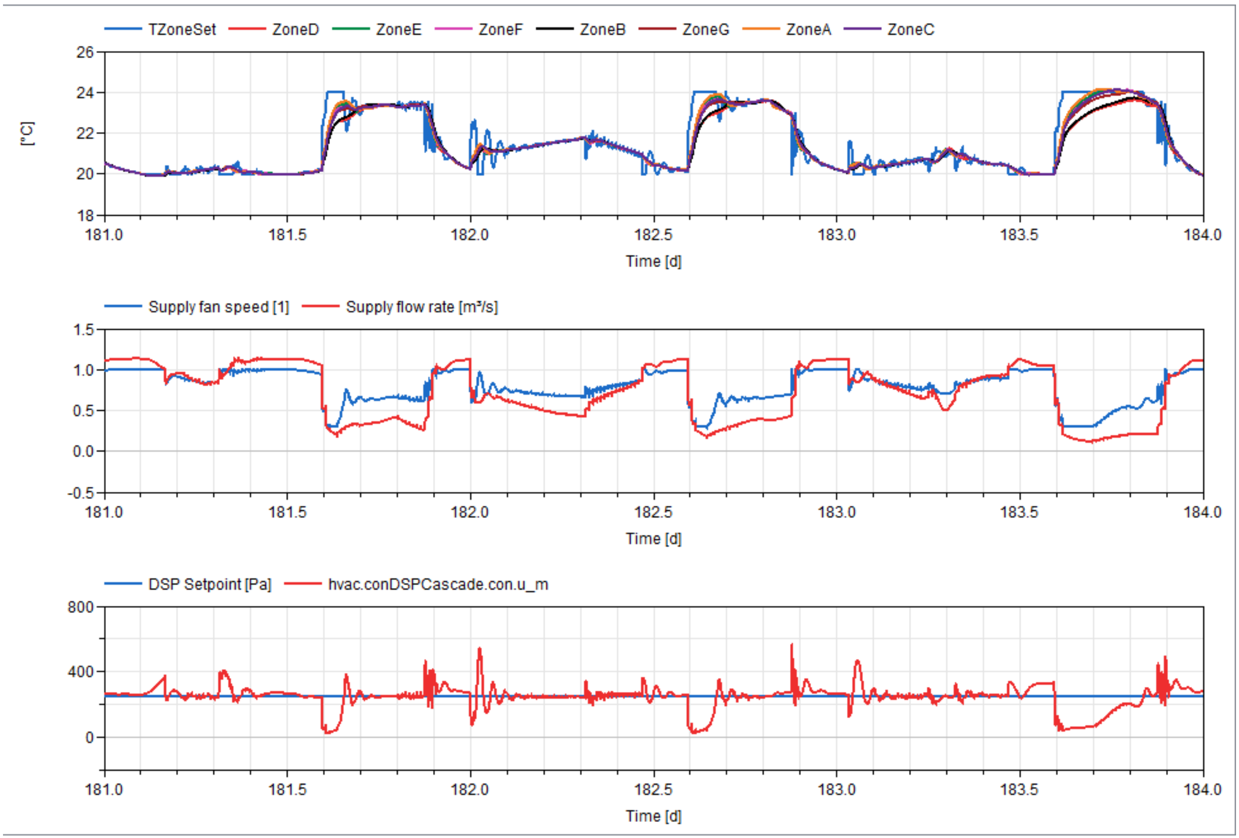

Figure 5.11: ZTs, supply fan airflow rate, and speed, duct static pressure for the Optimization-Based EF Control

5.3 Comparative Analysis and Discussion

This section evaluates the control strategies using different performance indices to compare their cooling energy use and electricity cost. Figure 5.12 shows the total cooling load profile and the average ZT for all three control strategies over the three-day simulation period.

The evaluated demand control strategies result in different cooling load profiles when compared with the baseline strategy. The baseline strategy, which utilizes GTA control during the on-peak period, does not directly regulate the cooling load. Consequently, the cooling load is not maintained at a prescribed setpoint, resulting in the highest cooling demand among the evaluated strategies, with a maximum TCL of 20 kW. During the on-peak period, the average ZT reaches approximately 24°C, corresponding to the upper limit of the thermal comfort range.

The EF control with Constant Setpoints accurately maintained the cooling load setpoints during both the precooling and load-shedding periods. The maximum TCL is 18.63 kW, which occurs after the on-peak period and is associated with the post demand response recovery of the building.

The Optimization-Based EF Control exhibits an adaptive cooling load profile, as the optimization algorithm continuously adjusts the cooling load setpoint while maintaining the ZTs within the prescribed thermal comfort bounds during both the off-peak and on-peak periods. The maximum TCL is 16.52 kW, which is the lowest among all the evaluated strategies. During the off-peak period, the average ZT remains within the prescribed thermal comfort range of 20–22°C, while during the on-peak period it remains between 22°C and 24°C. This indicates that the Optimization-Based EF controller satisfies the thermal comfort constraints throughout the simulation period, demonstrating that the comfort penalty formulation effectively prevents thermal comfort violations.

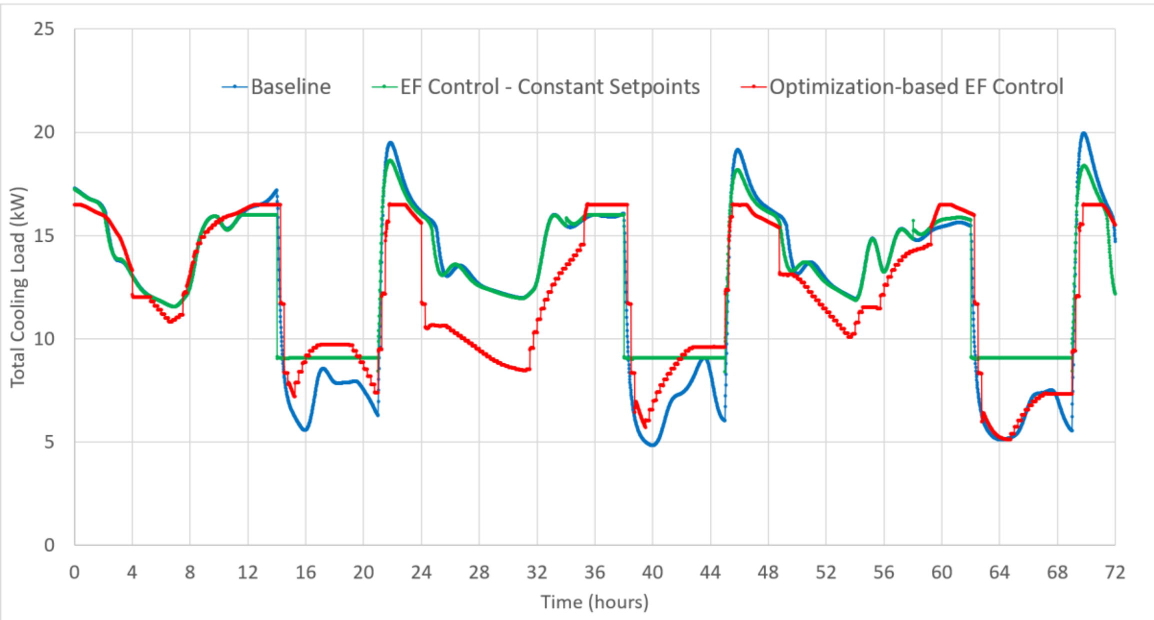

(a) Total Cooling load

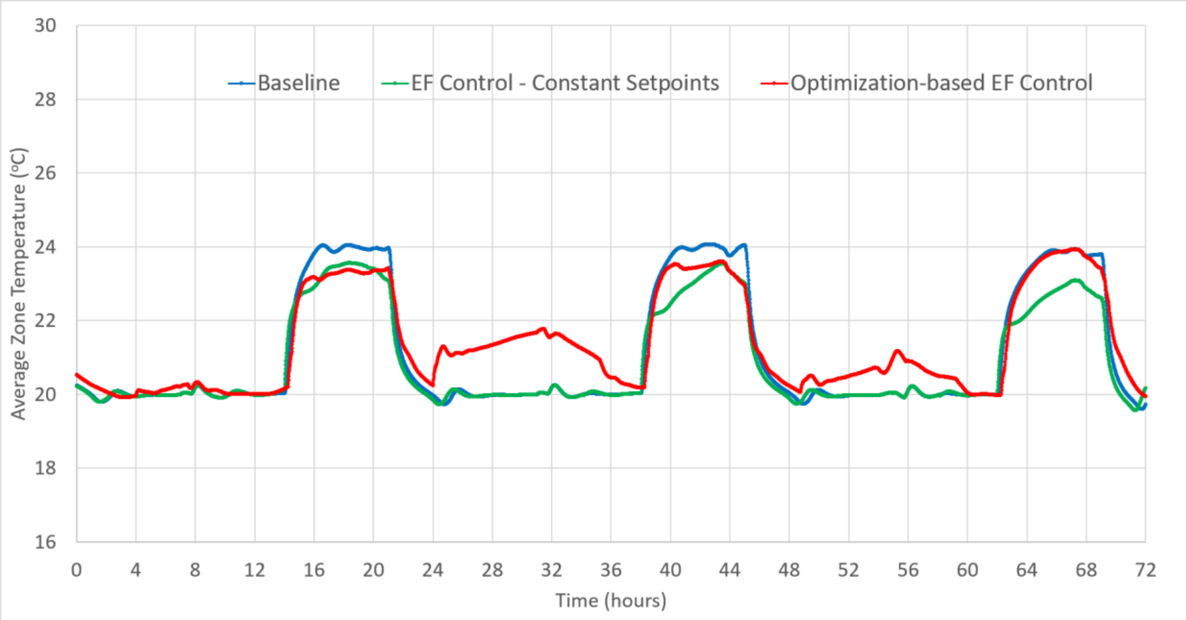

(a) Average ZT

Figure 5.12: Total cooling load profile and Average ZT of the evaluated strategies

The performance indices used to compare the control strategies are described in the following section.

5.3.1 Total Cooling Energy and Electricity Cost

The total cooling energy is used to quantify the overall cooling energy consumed during the simulation period. It is mathematically expressed as:

$$E_{cool}(Kwh) = \int_0^T TCL(t)\, dt$$

where E_{cool} is the total cooling energy (kWh), TCL is the total cooling load (kW), and T is the simulation duration (hours). The electricity cost is determined by first calculating the electrical energy consumption from the cooling load and the time-varying system coefficient of performance (COP(T_{oa})), after which the corresponding time-of-use (TOU) electricity tariff is applied. Table 5.5 shows the total cooling energy for the three-day simulation periods. The primary comparison is between the EF control with Constant Setpoints and Optimization-Based EF control, while the baseline strategy serves as a reference.

Table 5.5: Summary of the total cooling energy for the simulation scenarios

	Total [kWh]	Off-Peak [kWh]	On-Peak [kWh]
Baseline	915	765	150
EF Control with Constant Setpoints	951	758	193
Optimization-Based EF Control	880	702	178

The EF control with Constant Setpoints resulted in the highest total cooling energy consumption of 951 kWh, representing a 4% increase relative to the baseline and corresponding to an additional 36 kWh. It also consumed 71 kWh more cooling energy than the Optimization-Based EF Control, representing a 7.5% increase. This higher energy consumption is attributed to the use of constant cooling load setpoints, which do not adapt to the building's varying thermal conditions.

The Optimization-Based EF Control resulted in the lowest total cooling energy consumption of 880 kWh, as the optimization algorithm continuously adjusted the cooling load setpoint during both the off-peak and on-peak periods. During the off-peak period, the controller allowed the ZT to float within the prescribed thermal comfort bounds instead of maintaining a fixed cooling load or ZT setpoint. This flexibility reduced unnecessary cooling while maintaining thermal comfort. The Optimization-Based EF Control also resulted in the lowest off-peak cooling energy consumption of 702 kWh, whereas the baseline strategy produced the highest off-peak cooling energy consumption of 765 kWh. This difference is attributed to the baseline strategy maintaining the ZT at a fixed setpoint throughout the off-peak period, whereas the Optimization-Based EF Control exploited the allowable thermal comfort range to reduce unnecessary cooling energy consumption while maintaining occupant comfort.

The electricity cost of each control strategy was determined for both the off-peak and on-peak periods. The time-of-use (TOU) electricity tariff used for the comparison is based on Oklahoma's electricity pricing, where the electricity cost is \$0.32/kWh during the on-peak period (2:00 PM to 7:00 PM) and \$0.14/kWh during all other hours. The total electricity costs for the EF Control with Constant Setpoints, and Optimization-Based EF Control are \$39 and \$34, respectively. The EF Control with Constant Setpoints resulted in the highest total electricity cost, across both the on-peak and off-peak periods. Figure 5.13 shows the electricity cost profiles for the EF Control with Constant Setpoints and the Optimization-Based EF Control.

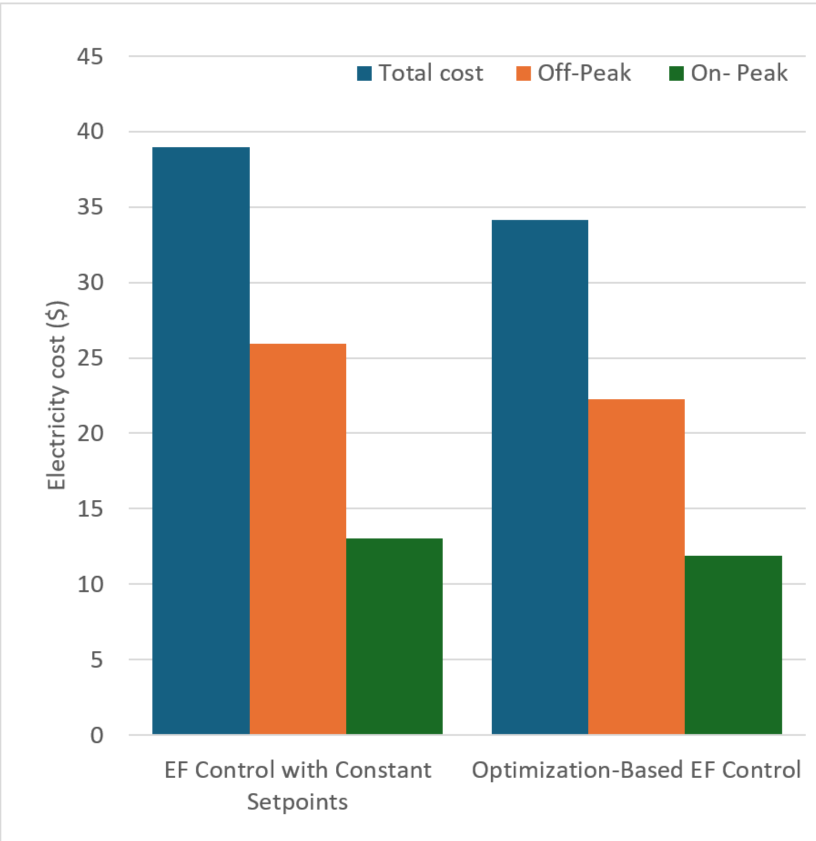

Figure 5.13: Electricity cost for the EF control scenarios

Compared with the EF Control with Constant Setpoints, the Optimization-Based EF Control reduced the total electricity cost by 12.8% over the 72-hour simulation period. During the on-peak period, the Optimization-Based EF Control reduced the electricity cost by 8.7% relative to the EF Control with Constant Setpoints. As shown in Figure 5.8, the EF Control with Constant Setpoints maintained a fixed TCL setpoint throughout the entire peak period. During the off-peak period, the Optimization-Based EF Control reduced the off-peak electricity cost by 15.4% compared with the EF Control with Constant Setpoints. The 12.8% reduction in total electricity cost demonstrates the economic advantage of the Optimization-Based EF Control over the EF Control with Constant Setpoints under a time-of-use electricity tariff. If extended over an entire cooling season, this reduction could result in substantial cumulative cost savings, particularly in locations with high summer cooling loads and significant exposure to peak electricity tariffs.

5.3.2 Rebound Energy

The rebound energy for each scenario was determined to evaluate the smoothness of thermal recovery following the on-peak period. The cumulative rebound energy is calculated from the end of the on-peak period over a defined recovery window, and is mathematically expressed as:

$$E_{rebound} = \int_{21}^{21+X} TCL \, dt$$

where X is the rebound evaluation window. Three recovery windows are considered: 1 hour, 2 hours, and 3 hours after the end of the on-peak period.

Table 5.6 shows the cumulative rebound energy for the different recovery windows. The baseline resulted in the highest rebound energy for the 2-hour and 3-hour recovery windows, while the baseline and the EF Control with Constant Setpoints have the same rebound energy for the 1-hour recovery window.

For comparison of the two EF control strategies, the EF Control with Constant Setpoints resulted in 17.3% higher rebound energy than the Optimization-Based EF Control for the 1-hour recovery window. The difference decreased to 8.6% for the 2-hour recovery window and 7.2% for the 3-hour recovery window. .The reduction in the relative difference as the recovery window increases indicates that the primary benefit of the Optimization-Based EF Control occurs during the initial recovery period immediately following the demand response event, where it suppresses the rebound more effectively than the EF Control with Constant Setpoints.

These results indicate that the Optimization-Based EF Control mitigates the rebound effect by continuously adjusting the cooling load setpoint during the recovery period. Consequently, the optimization-based strategy provides a smoother post-event recovery and reduces rebound energy compared with the EF Control with Constant Setpoints.

Table 5.6: Cumulative rebound energy during different windows

	1 hours [kWh]	2 hours [kWh]	3 hours [kWh]
Baseline	52	108	157
EF Control with Constant Setpoints	52	105	153
Optimization-Based EF Control	43	96	142

5.4 Summary

This study developed, implemented, and evaluated the performance of an Optimization-Based EF-DSP cascade control strategy for demand-flexible HVAC operations. A reduced-order gray-box thermal model was first developed and calibrated using parameter estimation techniques to accurately capture the dynamic thermal response of the building. The identified thermal model was then integrated with a optimization framework and coupled with the calibrated virtual test bed through the BuildingsPy interface and the Modelica-based HVAC model.

The Optimization-Based EF Control Strategy was evaluated against the EF Control with Constant Setpoints and the Baseline GTA control using performance indices, including total cooling energy, electricity cost, and rebound energy. The Optimization-Based EF Control achieved the lowest total cooling energy consumption among all evaluated strategies. Compared with the EF Control with Constant Setpoints, it reduced the total electricity cost by 12.8% over the 72-hour simulation period, with an 8.7% reduction during the on-peak period and a 15.4% reduction during the off-peak period. The 12.8% reduction in total electricity cost demonstrates the economic advantage of the Optimization-Based EF Control under a time-of-use electricity tariff. If extended over an entire cooling season, this reduction could result in substantial cumulative cost savings, particularly in climates with prolonged peak cooling demand. Regarding rebound mitigation, the EF Control with Constant Setpoints resulted in 17.3% higher rebound energy than the Optimization-Based EF Control for the 1-hour recovery window. The difference decreased to 8.6% for the 2-hour recovery window and 7.2% for the 3-hour recovery window, indicating that the Optimization-Based EF Control consistently provided a smoother post-peak thermal recovery.

Overall, these results demonstrate that incorporating optimization into the EF control framework improved both the energy and economic performance of demand response while providing smoother recovery following the on-peak demand response event. The proposed Optimization-Based EF Control provides an effective approach for achieving demand-flexible HVAC operation by simultaneously reducing cooling energy consumption, minimizing electricity cost, maintaining occupant thermal comfort, and mitigating rebound effects. The developed framework demonstrated the potential of integrating optimization-based supervisory control with EF and DSP cascade controls to improve the operational flexibility of commercial HVAC systems.

6. Experimental Validation of the Optimization-Based EF Controller for Demand-Flexible HVAC Operation

This chapter investigates the performance of the Optimization-Based EF Controller on an experimental test bed. The objective of this chapter is to experimentally validate the proposed controller and compare two practical implementation approaches for applying the optimization-derived EF setpoints on an HVAC system. The first EF implementation utilized a schedule of optimal EF setpoints generated offline from the optimization framework coupled with the virtual test bed. The schedule was subsequently implemented on the experimental test bed during a day with a similar, but not identical, outdoor weather profile to evaluate the robustness of the proposed control under realistic operating conditions. The second implementation utilized a regression-based formulation that relates the optimal EF setpoint to the outdoor air temperature for different periods of the day. Both experimental results were compared with the conventional ZT feedback control using performance indices such as normalized cooling load and cooling load factor.

6.1 Experimental Test Bed

The experimental test bed utilized in this study is a fully instrumented single-duct VAV AHU system that serves seven thermal zones in an office building located on a university campus (Figure 3.4). The specifications of the AHU system components are described in detail in Chapters 3 and 4. In Chapter 4, it was demonstrated that utilizing the total cooling load (TCL) as the EF control variable yields the best control performance in terms of response time, evaluated using the settling time, and control accuracy, evaluated using the relative error and mean absolute error. However, implementing this control strategy requires accurate enthalpy measurements derived from both dry-bulb temperature and relative humidity measurements.

To achieve this, duct-mounted humidity sensors were installed in the supply air, return air, and mixed air ducts of the AHU. These measurements, together with the corresponding air temperatures, are used to determine the air enthalpy. The measured total cooling load (TCL) for the EF controller is then calculated using the heat balance equation, which relates the supplied air flow rate and the enthalpy difference between the mixed air and the supply air. Figure 6.1 shows the Invensys Building Automation System (BAS) interface showing the installed humidity sensor points.

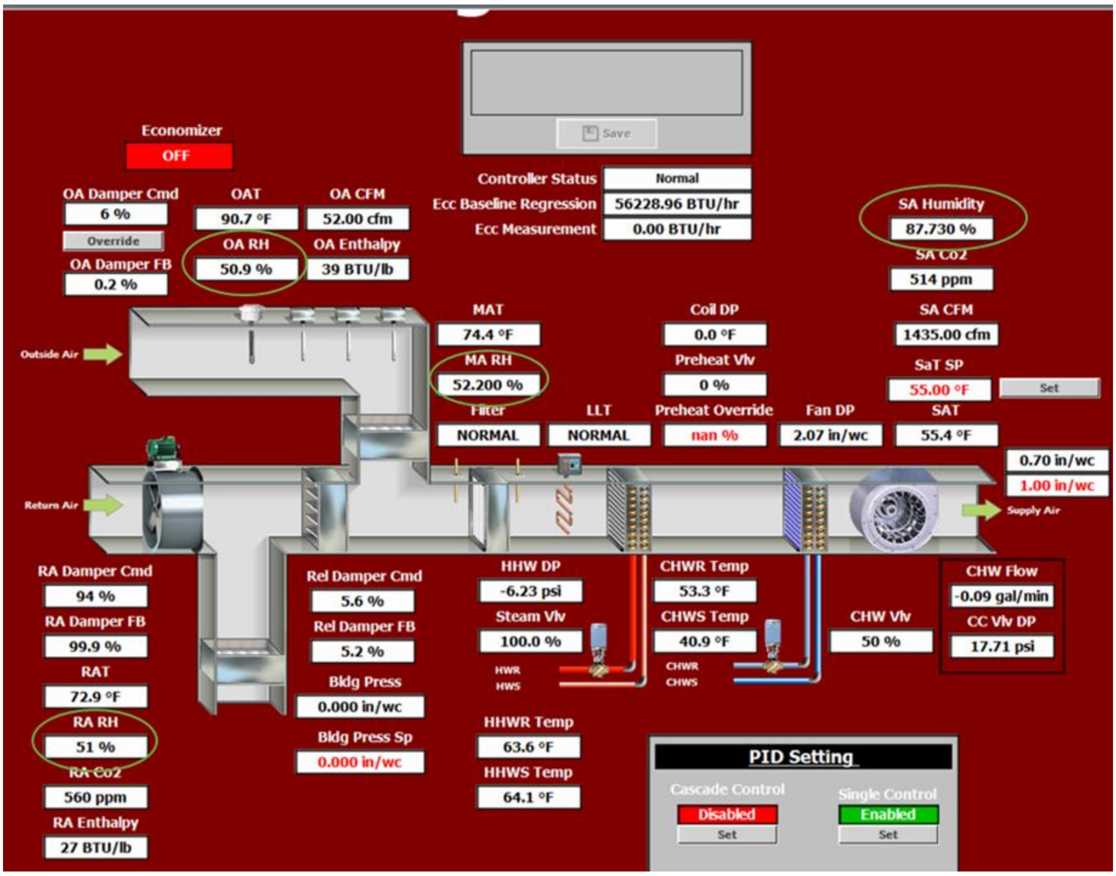

Figure 6.1: Invensys interface after installation of the humidity sensors

6.2 Experimental Test Scenarios

6.2.1 Conventional Control

This control strategy utilizes ZT feedback control and serves as the reference strategy for comparison. Figure 6.2 shows the conventional control loops implemented in the experimental test bed. The control sequence proceeds from the terminal boxes to the cooling coil and can be summarized as follows: (i) The terminal box (TB) dampers are modulated to maintain the zone temperature (ZT) at its setpoint. (ii) The supply fan speed is modulated through the variable frequency drive (VFD) to maintain the duct static pressure (DSP) at its setpoint. (iii) The cooling coil valve is modulated to maintain the supply air temperature (SAT) at its setpoint.

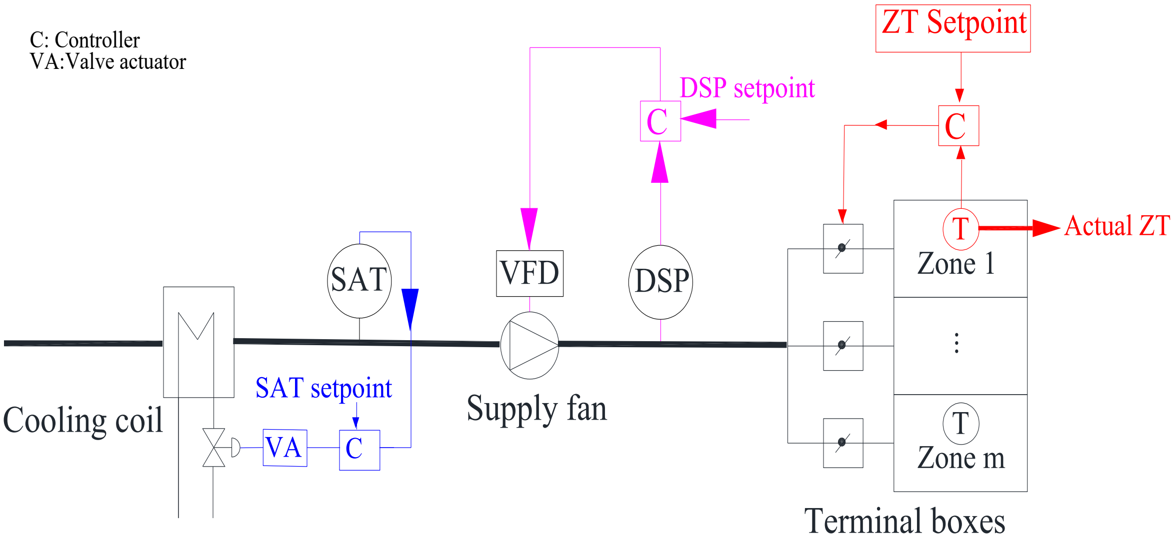

Figure 6.2: ZT feedback control

6.2.2 Schedule-Based EF Control

This Schedule-Based EF control test utilizes a time-varying TCL setpoint generated offline from the optimization framework. Figure 6.3 illustrates the configuration of the schedule-based EF control implemented in this study. The experiment was conducted on a summer day, and the DSP cascade control was not integrated into this control strategy.

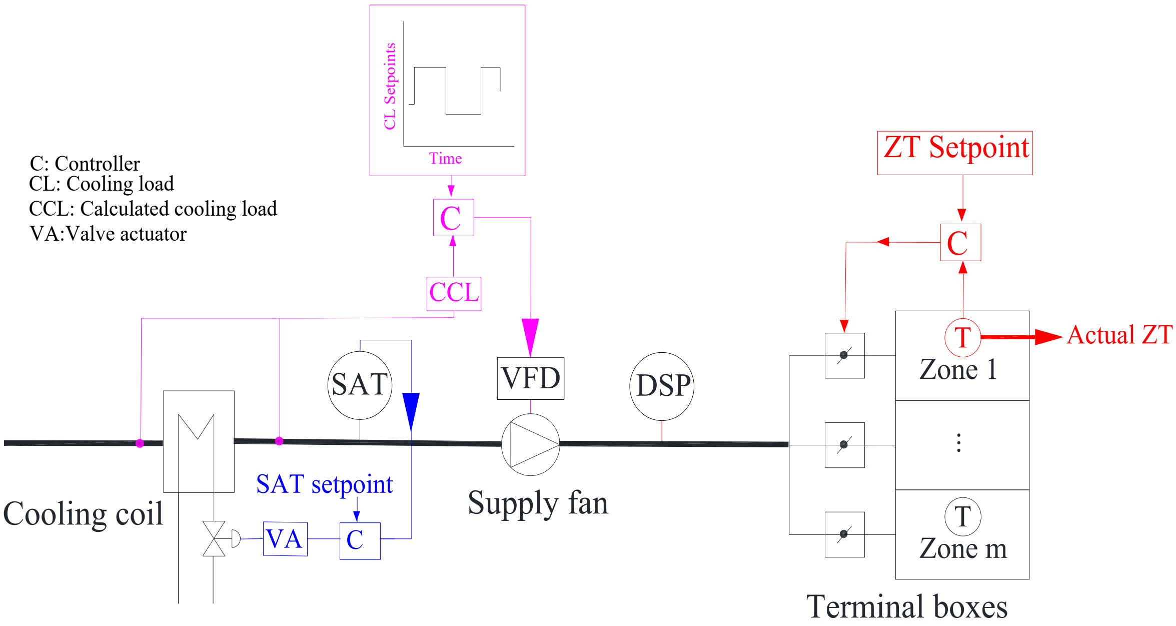

Figure 6.3: Schedule-Based EF Control

Figure 6.4 shows the operation of the EF controller and the corresponding supply fan speed response. During the early hours of the day, the TCL setpoint gradually increases. During the precooling period, the building experiences increased cooling demand, as indicated by the higher TCL setpoint. During the on-peak period, the TCL setpoint is reduced to achieve load shedding. Overall, the supply fan closely tracks the varying TCL setpoints, with the measured cooling load closely following the TCL setpoints for the majority of the test period. This demonstrates that the EF controller is well tuned, although minor oscillations are observed during the load-shedding period.

During the night and early morning hours, the supply fan modulates in response to the TCL setpoint. During the precooling period, the supply fan operates at its maximum speed (100%) to satisfy the increased cooling demand. As the TCL setpoint is reduced during the load-shedding period, the supply fan speed decreases accordingly and subsequently recovers after the peak period.

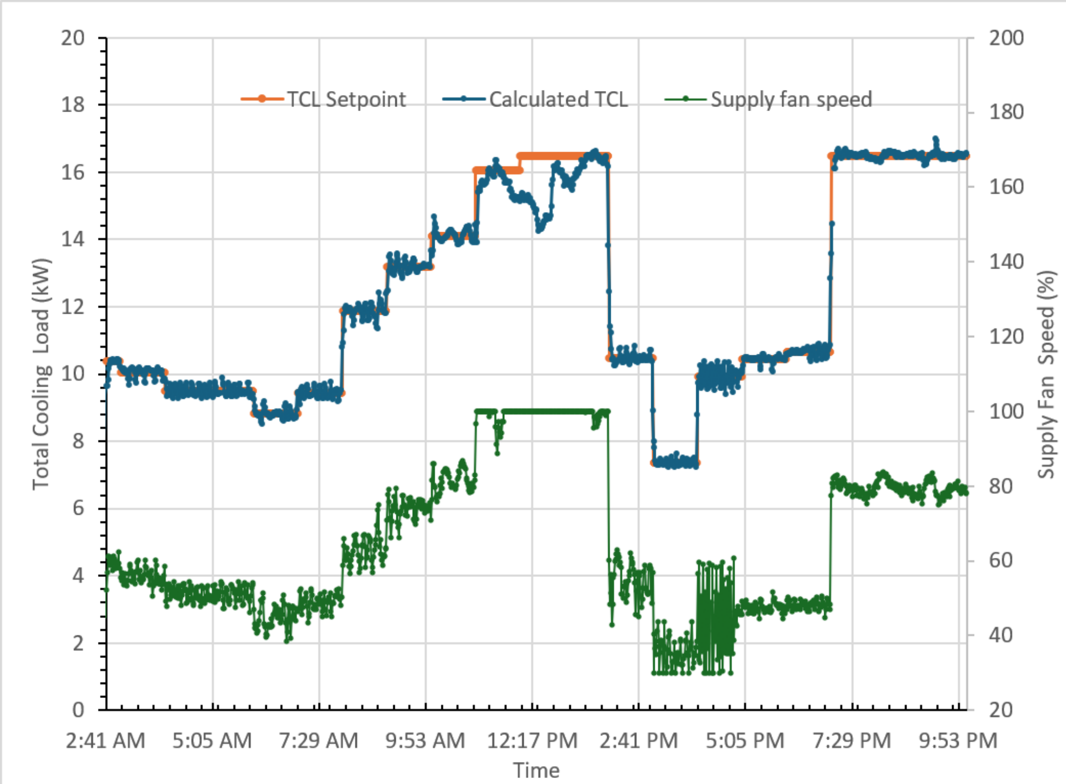

Figure 6.4: EF controller operation during the Scheduled based EF test

6.2.3 Adaptive EF Control

This control strategy utilizes a regression-based formulation to determine the TCL setpoint as a function of the outdoor air temperature. Depending on the time of day, the measured outdoor air temperature is used to estimate the appropriate TCL setpoint for the EF controller. Separate regression equations were developed from the optimization results presented in Chapter 4 for four operating periods: 12:00 AM–10:00 AM, the precooling period (10:00 AM–2:00 PM), the load-shedding period (2:00 PM–9:00 PM), and the post-load-shedding period (9:00 PM–11:59 PM). Figure 6.5 shows the regression equations developed for each operating period.

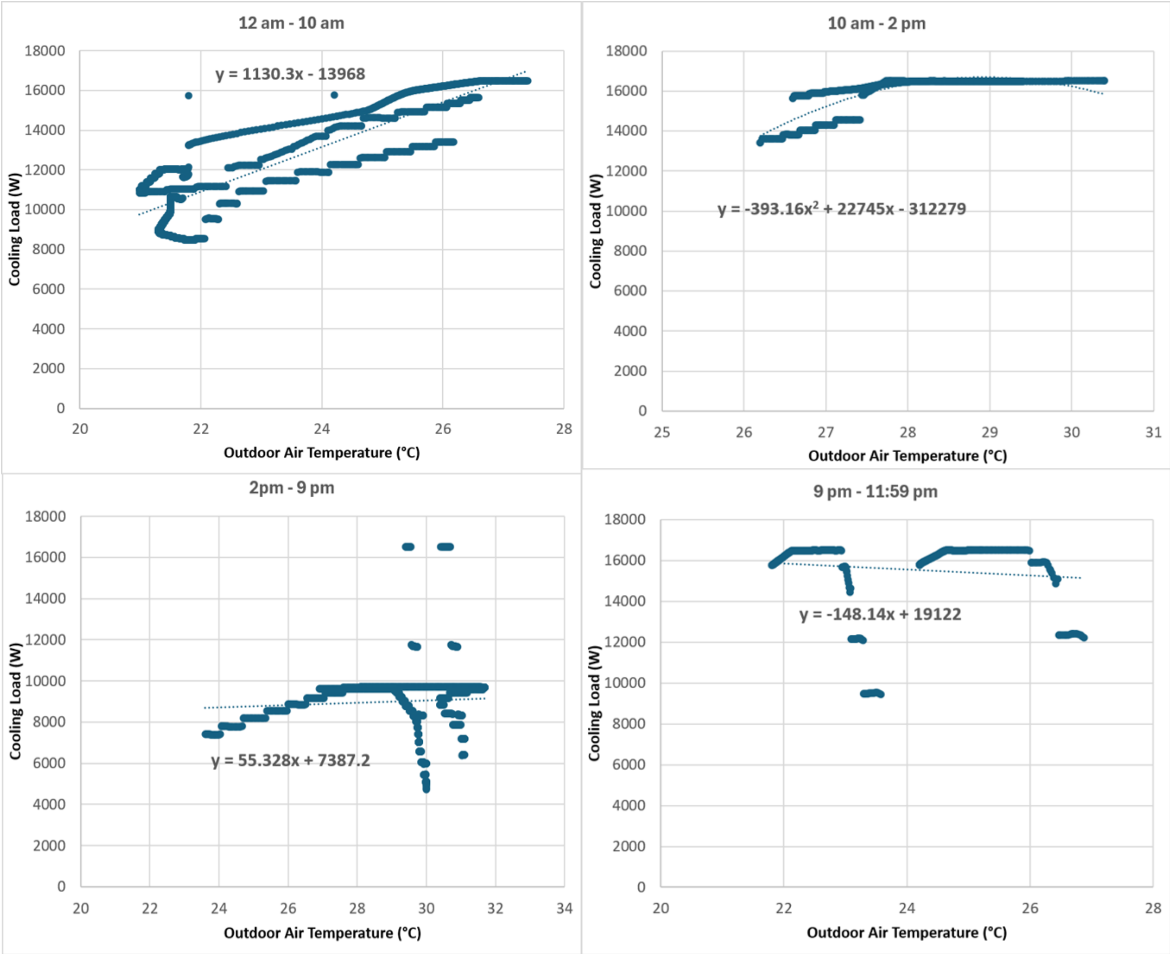

Figure 6.5: Regressed equation at different periods of the day

Figure 6.6 shows the schematic of the adaptive EF control implemented for the experimental test. Figure 6.7 illustrates the operation of the EF controller using the adaptive regression-based formulation and the corresponding supply fan speed response. For the majority of the test period, the measured total cooling load (TCL) closely tracks the estimated TCL setpoint, demonstrating that the EF controller effectively follows the adaptive setpoint generated from the regression equations.

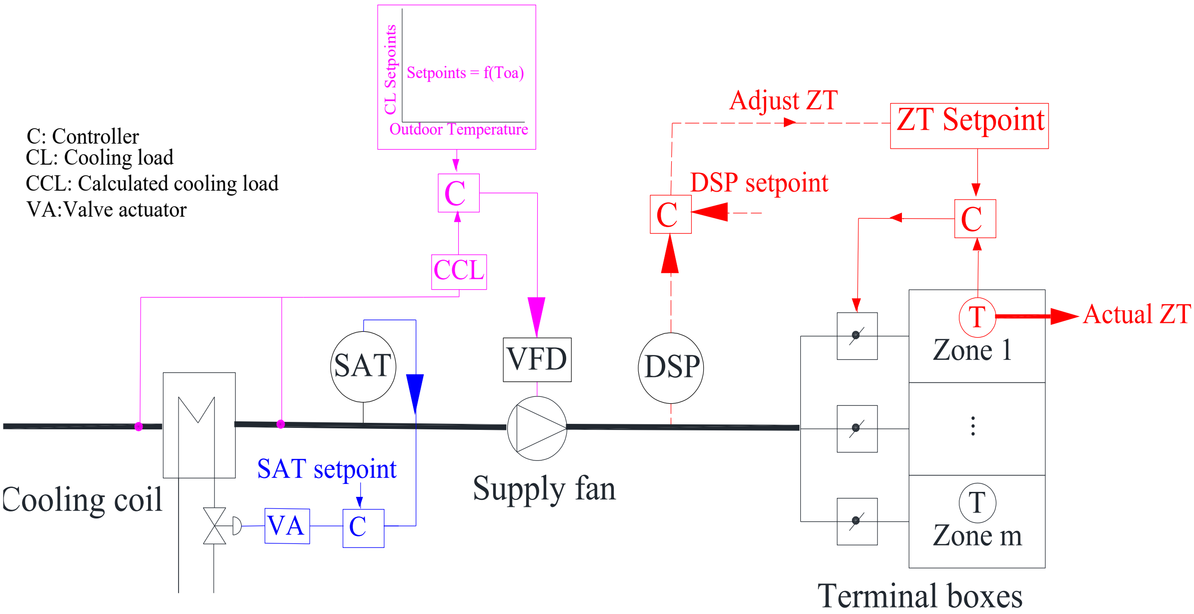

Figure 6.6: Adaptive EF Control

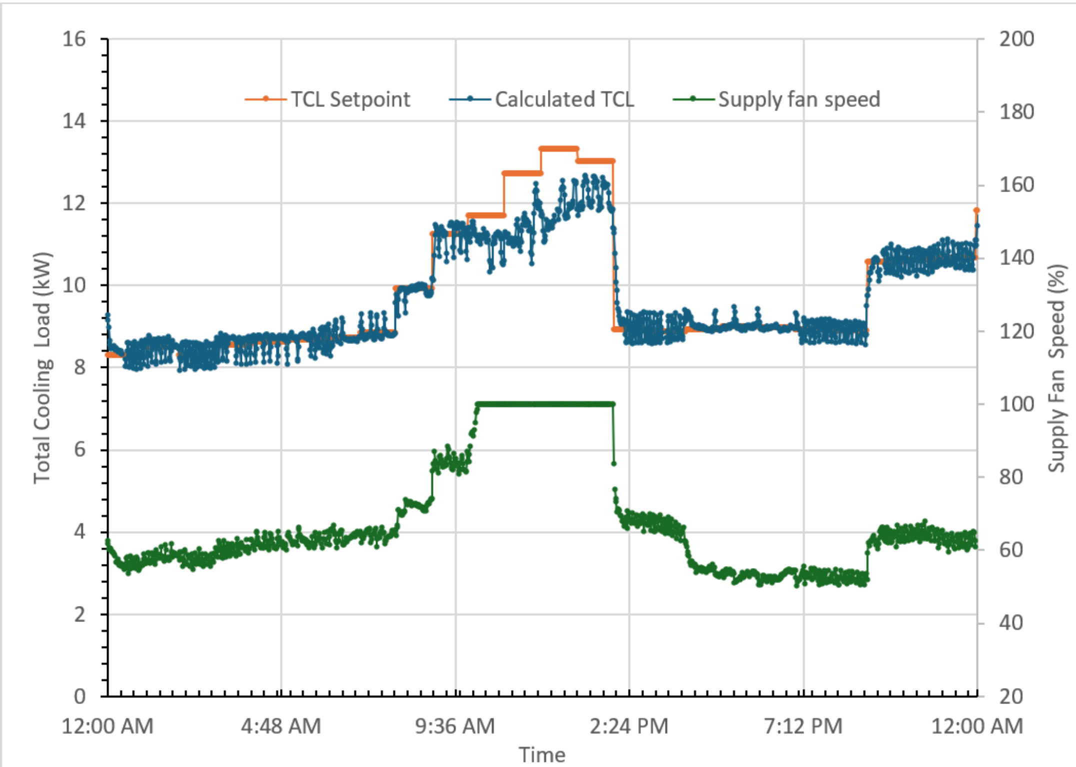

Figure 6.7: EF controller operation during the Adaptive EF Control test

6.3 Analysis and Discussion

6.3.1 Normalized Cooling Load

Figure 6.8 compares the normalized cooling load profiles of the Conventional ZT feedback control, Schedule-Based EF Control, and Adaptive EF Control. To account for differences in outdoor weather conditions between the experimental test days, the cooling load for each strategy is normalized by the mean TCL of its respective test day. Consequently, a normalized cooling load (NCL) greater than unity indicates cooling demand above the daily average, whereas values less than unity indicate cooling demand below the daily average. The NCL is mathematically expressed as

$$NCL = \frac{TCL(t)}{\overline{TCL}}$$

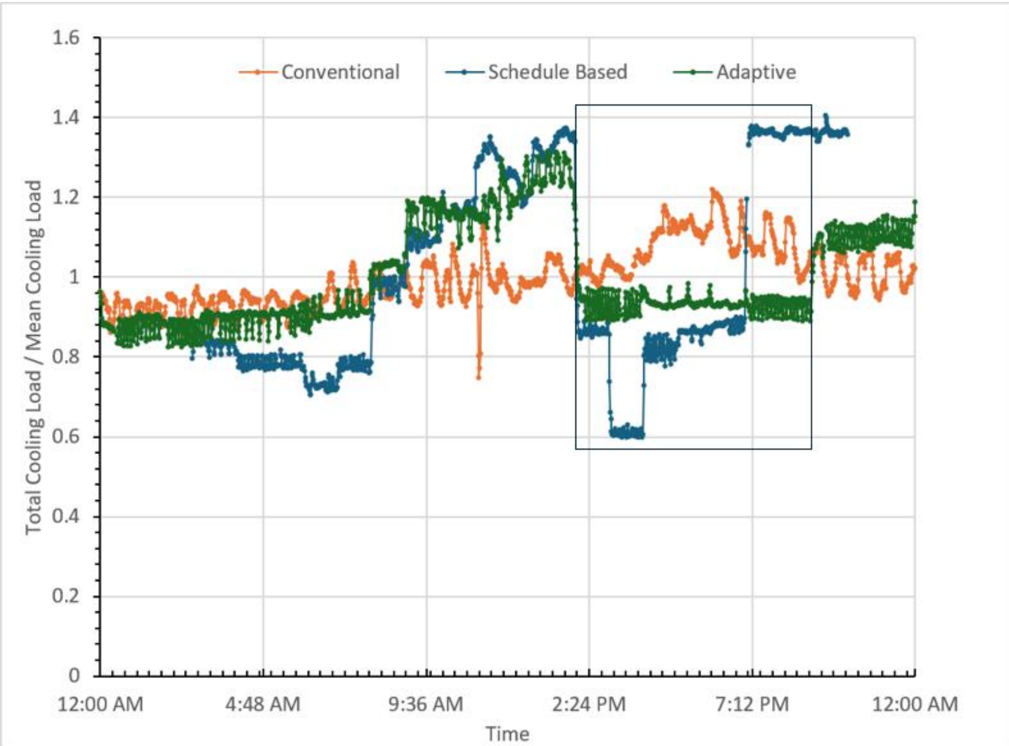

Figure 6.8: Normalized cooling load profile

The Conventional reference control maintained a relatively uniform cooling load throughout the day, with the NCL remaining close to unity for most of the occupied period, with a maximum NCL of 1.2. The gradual increase during the afternoon reflects the increasing building cooling demand as outdoor conditions become more severe. The Schedule-Based EF Control exhibits a distinct load-shifting and precooling behavior. During the early morning period, the normalized cooling load remains below unity, indicating reduced cooling demand before the precooling period. As precooling begins, the normalized cooling load increases rapidly to approximately 1.3–1.4, demonstrating aggressive thermal energy storage before the demand-response event. During the scheduled load-shedding period (2:00 PM–7:00 PM), the normalized cooling load decreases by approximately 37%, to 0.6–0.9, indicating a substantial reduction in cooling demand relative to the daily average. However, immediately after the end of the load-shedding period, the NCL increases sharply to approximately 1.33, representing a pronounced rebound. This rapid recovery indicates that a significant portion of the deferred cooling demand is recovered immediately after the demand-response event.

Although the normalized cooling load during the load-shedding period is slightly lower for the Schedule-Based EF Control than for the Adaptive EF Control, the two controllers operate over different demand-response durations. The Schedule-Based EF Control performs load shedding for 5 hours (2:00 PM–7:00 PM), whereas the Adaptive EF Control maintains reduced cooling demand for 7 hours (2:00 PM–9:00 PM). Consequently, the lower NCL achieved by the Schedule-Based EF Control should be interpreted together with its substantially larger rebound immediately after the event. In contrast, the Adaptive EF Control sustains load reduction over a longer period while avoiding the abrupt post-event recovery observed in the Schedule-Based EF Control.

Overall, the normalized cooling load profiles demonstrate the different operating characteristics of the three control strategies. The Conventional controller follows the building cooling demand with no demand flexibility. The Schedule-Based EF Control effectively shifts cooling demand away from the demand-response period but exhibits an aggressive post-event rebound due to its predetermined TCL schedule. In contrast, the Adaptive EF Control provides a more balanced demand response by continuously adjusting the TCL setpoint according to outdoor conditions, enabling sustained load reduction over a longer demand-response period while significantly mitigating rebound.

6.3.2 Cooling Load Factor

The Cooling Load Factor (CLF) of the evaluated control strategies is determined to assess the overall shape of the cooling demand profile. The CLF is used to quantify how uniformly the cooling load is distributed over the evaluation period and is defined as the ratio of the average cooling load to the maximum cooling load.

CLF is mathematically expressed as the ratio of the average TCL and the maximum TCL.

$$CLF(\%) = \frac{\overline{TCL}}{TCL_{max}} \times 100$$

A higher CLF indicates a more uniform cooling demand profile, characterized by reduced peak cooling demand and improved demand flexibility. Conversely, a lower CLF indicates that the cooling demand is concentrated over shorter periods, resulting in larger demand peaks and less effective load distribution.

Table 6.1: Summary of Cooling load factor

Control	CLF (%)
Conventional	82
Schedule-Based EF	71
Adaptive EF	76

Table 6.1 shows the summary of the CLF. The Conventional control, which serves as the reference, has the highest CLF of 82%, reflecting its relatively uniform cooling demand profile in the absence of demand-response operation. Among the two EF control strategies, the Adaptive EF Control achieved a higher CLF of 76% compared with 71% for the Schedule-Based EF Control. The higher CLF indicates that the Adaptive EF Control maintains a more uniformly distributed cooling demand throughout the evaluation period, avoiding the pronounced rebound peak observed in the Schedule-Based EF Control. This observation is consistent with the lower rebound energy and smoother post-demand-response recovery achieved by the Adaptive EF Control.

6.4 Summary

This chapter experimentally validated the proposed Optimization-Based EF Controller on a fully instrumented VAV AHU experimental test bed and compared two practical implementation approaches for applying optimization-derived EF setpoints. Both implementations successfully regulated the total cooling load in response to the setpoints, with the measured TCL closely tracking the TCL setpoint throughout the experiments. This confirms the feasibility of implementing optimization-derived supervisory control for the EF controller. A comparison of the two implementations showed that the Adaptive EF Control consistently outperformed the Schedule-Based EF Control. The Adaptive EF Control exhibited a smoother cooling load profile, lower rebound energy, and a higher CLF than the Schedule-Based EF Control, indicating more uniform cooling load distribution and more stable post-demand-response recovery. The normalized cooling load profiles further demonstrated that the adaptive strategy sustained load reduction over a longer demand-response period while avoiding the pronounced rebound observed with the scheduled implementation.

In summary, the experimental results validate the proposed Optimization-Based EF Controller as a practical approach for demand-flexible HVAC operation. The Adaptive EF implementation demonstrates that optimization-derived setpoints generated offline can be effectively translated into real-time supervisory control without requiring online optimization.

7. Conclusions and Future Work

This dissertation addressed the shortcomings of existing HVAC demand control strategies by developing and evaluating advanced control strategies capable of directly and precisely regulating the cooling load to provide on-demand load shifting and load shedding while minimizing the negative impact of demand control on indoor thermal comfort. Existing demand control strategies rely primarily on Global Temperature Adjustment (GTA) control and strategies such as duct static pressure setpoint reduction, supply fan speed limiting, and supply air temperature (SAT) reset. These approaches result in slow response, inaccurate demand reduction, uneven distribution of the demand control burden across thermal zones, and the inability to guarantee precise demand control. To overcome these limitations, this dissertation proposed novel control strategies that enable direct cooling load regulation while minimizing the adverse impact of demand control on occupant thermal comfort.

The first contribution of this dissertation is the development and experimental validation of the Energy Feedback (EF) Control and the Duct Static Pressure (DSP) Cascade Control. The proposed EF Control directly regulates the cooling load by modulating the supply fan speed, enabling fast, precise, and direct demand control. The proposed DSP Cascade Control maintains the duct static pressure at its setpoint by uniformly adjusting the zone temperature setpoints within prescribed comfort limits, thereby distributing the reduced cooling load evenly across all thermal zones. Experimental evaluation on a fully instrumented VAV AHU experimental test bed demonstrated the feasibility of implementing both controllers and confirmed that they successfully achieved their intended control objectives under experimental operating conditions.

The second contribution is the development and comprehensive evaluation of an integrated EF–DSP Cascade Control using a calibrated Modelica-based virtual test bed. Four AHU demand control strategies were developed and evaluated under identical operating conditions. The results demonstrated that integrating the DSP Cascade Control with the EF Control significantly improved demand control performance by providing faster response, higher demand control accuracy, and more uniform distribution of the reduced cooling load across all thermal zones. The integrated EF–DSP Cascade Control successfully achieved precise load shedding while minimizing the adverse impact of demand control on indoor thermal comfort.

The third contribution is the development of an Optimization-Based EF Controller for demand-flexible HVAC operation. A reduced-order gray-box thermal model was developed and calibrated for control-oriented optimization and integrated with the calibrated virtual test bed. The optimization framework dynamically determined cooling load setpoints based on weather conditions and the building's daily load profile. Compared with the baseline demand control strategy and the EF–DSP Control with constant cooling load setpoints, the proposed Optimization-Based EF–DSP Cascade Control reduced cooling energy consumption, minimized electricity cost, mitigated rebound effects, and maintained occupant thermal comfort within the prescribed comfort bounds. These results demonstrated the effectiveness of optimization-based supervisory control for enhancing demand-flexible HVAC operation.

The fourth contribution is the experimental validation of the Optimization-Based EF Controller and the evaluation of two practical implementation approaches for applying optimization-derived cooling load setpoints on an HVAC system. Both the Schedule-Based EF Control and the Adaptive EF Control successfully regulated the cooling load in accordance with the optimization-derived setpoints, confirming the feasibility of implementing optimization-based supervisory control on a real HVAC system. The Adaptive EF Control provided smoother cooling load regulation, lower rebound energy, and more effective demand response performance than the Schedule-Based EF Control, demonstrating its potential for practical implementation.

Overall, this dissertation demonstrated that the proposed EF Control, DSP Cascade Control, and Optimization-Based EF–DSP Cascade Control provide an effective framework for demand-flexible HVAC operation. Together, these control strategies enable fast, direct, and precise demand control through direct regulation of the cooling load, distribute the reduced cooling load evenly across thermal zones to preserve occupant thermal comfort, and dynamically determine optimal cooling load setpoints that reduce cooling energy consumption, minimize electricity cost, and mitigate rebound effects. Collectively, the simulation and experimental results demonstrate that the proposed control framework achieves accurate demand control, improves occupant thermal comfort, reduces operating costs, and provides a practical, scalable, and effective approach for demand-responsive control of commercial HVAC systems

7.1 Limitations

This dissertation focused on demand control on the air side of the HVAC system through the development of the Energy Feedback (EF) Control and Duct Static Pressure (DSP) Cascade Control. The proposed control strategies were developed and validated on a single VAV AHU experimental test bed and a calibrated virtual test bed, with demand flexibility achieved through direct regulation of the AHU cooling load. Although the proposed framework effectively controls the air-side cooling demand, it does not extend demand control to the chilled water plant, including the chillers, chilled water pumps, cooling towers, and other water-side HVAC components. Consequently, the interaction between the proposed air-side control strategies and the operation of the chilled water system was not investigated.

Furthermore, this study primarily evaluated the performance of the proposed control strategies in terms of demand control accuracy, thermal comfort, cooling energy consumption, electricity cost, and rebound mitigation. The long-term impact of continuous cooling load modulation on HVAC equipment was not investigated. Frequent modulation of the supply fan speed, terminal box dampers, chilled water control valves, pumps, and other mechanical components may influence equipment wear, actuator cycling, maintenance requirements, component lifespan, and overall system reliability.

7.2 Future Work

Long-Term Equipment Impact and Life-Cycle Cost

Future work should evaluate the long-term impact of the proposed EF–DSP Cascade Control strategy on HVAC equipment performance and reliability. Although the EF Control provides fast and precise demand control through continuous modulation of the supply fan speed, the long-term effects of frequent modulation on the supply fan, terminal box dampers, and other mechanical components were not investigated in this dissertation. Future research should examine the effects of the proposed control strategy on equipment wear, actuator cycling, maintenance requirements, component lifespan, and overall system reliability. In addition, future research should conduct a comprehensive life-cycle cost analysis to quantify the economic benefits of the proposed control strategies. Such an analysis should consider capital investment, instrumentation and implementation costs, operational energy savings, maintenance costs, equipment replacement costs, and life-cycle performance under different building types and climatic conditions. This would provide a more comprehensive assessment of the long-term economic viability of the proposed control framework for commercial HVAC systems.

Integration of Water-Side HVAC Systems

Future research should extend the proposed control framework by integrating the EF–DSP Cascade Control with the operation of the chilled water plant, including the chillers, chilled water pumps, and cooling towers. This integration could coordinate the operation of the entire cooling plant with air-side demand control, further improving energy efficiency, reducing electricity cost, and enhancing building-level load shifting and load shedding capability.

Implementation of the Optimization-Based EF Controller

Future work should implement the Optimization-Based EF Controller within a Building Automation System by developing an online optimization framework that automatically determines the optimal cooling load setpoint in real time. To maintain optimization accuracy under changing building operating conditions, weather conditions, and occupancy patterns, the framework should continuously update the building thermal model and optimization parameters online. This would enable fully autonomous supervisory control, eliminate the need for offline optimization, and improve the long-term robustness and performance of the proposed control framework. In addition, future research should investigate robust and fault-tolerant control strategies that account for measurement uncertainty, communication delays, missing data, and sensor faults, particularly because the EF Control relies on cooling load calculations derived from multiple sensor measurements. Addressing these challenges would improve the reliability and practical deployment of the proposed optimization framework.

Long-Term Field Demonstration and Validation

While the proposed control strategies were experimentally validated on a fully instrumented VAV AHU test bed and evaluated using a calibrated Modelica-based virtual test bed, future work should extend this validation to different building types, climatic regions, occupancy patterns, and operating conditions to establish their robustness, scalability, and generalizability. In addition, long-term field demonstrations over entire cooling seasons in occupied commercial buildings should be conducted to further verify the sustained performance of the proposed control strategies under diverse utility rate structures and grid programs, including time-of-use electricity pricing, demand response programs, demand charges, grid service participation, and carbon-intensity-based electricity signals.

7.3 Publications

In addition to the research presented in this dissertation, I have contributed to several funded research projects that have resulted in peer-reviewed journal and conference publications. A list of publications and manuscripts completed during my doctoral studies at the University of Oklahoma is provided below:

<u>Published</u>

(1) **Nurayn Tiamiyu**, Kevwe Ejenakevwe, Philani Hlanze, Li Song. (2026). Evaluating the performance of ground source heat pumps under different vertical borehole ground heat exchanger design methods using Modelica-based dynamic modeling and simulation. *Science and Technology for the Built Environment*, *32*(1), 130–147 (Tiamiyu et al., 2026).

(2) **Nurayn Tiamiyu**, Junke Wang, Zufen Wang, Li Song, Gang Wang (2024). Occupancy Sensor-enabled Demand Control Ventilation Using Virtual Outdoor Air Flow Meters in Air Handling Units. *Building and Environment*. *111501* (Tiamiyu et al., 2024).

(3) **Nurayn Tiamiyu**, Kevwe Ejenakevwe, Li Song (2024). Performance Analysis of Vertical Borehole Ground Heat Exchanger Design Methods using Modelica-Based Modeling and Simulation. *ASHRAE Transactions 130, 464-473* (Tiamiyu et al., 2024).

(4) Kevwe Ejenakevwe**, Nurayn Tiamiyu**, Rodney Hurt, Gang Wang, Li Song (2026). Impact of Unmeasurable Building Load Disturbances on the Performance of Smart Thermostat-Based Fault Detection and Diagnosis Methods. *Energy and Building* (Ejenakevwe et al., 2026)

(5) Gang Wang, Junke Wang, **Nurayn Tiamiyu**, Zufen Wang, Li Song (2023). Development and Investigation of Advanced HVAC Demand Control. *ASHRAE Transactions, 129, 176-183* (Wang et al., 2023).

(6) Gang Wang, Junke Wang, **Nurayn Tiamiyu**, Zufen Wang, Li Song (2023). Loose Belt Fault Detection and Virtual Flow Meter Development Using Identified Data-driven Energy Model for Fan Systems. *Journal of Sustainability 2023, 15, 12113 (Wang et al., 2023b).*

(7) Rodney Hurt, Kevwe Ejenakevwe**, Nurayn Tiamiyu**, Gang Wang, Li Song. Study of Different Single-Pipe District Geothermal Heating and Cooling System Designs Using Modelica-Based Simulation Test Bed. *15th IEA Heat Pump Conference at Vienna, May 26- 29, 2026*

<u>Under- Review and In- Preparation</u>

(8) **(***Under Review***) Nurayn Tiamiyu**, Gang Wang, Li Song. Performance Comparison of Four Air Handling Unit Control Strategies for Building Demand Control and Thermal Comfort Using a Modelica-Based Virtual Test Bed. *Submitted to Science and Technology for the Built Environment (June 2026),* STBE-0179-2026

(9) **(***In Preparation***)** **Nurayn Tiamiyu**, Gang Wang, Li Song. Development and Validation of an Optimization-Based Energy Feedback and Duct Static Pressure Cascade Control for Building Demand Flexibility and Thermal Comfort

8. Appendix

8.1 Supplementary Results for Chapter 4

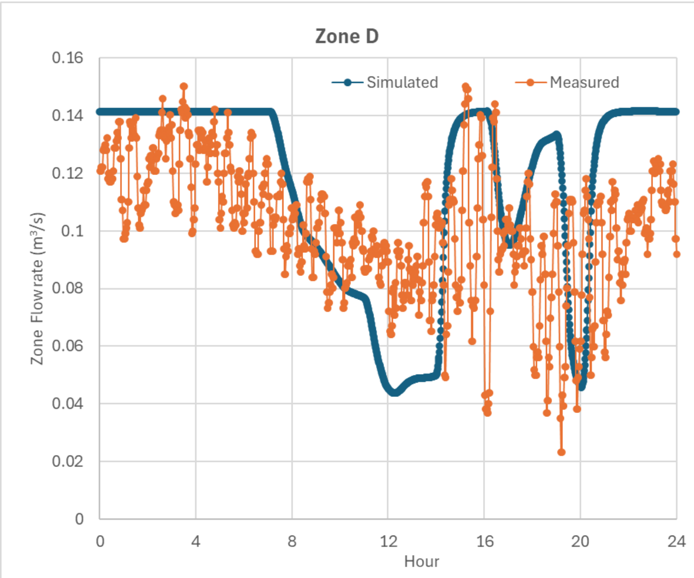

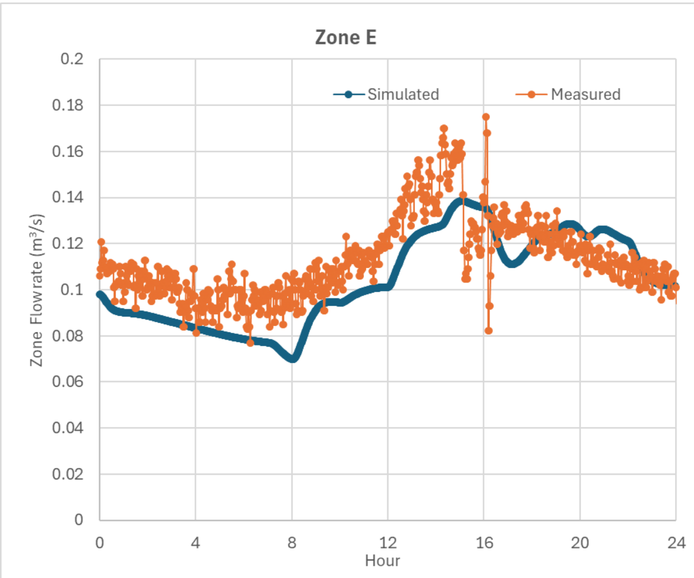

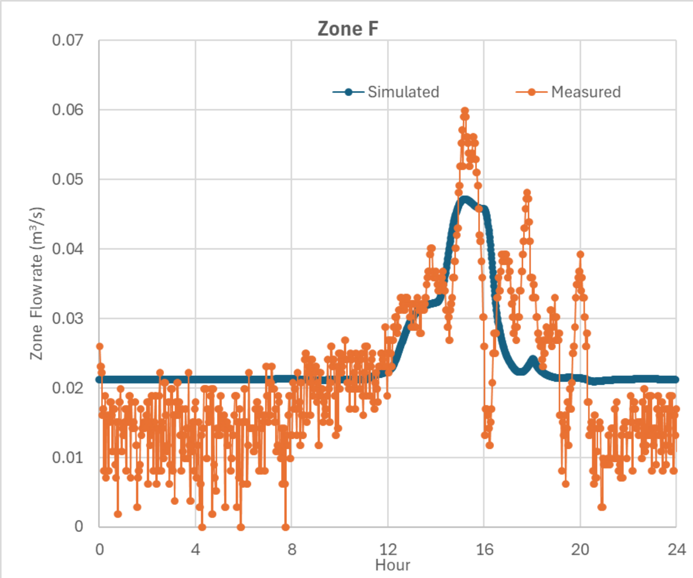
Zone F
Simulated
Measured
Zone Flowrate (m³/s)
0.07
0.06
0.05
0.04
0.03
0.02
0.01
0
0
4
8
12
16
20
24
Hour

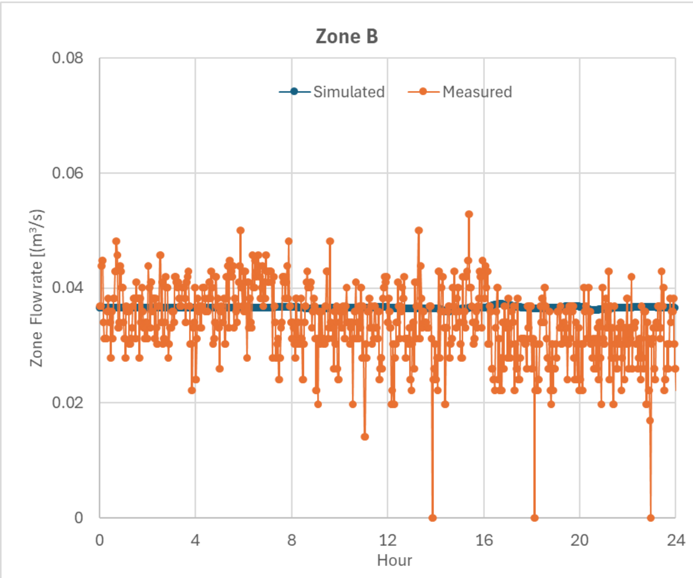
Zone B
Simulated
Measured
Zone Flowrate [(m³/s)
0.08
0.06
0.04
0.02
0
0
4
8
12
16
20
24
Hour

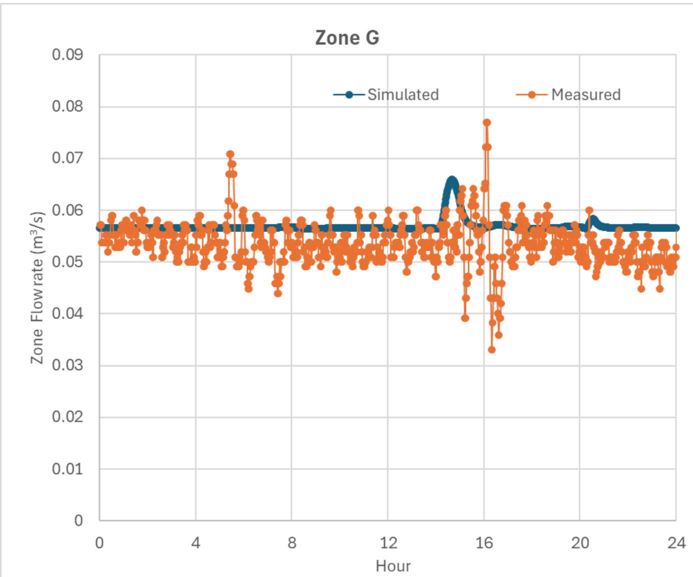
Zone G
Simulated
Measured
Zone Flowrate (m³/s)
0.09
0.08
0.07
0.06
0.05
0.04
0.03
0.02
0.01
0
0
4
8
12
16
20
24
Hour

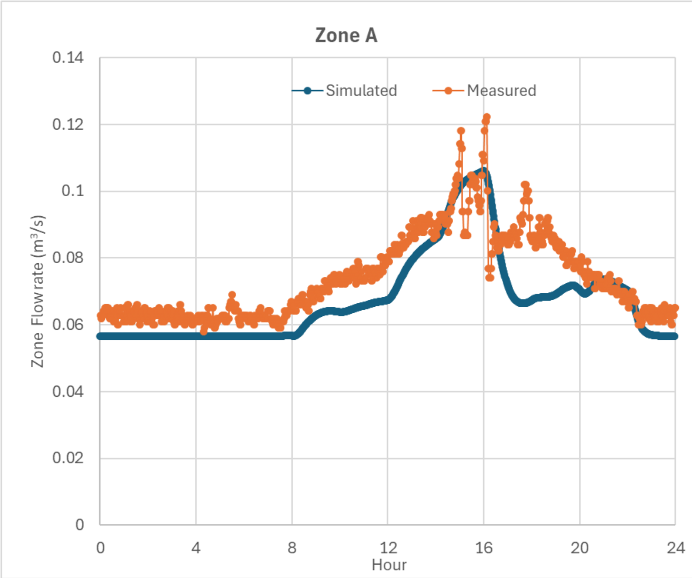

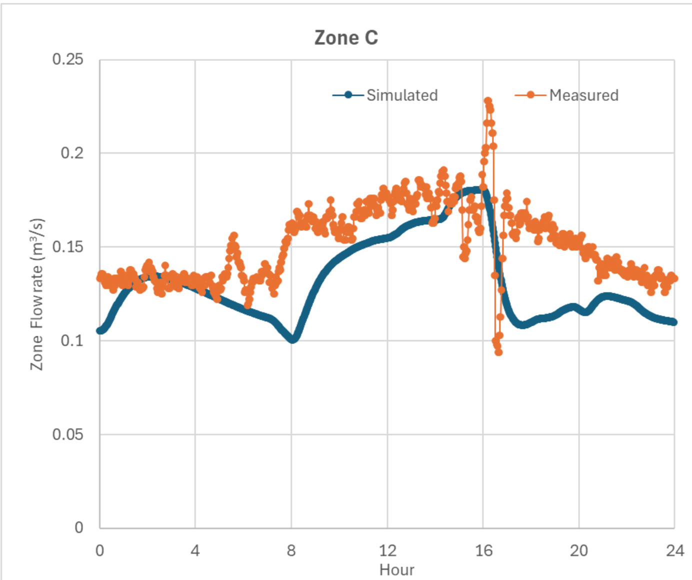

Figure 8.1: Comparison of the simulated and measured thermal zones flow rates

8.2 Supplementary Materials for Chapter 5

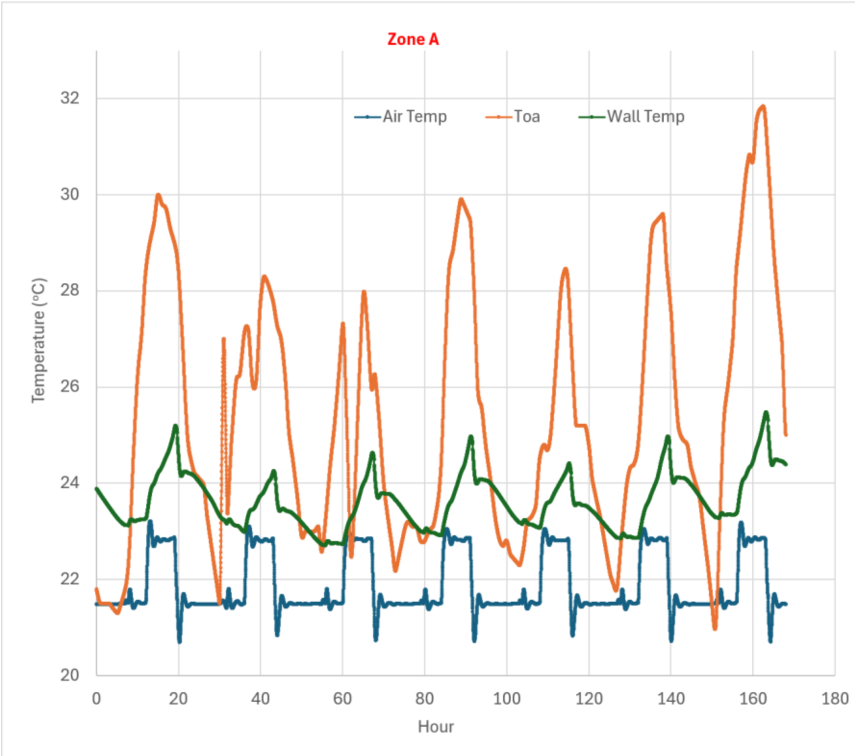

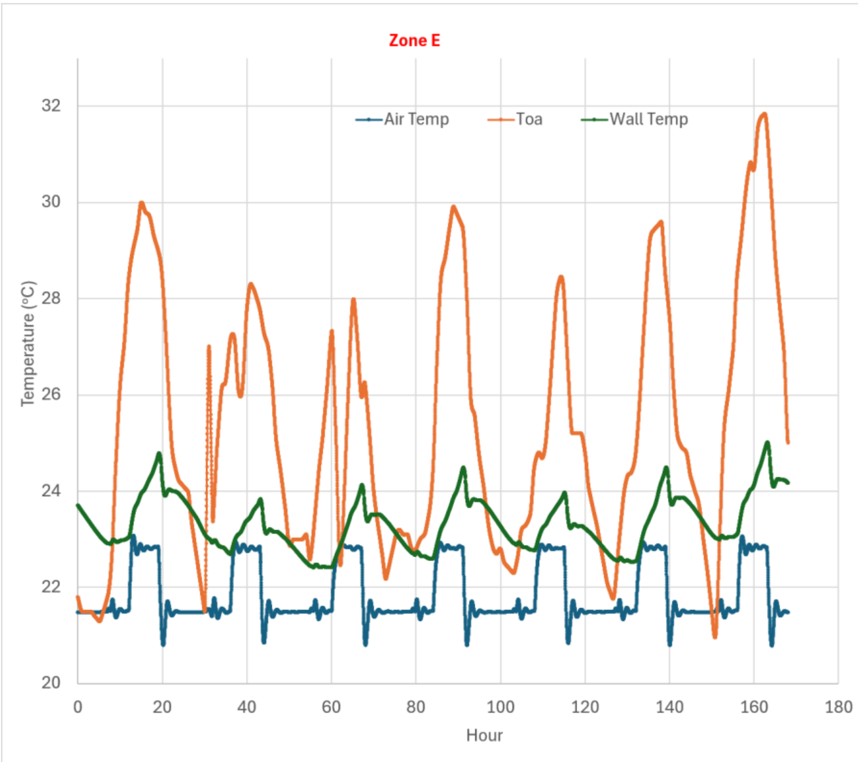

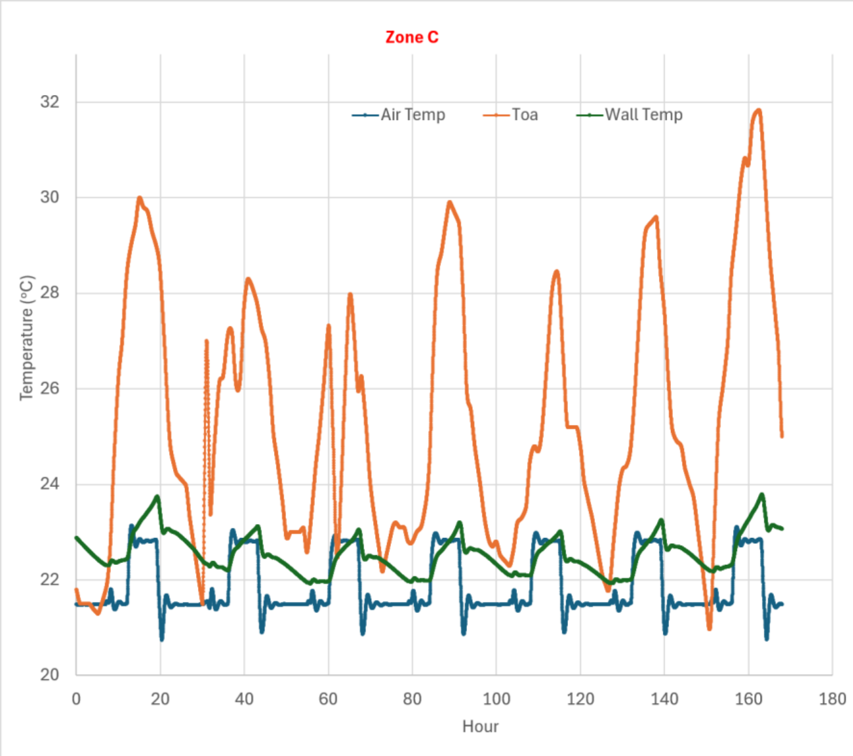
Zone C
Air Temp
Toa
Wall Temp
Temperature (°C)
32
30
28
26
24
22
20
0
20
40
60
80
100
120
140
160
180
Hour

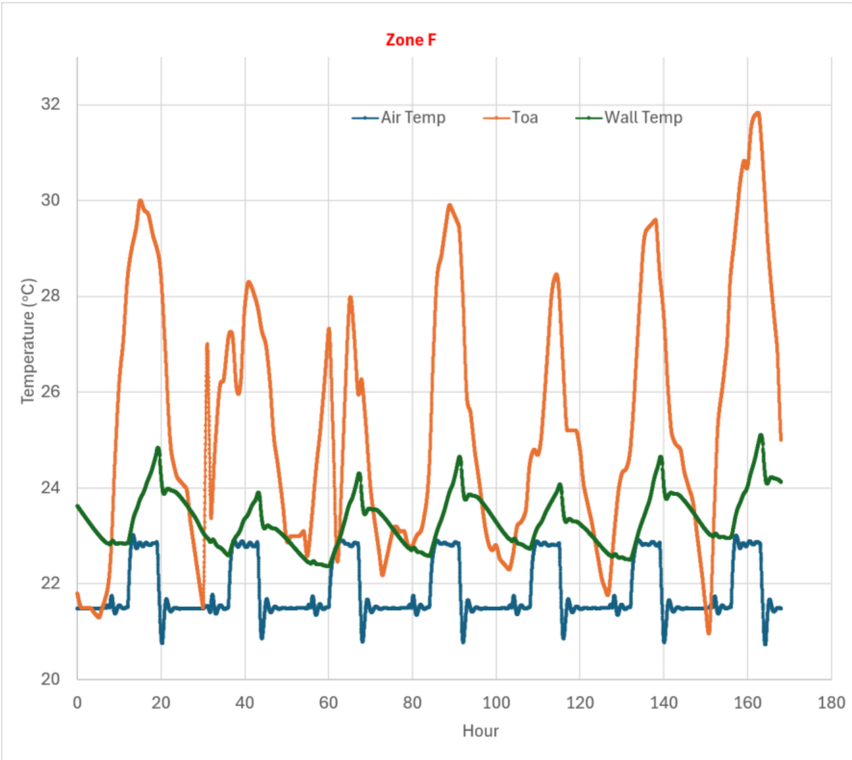
Zone F
Air Temp
Toa
Wall Temp
Temperature (°C)
32
30
28
26
24
22
20
0
20
40
60
80
100
120
140
160
180
Hour

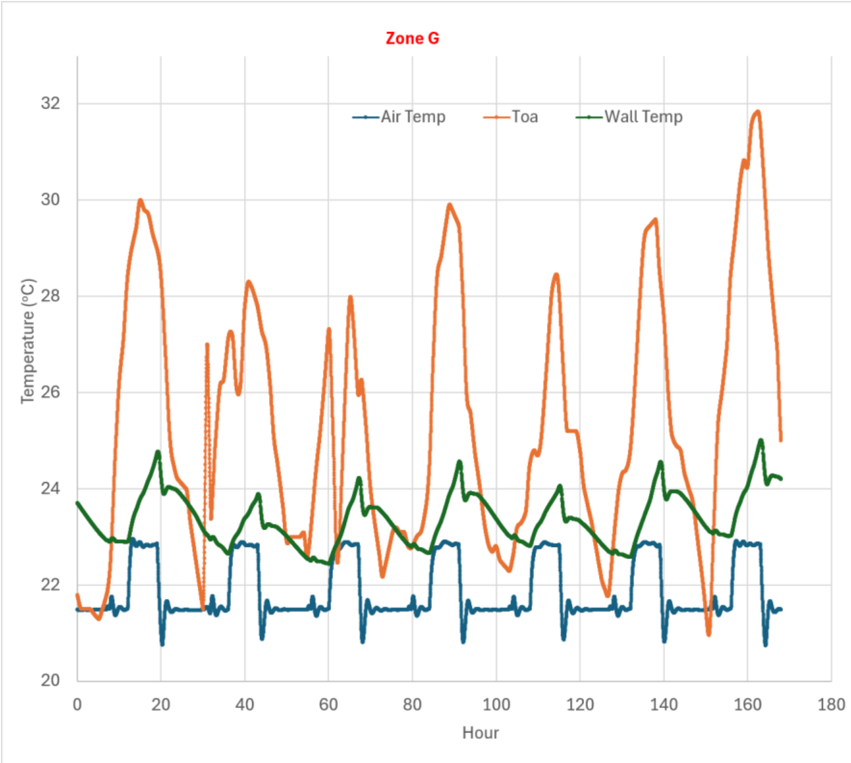

Figure 8.2: Air and wall temperature for exterior zones

Parameter Bounds for Optimization

Exterior Zones

Parameter	Symbol	Physical range
Envelope resistance	R_{env}	1.0×10^{-3}– 3.16×10^{-1} K/W
Air–mass resistance	R_{am}	1.0×10^{-4}–3.16×10^{-1} K/W
Air capacitance	C_{air}	1.0×10^{3}–3.16×10^{6} J/K
Mass capacitance	C_{mass}	3.16×10^{5} –3.16×10^{8} J/K
Internal-gain scale	γ	0.01 – 5
Effective Solar aperture	Sol_f	0 – 100
Infiltration conductance	h_f	1.0×10^{-1}–1.0×10^{4} W/K
Solar air fraction	α	0.001– 1
Inter-zone resistance	R_{ij}	1.0×10^{-4}–3.16×10^{-1} K/W
Air capacitance	C_{air}	1.0×10^{3}–3.16×10^{6} J/K

Parameter	Symbol	Physical range
Interior Zones		
Internal-gain scale	γ	0.01 – 5
Infiltration conductance	h_f	1.0×10^{-1}–1.0×10^{2} W/K
Inter-zone resistance	R_{ij}	1.0×10^{-4}–3.16×10^{-1} K/W

References

Afroz, Z., Goldsworthy, M., & White, S. D. (2023). Energy flexibility of commercial buildings for demand response applications in Australia. Energy and Buildings, 300. https://doi.org/10.1016/j.enbuild.2023.113533

Aghniaey, S., & Lawrence, T. M. (2018). The impact of increased cooling setpoint temperature during demand response events on occupant thermal comfort in commercial buildings: A review. In Energy and Buildings (Vol. 173, pp. 19–27). Elsevier Ltd. https://doi.org/10.1016/j.enbuild.2018.04.068

ASHRAE. (2006). Sequences of Operation for Common HVAC Systems (ASHRAE). Atlanta, GA.

ASHRAE, A. G. (2014). Guideline 14-2014: Measurement of energy, demand, and water savings. American Society of Heating, Refrigerating, and Air Conditioning Engineers, Atlanta, Georgia. www.ashrae.org

Byrdt, R. H., Lut, P., Nocedalt, J., & Zhu, C. (1995). A limited memory algorithm for bound constrained optimization. SIAM Journal on Scientific Computing, 16(5), 1190–1208. https://epubs.siam.org/terms-privacy

Chen, Y., Xu, P., Gu, J., Schmidt, F., & Li, W. (2018). Measures to improve energy demand flexibility in buildings for demand response (DR): A review. Energy and Buildings, 177, 125–139. https://doi.org/10.1016/j.enbuild.2018.08.003

Dai, M., Li, H., & Wang, S. (2023). Multi-agent based distributed cooperative control of air-conditioning systems for building fast demand response. Journal of Building Engineering, 77. https://doi.org/10.1016/j.jobe.2023.107463

Deng, Z., Hao, X., Yin, W., Zhang, S., & Chen, Y. (2025). Quantification of energy flexibility potential in commercial buildings for demand response across various climate zones in China. Journal of Building Engineering, 105. https://doi.org/10.1016/j.jobe.2025.112595

EIA. (2022, December). Electricity explained: Use of Electricity . US Energy Information Administration. https://www.eia.gov/energyexplained/electricity/use-of-electricity.php

Ejenakevwe, K. A., Tiamiyu, N., Hurt, R., Wang, G., & Song, L. (2026). A framework for assessing smart thermostat fault detection and diagnosis under unmeasurable building load disturbances. Energy and Buildings, 368, 117856. https://doi.org/10.1016/j.enbuild.2026.117856

Elehwany, H., Gunay, B., Ouf, M., Cotrufo, N., & Venne, J. S. (2024). Evaluating common supply air temperature setpoint reset strategies with varying occupancy patterns and behaviours. Building and Environment, 266(112129). https://doi.org/10.1016/j.buildenv.2024.112129

Fuchs, M., Teichmann, J., Lauster, M., Remmen, P., Streblow, R., & Müller, D. (2016). Workflow automation for combined modeling of buildings and district energy systems. Energy, 117, 478–484. https://doi.org/10.1016/j.energy.2016.04.023

Ghahramani, A., Zhang, K., Dutta, K., Yang, Z., & Becerik-Gerber, B. (2016). Energy savings from temperature setpoints and deadband: Quantifying the influence of building and system properties on savings. Applied Energy, 165, 930–942. https://doi.org/10.1016/j.apenergy.2015.12.115

Goetsch, H., & Deru, M. (2022). Operational Emissions Accounting for Commercial Buildings. www.nrel.gov/publications.

Goetzler, B., Guernsey, M., & Kassuga, T. (2019). Grid-interactive Efficient Buildings Technical Report Series: Heating, Ventilation, and Air Conditioning (HVAC); Water Heating; Appliances; and Refrigeration.

Hoyt, T., Arens, E., & Zhang, H. (2015). Extending air temperature setpoints: Simulated energy savings and design considerations for new and retrofit buildings. Building and Environment, 88, 89–96. https://doi.org/10.1016/j.buildenv.2014.09.010

Hoyt, T., Ho Lee, K., Zhang, H., Arens, E., & Webster, T. (2009). Energy Savings From Extended Air Temperature Setpoints and Reductions in Room Air Mixing. In Environmental Ergonomics. https://escholarship.org/uc/item/28x9d7xj

Hurt, R. (2021). Distributed energy feedback control for demand response operations in commercial hvac systems [master's thesis]. University of Oklahoma.

Jiang, Y. (2023). Design and analysis of smart home energy management system for energy-efficient and demand response operations [PhD's dissertation]. University of Oklahoma.

Keskar, A., Lei, S., Webb, T., Nagy, S., Hiskens, I. A., Mathieu, J. L., & Johnson, J. X. (2022). Assessing the performance of global thermostat adjustment in commercial buildings for load shifting demand response. Environmental Research: Infrastructure and Sustainability, 2(1), 015003. https://doi.org/10.1088/2634-4505/ac51c5

Kim, D., & Braun, J. E. (2022). MPC solution for optimal load shifting for buildings with ON/OFF staged packaged units: Experimental demonstration, and lessons learned. Energy and Buildings, 266, 112118. https://doi.org/https://doi.org/10.1016/j.enbuild.2022.112118

Lee, K. ho, & Braun, J. E. (2008). Model-based demand-limiting control of building thermal mass. Building and Environment, 43(10), 1633–1646. https://doi.org/10.1016/j.buildenv.2007.10.009

Li, H., Wang, Z., Hong, T., & Piette, M. A. (2021a). Energy flexibility of residential buildings: A systematic review of characterization and quantification methods and applications. In Advances in Applied Energy (Vol. 3). Elsevier Ltd. https://doi.org/10.1016/j.adapen.2021.100054

Li, H., Wang, Z., Hong, T., & Piette, M. A. (2021b). Energy flexibility of residential buildings: A systematic review of characterization and quantification methods and applications. In Advances in Applied Energy (Vol. 3). Elsevier Ltd. https://doi.org/10.1016/j.adapen.2021.100054

Li, Y., O'Neill, Z., Zhang, L., Chen, J., Im, P., & DeGraw, J. (2021). Grey-box modeling and application for building energy simulations - A critical review. In Renewable and Sustainable Energy Reviews (Vol. 146). Elsevier Ltd. https://doi.org/10.1016/j.rser.2021.111174

Liu, J., Yin, R., & Pritoni, M. (2021). Developing and Evaluating Metrics for Demand Flexibility in Buildings: Comparing Simulations and Field Data. https://doi.org/10.20357/B7WW34

Lu, X., Fu, Y., & O'Neill, Z. (2023). Benchmarking high performance HVAC Rule-Based controls with advanced intelligent Controllers: A case study in a Multi-Zone system in Modelica. Energy and Buildings, 284. https://doi.org/10.1016/j.enbuild.2023.112854

Lu, X., Fu, Y., O'Neill, Z., & Wen, J. (2021). A holistic fault impact analysis of the high-performance sequences of operation for HVAC systems: Modelica-based case study in a medium-office building. Energy and Buildings, 252. https://doi.org/10.1016/j.enbuild.2021.111448

Motegi, N., Piette, M. A., Watson, D. S., Kiliccote, S., & Xu, P. (2007). Introduction to Commercial Building Control Strategies and Techniques for Demand Response. Lawrence Berkeley National Laboratory LBNL-59975, 4.

Okochi, G. S., & Yao, Y. (2016). A review of recent developments and technological advancements of variable-air-volume (VAV) air-conditioning systems. In Renewable and Sustainable Energy Reviews (Vol. 59, pp. 784–817). Elsevier Ltd. https://doi.org/10.1016/j.rser.2015.12.328

O'Neill, Z., Li, Y., & Williams, K. (2017). HVAC control loop performance assessment: A critical review (1587-RP). Science and Technology for the Built Environment, 23(4), 619–636. https://doi.org/10.1080/23744731.2016.1239466

Papadopoulos, S., Kontokosta, C. E., Vlachokostas, A., & Azar, E. (2019). Rethinking HVAC temperature setpoints in commercial buildings: The potential for zero-cost energy savings and comfort improvement in different climates. Building and Environment, 155, 350–359. https://doi.org/10.1016/j.buildenv.2019.03.062

PNNL. (2021). Variable Air Volume (VAV) Systems Operations and Maintenance. https://www.pnnl.gov/projects/om-best-practices/variable-air-volume-systems#Description%20of%20Technology

Satchwell, A., Piette, M. A., & Khandekar, A. (2021). A National Roadmap for Grid-Interactive Efficient Buildings. https://escholarship.org/uc/item/78k303s5

Schwartz, L., Leventis, G., & Zetterberg, J. (2020). Grid-Interactive Efficient Buildings: An Introduction for State and Local Governments. www.seeaction.energy.gov

Sehar, F., Pipattanasomporn, M., & Rahman, S. (2016). An energy management model to study energy and peak power savings from PV and storage in demand responsive buildings. Applied Energy, 173, 406–417. https://doi.org/10.1016/j.apenergy.2016.04.039

Shan, K., Wang, S., Yan, C., & Xiao, F. (2016). Building demand response and control methods for smart grids: A review. Science and Technology for the Built Environment, 22(6), 692–704. https://doi.org/10.1080/23744731.2016.1192878

Shehadi, M. (2018). Review of humidity control technologies in buildings. Journal of Building Engineering, 19, 539–551. https://doi.org/10.1016/j.jobe.2018.06.009

Shen, P. (2026). RCBldEng - a computationally efficient RC network modeling method and engine for multizone building simulation. Energy, 346. https://doi.org/10.1016/j.energy.2026.140260

Storn, R., & Price, K. (1997). Differential Evolution-A simple and efficient adaptive scheme for global optimization over continuous spaces. Journal of Global Optimization, 11(4), 341–359.

Tang, H., Wang, S., & Li, H. (2021). Flexibility categorization, sources, capabilities and technologies for energy-flexible and grid-responsive buildings: State-of-the-art and future perspective. Energy, 219, 119598. https://doi.org/https://doi.org/10.1016/j.energy.2020.119598

Tiamiyu, N., Ejenakevwe, A., & Song, L. (2024). Performance Analysis of Vertical Borehole Ground Heat Exchanger Design Methods using Modelica-Based Modeling and Simulation. ASHRAE Transactions, 130, 464–473.

Tiamiyu, N., Ejenakevwe, K. A., Hlanze, P., & Song, L. (2026). Evaluating the performance of ground source heat pumps under different vertical borehole ground heat exchanger design methods using Modelica-based dynamic modeling and simulation. Science and Technology for the Built Environment, 32(1), 130–147. https://doi.org/10.1080/23744731.2025.2583886

Tiamiyu, N., Wang, J., Wang, Z., Song, L., & Wang, G. (2024). Occupancy Sensor-enabled Demand Control Ventilation Using Virtual Outdoor Air Flow Meters in Air Handling Units without an Outdoor Air Flow Meter. Building and Environment, 111501. https://doi.org/10.1016/j.buildenv.2024.111501

Torabi, N., Gunay, H. B., O'Brien, W., & Barton, T. (2022). Common human errors in design, installation, and operation of VAV AHU control systems – A review and a practitioner interview. In Building and Environment (Vol. 221). Elsevier Ltd. https://doi.org/10.1016/j.buildenv.2022.109333

US DOE. (2019). Grid-interactive Efficient Buildings Why are buildings important to grid modernization?

US EPA. (2022). Inventory of U.S. greenhouse gas emissions and sinks: 1990–2020. EPA 430-R-22-003. www.epa.gov/ghgemissions/inventory-us-greenhouse-gas-emissions-and-sinks.

Wang, G., Wang, J., Tiamiyu, N., Wang, Z., & Song, L. (2023a). Development and Investigation of Advanced HVAC Demand Control . ASHRAE Transactions, 129, 176–183.

Wang, G., Wang, J., Tiamiyu, N., Wang, Z., & Song, L. (2023b). Loose Belt Fault Detection and Virtual Flow Meter Development Using Identified Data-driven Energy Model for Fan Systems. Sustainability (Switzerland), 15(16), 12113. https://doi.org/10.3390/su151612113

Wang, H., Wang, S., & Tang, R. (2019). Development of grid-responsive buildings: Opportunities, challenges, capabilities and applications of HVAC systems in non-residential buildings in providing ancillary services by fast demand responses to smart grids. Applied Energy, 250, 697–712. https://doi.org/https://doi.org/10.1016/j.apenergy.2019.04.159

Watson, D. S., Kiliccote, S., Motegi, N., & Piette, M. A. (2006). Strategies for Demand Response in Commercial Buildings.

Wetter, M., Benne, K., Tummescheit, H., & Winther, C. (2024). Spawn: coupling Modelica Buildings Library and EnergyPlus to enable new energy system and control applications. Journal of Building Performance Simulation, 17(2), 274–292. https://doi.org/10.1080/19401493.2023.2266414

Wetter, M., Hu, J., Grahovac, M., Eubanks, B., & Haves, P. (2018, September 26). OpenBuildingControl: Modeling feedback control as a step towards formal design, specification, deployment and verification of building control sequences. Building Performance Modeling Conference and SimBuild. http://project-haystack.org/

Xu, P. (2009). Demand Shifting with Thermal Mass in Light and Heavy Mass Commercial Buildings.

Xu, P., & Haves, P. (2006). Case study of demand shifting with thermal mass in two large commercial buildings. ASHRAE Transactions, 112, 572.

Xu, P., Haves, P., Piette, M. A., Braun, J., & ten Hope, L. (2004, August 22). Peak Demand Reduction from Pre-Cooling with Zone Temperature Reset in an Office Building. ACEEE 2004 Summer Study on Energy Efficiency in Buildings: Breaking out of the Box. https://escholarship.org/uc/item/1205612d

Xue, X., Wang, S., Yan, C., & Cui, B. (2015). A fast chiller power demand response control strategy for buildings connected to smart grid. Applied Energy, 137, 77–87. https://doi.org/10.1016/j.apenergy.2014.09.084

Yang, Y., Chen, Y., Wang, Y., Li, C., & Li, L. (2016). Modelling a combined method based on ANFIS and neural network improved by DE algorithm: A case study for short-term electricity demand forecasting. In Applied Soft Computing Journal (Vol. 49, pp. 663–675). Elsevier Ltd. https://doi.org/10.1016/j.asoc.2016.07.053

Yin, R., Kara, E. C., Li, Y., DeForest, N., Wang, K., Yong, T., & Stadler, M. (2016). Quantifying flexibility of commercial and residential loads for demand response using setpoint changes. Applied Energy, 177, 149–164. https://doi.org/10.1016/j.apenergy.2016.05.090

Yin, R., Liu, J., Piette, M. A., Xie, J., Pritoni, M., Casillas, A., Yu, L., & Schwartz, P. (2023). Comparing simulated demand flexibility against actual performance in commercial office buildings. Building and Environment, 243. https://doi.org/10.1016/j.buildenv.2023.110663

Young, M., Less, B. D., Dutton, S. M., Walker, I. S., Sherman, M. H., & Clark, J. D. (2020). Assessment of peak power demand reduction available via modulation of building ventilation systems. Energy and Buildings, 214. https://doi.org/10.1016/j.enbuild.2020.109867

Zanetti, E., Blum, D., Fu, H., Weyandt, C., Pritoni, M., & Piette, M. A. (2025). Commercial building HVAC demand flexibility with model predictive control: Field demonstration and literature insights. Energy and Buildings, 345. https://doi.org/10.1016/j.enbuild.2025.116097

Zhao, X., Luo, L., Zhu, Q., Li, P., Luo, M., & Shi, X. (2026). Increasing demand-response flexibility for office buildings: A multi-scenario strategy integrating thermal tolerance and adaptive behaviors. Building and Environment, 288. https://doi.org/10.1016/j.buildenv.2025.113974

Zhou, X., Yap, E. W., Dou, W., Huang, M., Aziz, M. S., Robinson, D. A., McDowell, C., White, S. D., Goldsworthy, M., Sethuvenkatraman, S., Shah, S. K., Amos, M., & Ma, Z. (2025). Demand flexibility characterisation in non-residential buildings: A review. Applied Energy, 393. https://doi.org/10.1016/j.apenergy.2025.126100

Zhu, C., Byrd, R. H., Peihuang Lu, & Jorge Nocedal. (1997). Algorithm 778: L-BFGS-B: Fortran Subroutines for Large-Scale Bound-Constrained Optimization. ACM Transactions on Mathematical Software (TOMS), 23(4), 550–560.